Applications of Droplet Microarray in Microbiology: from Miniaturized High Throughput Screening Platform to Biofilm Control

Zur Erlangung des akademischen Grades einer
DOKTORIN DER NATURWISSENSCHAFTEN
(Dr. rer. nat.)
von der KIT-Fakultät für Chemie und Biowissenschaften
des Karlsruher Instituts für Technologie (KIT)
genehmigte
DISSERTATION
von
M. Sc (Eng). Wenxi Lei

1. Referent: Prof. Dr. Pavel A. Levkin

2. Referentin: Prof. Dr. Anne-Kristin Kaster

Tag der mündlichen Prüfung: 16.07.2021

Eidesstattliche Erklärung

Hiermit versichere ich, dass ich die vorliegende Arbeit selbständig verfasst und keine anderen als die angegebenen Quellen und Hilfsmittel verwendet, sowie Literaturzitate kenntlich gemacht habe. Die Satzung des Karlsruher Instituts für Technologie (KIT) zur Sicherung guter wissenschaftlicher Praxis wurde beachtet. Ich erkläre außerdem, dass diese Dissertation weder in gleicher oder ähnlicher Form bisher in einem anderen Prüfungsverfahren vorgelegen hat. Die elecktroische Version der Arbeit stimmt mit der schriftlichen überein und die Abgabe und Archivierung der Primärdaten gemäß Abs. A (6) der Regeln zur Sicherung guter wissenschaftlicher Praxis der KIT beim Institut ist gesichert.

Ort, Datum Unterschrift

Acknowledgement

First of all and at most, I am thankful to Prof. Pavel Levkin for accepting me as a PhD student. In the past almost four years, I have learned not only knowledge but also academic thinking from him. Whenever I needed discussion about my projects, his door was always open to me. He made everything clear and easy for me. Whether it is his criticism or affirmation of me, I am very grateful. I saw his great passion for science, which had great impact on me and made me think about my academic aims. Thank you, Pavel!

I would like to thank Prof. Thomas Schwartz for his kind help in my PhD study. I am grateful for his suggestions and guidance to my research projects. He gave me great encouragement and confidence when I was frustrated with my projects. He provided me with a very safe, clean, and equipped microbiology lab, where I spent most of my time. I am grateful for all of these.

I would like to thank Dipl.-Biol. Peter Krolla. I am very impressed by his cautious attitude and open mind in lab work. I will always remember the time we worked together in the lab and his question ‘But why is it like this, why? Wenxi.’ He gave me great help in my projects and he is also a good friend to me. Peter, thank you for everything!

I am thankful to all my group members and group members of Thomas’ group. For your help, kindness, and patience. You are all excellent and I learned a lot from all of you. Lei, Zheqin, Julia, Jacky, and Johannes, thank you for your warm heart to help me adapt to the new environment when I was first the lab. Shraddha, Tina, Haijun, thank you for offering me a nice office and all the kind help to my study and to my personal life. Anna, Ye, Johannes Alexander, Jan Las, thank you for your great help in my projects. I am thankful to Zhenwu, Shuai, Janne, Maria, Ynaxi, Marius, Gerile, Julius, Max, Yaqi, Weiyi, Xiaotao, Dorothea, Razan, Joaquin for offering me

a friendly working environment. All the time I spent with you was nice and inspirational.

I would like to thank Prof. Markus Reischl for his support in my TAC meetings and his help in my bacterial screening project. I am thankful to Dr. Sergiy Afonin for all helpful discussion and his help in MALDI-ToF measurements.

I am thankful to the China Scholarship Council. Without the scholarship supporting overseas PhD studies, I would never have the chance to study abroad. Now I am happy to be back in China and do something useful to my country.

Abstract*

Our health systems are facing an increasing number of infections involving antibiotic-resistant bacteria, which can no longer be treated with previously potent antimicrobial agents. High-throughput screening (HTS) method is widely used in drug discovery that allows researchers to quickly identify novel antimicrobial agents from various libraries of natural products or synthetic compounds. However, currently there are no time-saving and cost-effective high-throughput screening methods for discovery of antimicrobial compounds.

In Chapter 4.1, a droplet microarray (DMA) system was established as a miniaturized platform for high-throughput screening of antibacterial compounds using the pathogen *Pseudomonas aeruginosa* (*P. aeruginosa*) as a target. Due to the differences in wettability of the DMA surface, it was possible to develop a rapid method for generating microarrays of nanoliter-sized droplets containing bacteria. A sandwiching method enabled immediate screening with libraries of antibiotics. A novel simple colorimetric readout method compatible with the nanoliter size of the droplets was established. Furthermore, the drug-resistance of *P. aeruginosa* PA49, an environmental isolate was investigated by using the DMA platform to screen a small antibiotic library.

Subsequently, in Chapter 4.2, the work flow of HTS using DMA is optimized to adapt to a larger library screening. To develop new antibiotics against carbapenem-resistant *Klebsiella pneumoniae*, an important pathogen, DMA based HTS system was used to screen commercially unavailable compounds from the ComPlat library. The screening pipeline was validated, including the influence of the dispensing process on bacteria viability, the establishment of the colorimetric readout of screening results, and the data analyzing. With the developed colorimetric readout method,

*Parts of the abstract are adapted from the following publications: Lei, W., Demir, K., Overhage, J., Grunze, M., Schwartz, T., & Levkin, P. A. (**2020**). *Advanced Biosystems*, 4(10), 2000073.
Lei, W., Bruchmann, J., Rüping, J. L., Levkin, P. A., & Schwartz, T. (**2019**). *Advanced Science*, 6(13), 1900519.
Lei, W., Krolla, P., Schwartz, T., & Levkin, P. A. (**2020**). *Small*, 16(52), 2004575.

antibacterial effects of compounds can be evaluated visibly by reading the color of droplets. Quantitative evaluation can be achieved with a cheap paper scanner. This research builds solid foundation for further miniaturization of HTS of compound libraries in order to identify novel antimicrobial substances.

When planktonic bacteria form biofilms in the human body, persistent infections could be caused and become a serious problem in healthcare. Despite many decades of research, biofilm architecture and spreading mechanisms are still not clear partly due to the high heterogeneity within biofilms.

In Chapter 4.3, patterned liquid infused surfaces (pLIS) are introduced and utilized to study biofilm structure of *P. aeruginosa*, *Stenotrophomonas maltophilia*, and *Staphylococcus aureus*. Biofilm patterns of different species have been formed on hydrophilic regions, which were separated by liquid infused borders. It is found that there were string-like connections between biofilm patterns, which were termed as 'biofilm bridges'. Fluorescence staining methods were used to investigate the detailed structure of bridges, showing a spatial distribution of respiratory active bacteria and biomass in the bridges. The core–shell structure of bridges formed by two-species mixed populations is illustrated. pLIS can be useful to reveal more details about the fine structures within biofilm communities as well as to understand the spreading of biofilms and complex communication in multi-species biofilms.

Ultimately, in Chapter 4.4, the mechanism of formation of biofilm bridges is illustrated. pLIS are utilized to fabricate connective structures between bacterial colonies of *P. aeruginosa* by a simple dewetting method. It is demonstrated that the bacteria attached to hydrophilic areas and bacteria precipitated on lubricant infused borders both contribute to the formation of bacterial bridges. The geometry and distribution of bridges can be controlled using pre designed superhydrophobic–hydrophilic patterns. It is demonstrated that bacterial bridges connecting bacteria colonies act as bio-microfluidic channels and can transport liquids, nutrients, and antibacterial substances between neighboring bacteria clusters. Thus, bacterial

bridges can be used to study formation, spreading, and development of bacterial colonies, and communication within and between isolated biofilms.

Overall, this thesis shows applications of DMA in microbiology to promote the drug discovery, as well as to understand structures and organizations of biofilms. We explored the ability of DMA as a miniaturized HTS platform to identify novel antibiotics. This HTS system based on DMA would facilitate drug developments in laboratories and provide new perspectives to conduct antibacterial assays. Combined with lubricant infused surfaces, DMA enables fabrication of patterned biofilms. With a clear demonstration of structures and formation mechanism of biofilm bridges in this thesis, it is possible to control biofilm distribution on DMA, which will open opportunities to study complex architecture, heterogeneity, and interactions in biofilms. These results were published in three publications, while the manuscript of content of Chapter 4.2 is in preparation. [1-3]

Zusammenfassung

Unsere Gesundheitssysteme sind mit der zunehmenden Zahl von Infektionen mit antibiotikaresistenten Bakterien konfrontiert, die mit bisher wirksamen antimikrobiellen Mitteln nicht mehr behandelbar sind. Die Hochdurchsatz-Screening-Methode (HTS) wird häufig in der Wirkstoffforschung eingesetzt und ermöglicht es Forschern, schnell neue antimikrobielle Wirkstoffe aus verschiedenen Bibliotheken von Naturstoffen oder synthetischen Verbindungen zu identifizieren. Derzeit gibt es jedoch keine zeitsparenden und kostengünstigen Hochdurchsatz-Screening-Methoden zur Entdeckung antimikrobieller Verbindungen.

In Kapitel 4.1 wurde ein Tröpfchen-Microarray (DMA)-System als miniaturisierte Plattform für das Hochdurchsatz-Screening von antibakteriellen Wirkstoffen mit dem Erreger *Pseudomonas aeruginosa* (*P. aeruginosa*) als Target etabliert. Aufgrund der unterschiedlichen Benetzbarkeit der DMA-Oberfläche war es möglich, eine schnelle Methode zur Erzeugung von Mikroarrays aus bakterienhaltigen Tröpfchen im Nanoliterbereich zu entwickeln. Eine Sandwiching-Methode ermöglichte ein sofortiges Screening mit Bibliotheken von Antibiotika. Es wurde eine neue einfache kolorimetrische Auslesemethode entwickelt, die mit der Nanolitergröße der Tröpfchen kompatibel ist. Darüber hinaus wurde die Arzneimittelresistenz von *P. aeruginosa* PA49, einem Umweltisolat, untersucht, indem die DMA-Plattform zum Screening einer kleinen Antibiotikabibliothek verwendet wurde.

Anschließend wird in Kapitel 4.2 der Arbeitsablauf von HTS unter Verwendung von DMA optimiert, um sich an ein größeres Bibliotheksscreening anzupassen. Um ein neues Antibiotikum gegen Carbapenem-resistente *Klebsiella pneumoniae*, einen wichtigen Krankheitserreger, zu entwickeln, wurde ein DMA-basiertes HTS-System verwendet, um kommerziell nicht verfügbare Verbindungen aus der ComPlat-Bibliothek zu screenen. Die Screening-Pipeline wurde validiert, einschließlich des Einflusses des Dosierprozesses auf die Lebensfähigkeit der Bakterien, der Etablierung der kolorimetrischen Anzeige der Screening-Ergebnisse und der Datenanalyse. Mit der entwickelten kolorimetrischen Auslesemethode kann die

antibakterielle Wirkung von Verbindungen durch Ablesen der Farbe von Tröpfchen sichtbar bewertet werden. Eine quantitative Auswertung kann mit einem billigen Papierscanner erreicht werden. Diese Forschung bildet eine solide Grundlage für die weitere Miniaturisierung der HTS von Verbindungsbibliotheken, um neue antimikrobielle Substanzen zu identifizieren.

Wenn planktonische Bakterien im menschlichen Körper Biofilme bilden, können anhaltende Infektionen verursacht und zu einem ernsthaften Problem im Gesundheitswesen werden. Trotz jahrzehntelanger Forschung sind Biofilmarchitektur und Ausbreitungsmechanismen immer noch nicht klar, teilweise aufgrund der hohen Heterogenität innerhalb von Biofilmen.

In Kapitel 4.3 werden gemusterte flüssige infundierte Oberflächen (pLIS) vorgestellt und verwendet, um die Biofilmstruktur von *P. aeruginosa*, *Stenotrophomonas maltophilia* und *Staphylococcus aureus* zu untersuchen. Biofilmmuster verschiedener Spezies wurden auf hydrophilen Regionen gebildet, die durch flüssigkeitsinfundierte Ränder getrennt waren. Es wurde festgestellt, dass es fadenartige Verbindungen zwischen Biofilmmustern gab, die als „Biofilmbrücken“ bezeichnet wurden. Mit Fluoreszenz-Färbungsmethoden wurde die detaillierte Struktur von Brücken untersucht, die eine räumliche Verteilung von atemaktiven Bakterien und Biomasse in den Brücken zeigten. Die Kern-Schale-Struktur von Brücken, die von einer gemischten Population aus zwei Arten gebildet werden, wird veranschaulicht. pLIS kann nützlich sein, um mehr Details über die feinen Strukturen innerhalb von Biofilmgemeinschaften aufzudecken sowie die Ausbreitung von Biofilmen und die komplexe Kommunikation in Biofilmen mehrerer Arten zu verstehen.

Schließlich wird in Kapitel 4.4 der Mechanismus der Bildung von Biofilmbrücken dargestellt. pLIS werden verwendet, um durch ein einfaches Entnetzungsverfahren Bindestrukturen zwischen Bakterienkolonien von *P. aeruginosa* herzustellen. Es wird gezeigt, dass sowohl die an hydrophilen Bereichen haftenden Bakterien als auch die an mit Schmiermittel infundierten Grenzen ausgefällten Bakterien zur Bildung von Bakterienbrücken beitragen. Die Geometrie und Verteilung von Brücken kann

durch vorgefertigte superhydrophob-hydrophile Muster gesteuert werden. Es wird gezeigt, dass Bakterienbrücken, die Bakterienkolonien verbinden, als bio-mikrofluidische Kanäle wirken und Flüssigkeiten, Nährstoffe und antibakterielle Substanzen zwischen benachbarten Bakterienclustern transportieren können. Somit können Bakterienbrücken verwendet werden, um die Bildung, Ausbreitung und Entwicklung von Bakterienkolonien sowie die Kommunikation innerhalb und zwischen isolierten Biofilmen zu untersuchen .

Insgesamt zeigt diese Dissertation Anwendungen von DMA in der Mikrobiologie zur Förderung der Wirkstoffforschung sowie zum Verständnis von Strukturen und Organisationen von Biofilmen. Wir untersuchten die Fähigkeit von DMA als miniaturisierte HTS-Plattform, um neuartige Antibiotika zu identifizieren. Dieses auf DMA basierende HTS-System würde die Arzneimittelentwicklung in Labors erleichtern und neue Perspektiven für die Durchführung antibakterieller HTS eröffnen. In Kombination mit schmiermittelinfundierten Oberflächen ermöglicht DMA die Herstellung gemusterter Biofilme. Mit einer klaren Demonstration der Strukturen und des Bildungsmechanismus von Biofilmbrücken in dieser Arbeit ist es möglich, die Biofilmverteilung auf DMA zu kontrollieren, was Möglichkeiten zur Untersuchung komplexer Architektur, Heterogenität und Wechselwirkungen in Biofilmen eröffnet. Diese Ergebnisse wurden in drei Publikationen veröffentlicht, während das Inhaltsmanuskript von Kapitel 4.2 vorbereitet wird. [1-3]

Table of Contents

1 Introduction

1.1 Miniaturized HTS of Bacteria and Biofilms

1.1.1 The Threat of Multi-Resistant Bacteria

Antibiotics were once considered as a 'medical miracle' when they saved innumerable lives in the 20th century. Before the commercialization of antibiotics, infectious diseases had been the leading cause of death in Europe. At that time, 25% of England's mortality was due to infectious diseases. [4] Later, a large number of antibiotics including streptomycin, chloramphenicol, macrolides etc. were discovered during 1940-1960s, leading to the antibiotic golden age. Considering the rapid development of antibiotic identification, it was believed that infectious diseases were under perfect control and would no longer pose a threat to life. [5]

Are things now really as people expected? Currently, in Europe, there are still nearly 700,000 people suffering from antibiotic-resistant infections and 33,000 deaths every year. It was estimated that the cost for antibiotic-resistant infections is over €1.5 billion yearly in Europe. [6] In North America, more than 2 million people are involved in antibiotic-resistant infections yearly and 23,000 people pass away due to ineffective treatments every year. [5] From 2000 to 2010, the consumption of antibiotics in 71 countries has increased 36%, meanwhile the antibiotics that people are using tend to be more and more broad-spectrum. Even with the two classes of last-resort antibiotics, carbapenems and polymyxins, the consumption has increased by 45% and 13%, respectively, which is not a good sign of control of antibiotic resistant infections. Today, the fact is that infectious diseases have been involved in about 20% of deaths globally. [7]

Usually, the initial susceptive bacteria become resistant to antimicrobial agents in the following two manners including: I. mutation and selection, II. gene exchange. Mutated bacteria are able to eliminate the effect of antibiotics by altering antibiotic targets, increasing the expression of efflux genes, downregulating the membrane

protein to hinder the entry of antibiotics, upregulating proteins inactivating antimicrobial agents etc. [8] Such mutations are selected by the pressure of antimicrobial agents, meaning that susceptible strains are killed by antibiotics while the resistant strains are able to survive and proliferate. This process is termed 'vertical evolution'. [9] By gene exchange, or so-called 'horizontal evolution', bacteria obtain resistance gene materials from other bacteria even from different species by conjugating together using pilus, infecting with bacteriophage carrying resistance genes, or acquiring resistance genes spreading in environment. [9] Tens of years of selection with various antibiotics resulted in the appearance of multidrug-resistant bacteria or so called 'superbugs' as a severe threat to human health. Typical multidrug-resistant bacteria include the 'ESKAPE' pathogens (*Enterococcus faecium*, *Staphylococcus aureus*, *Klebsiella pneumoniae*, *Acinetobacter baumannii*, *Pseudomonas aeruginosa*, and *Enterobacter spp.*). [10] It has been reported that over 15% of nosocomial infections are caused by multi-resistant pathogens, which are not able to be treated with most antibiotics. [11] For example, it is estimated that in Asia, the average prevalence of methicillin-resistant *Staphylococcus aureus* (MRSA) in hospitals is at 67.4%. [12] Another important pathogen, carbapenem-resistant *Enterobacteriaceae* (CRE) which produces New Delhi metallo-β-lactamase reported in 2008, has now been detected worldwide. [13, 14]

One direct strategy to combat multidrug-resistant bacteria is to discover new antibiotics. However, the last new class of antibiotics was daptomycin discovered in 1986. For a long time no breakthrough has been made in the market of antibiotics (Figure 1). For example, recently marketed tedizolid, dalbavancin and ceftobiprole in fact belong to already known antibiotic classes of oxazolidinones, lipoglycopeptides and cephalosporins. [15]

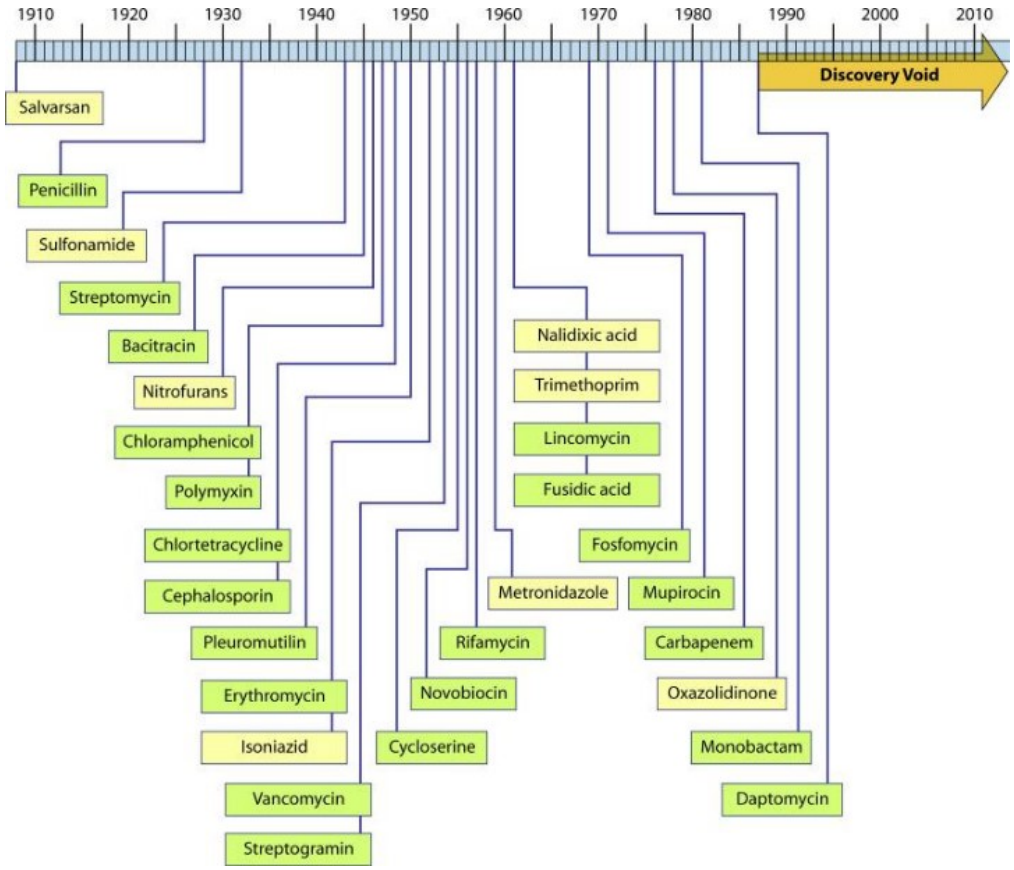

Figure 1. Timeline of discovery of antibiotics of different classes. [16]

Besides scientific difficulties, the reason for slow discovery of antibiotics lies in financial hurdles. It has been reported that it takes more than 20 years of work and costs of over 2 billion dollars to discover a new drug. [17] Therefore, major pharmaceutical companies have stopped or drastically cut their research efforts for developing new antimicrobials. By not addressing this issue, even minor infections that are currently easily treated can become a serious health risk in the future. The O'Neil Report estimates that by 2050, 10 million people will die per year from infections caused by drug-resistant microbes. [18] The number is even higher than the deaths caused by COVID-19 from January, 2020 to January, 2021, which is about 2 million. (data from https://www.worldometers.info/coronavirus/worldwide-graphs/#total-deaths)

1.1.2 In Vitro Platforms for Screening of Antibacterial Agents

The high-throughput screening (HTS) method is widely used in drug discovery as well as in fields of chemistry, biology, chemical biology, etc. In microbiological studies, HTS allows researchers to quickly identify novel antimicrobial agents from various libraries of natural products or synthetic compounds. [19-22] The platforms used in HTS play an important role, as they decide the efficiency and cost of the screening process. In this progress report, the state-of-the-art examples of various platforms in HTS of antibiotics are reviewed.

1.1.2.1 Agar Plates

Agar plates are one of the most commonly used tools for drug-resistance test with bacteria. Even though the agar plate is not a preferred platform for HTS, it is discussed here as well, due to its importance in antibacterial assays and new techniques that adapt agar plates to HTS. Among various antibacterial assays on agar plates, the disk diffusion assay is widely applied as an official method for testing antimicrobial susceptibility in many laboratories. [23] Many standards based on the disk diffusion assay are well accepted and approved. The procedure for the disk diffusion assay includes inoculation of testing bacteria on agar plates with a standard inoculum, placement of paper disks containing antibiotics on inoculated agar plates, incubation and measurement of diameter of inhibition zone of bacteria growth. Bacteria then could be categorized as susceptible, intermediate, or resistant stain according to the diameter data (Figure 2). [23] The principle of the disk diffusion assay is that diffused antibiotics from paper disks inhibit the growth and reproduction of testing bacteria. Advantages of this assay include reliability, simplicity, and low cost.

As a robust method, disk diffusion assay has been applied to screen antimicrobial susceptibility of various bacteria. [24-26] For example, Gleeson et al. screened susceptibility of 12 mastitis-associated bacteria to 11 commercial products for teat disinfectant using the disk diffusion assay. They demonstrated that products with

combined ingredients show better antibacterial effects than products with single ingredients. [27] By screening using agar plates, a new antibiotic named darobactin was obtained from *Photorhabdus* isolates (67 isolates in total) in 2019. Darobactin is selectively effective to Gram-negative bacteria [28]. Nevertheless, to realize high throughput screening with the disk diffusion assay, automation equipment is essential. [29] Otherwise it is time-consuming and skill-depended to obtain reliable results. There are other assays operated on agar plates such as antimicrobial gradient method, thin-layer chromatography (TLC) bioautography, agar well diffusion method, etc. [23] However, they have similar limitations with the disk diffusion method in HTS.

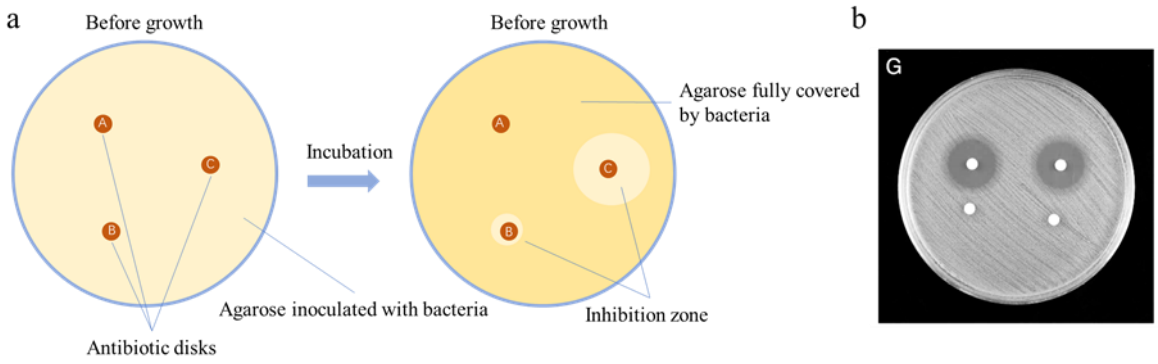

Figure 2. Illustration of the disk diffussion test on agar plates. (a) Schematic illustration. (b) A digital image of a representative sample with inhibition zones. [30]

In order to adapt agar plates to HTS, microwell arrays have been exploited to generate small compartments on agar surfaces while using each compartment as an independent growing area of bacteria. [31] For example, M. de Vos et al. reported a microbial culture chip fabricated by etching acrylic polymers on the surface of porous ceramic contains up to one million growth compartments. This culture chip enables screenings of fluorescent microcolony and galactosidase-producing microcolony on agar surfaces. [32] The microwell array/agar system miniaturized conventional agar plates by simple space separation, which is promising in future to culture bacteria on agar and conduct antibiotic susceptibility tests.

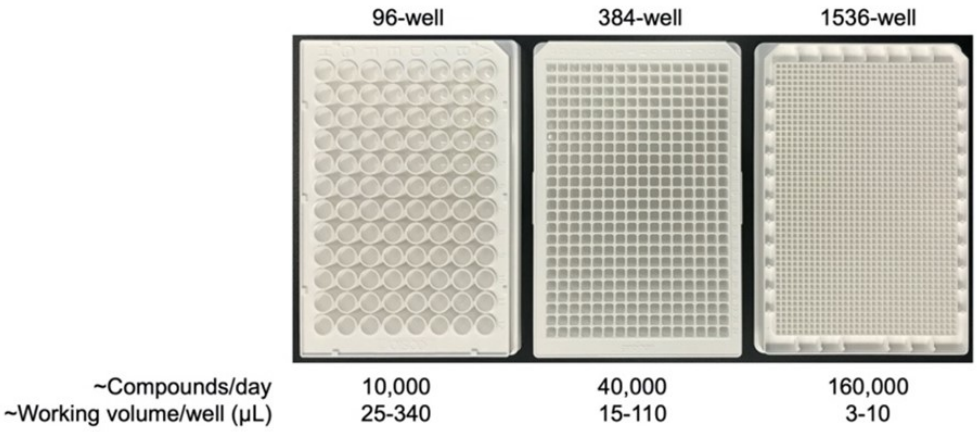

Figure 3. Typical microplate formats and corresponding working volumes. [33]

1.1.2.2 Microtiter Plates

Since the laboratory of Dr. Gyula Takatsy invented the first plate with 6 × 12 wells using plexiglass, microtiter plates such as 96-well plates and 384-well plates have been widely used in biology testing, including cell based HTS. [33-37] The design of plates was standardized by the Society for Biomolecular Screening together with American National Standards Institute (ANSI) as the SBS/ANSI standard to adapt plates to screening instruments and automatization. [33]

As a conventional platform, microtiter plates have the advantage that they are compatible with various instruments such as liquid-moving machines, microscopes, microplate readers, etc. to conduct biological assays. Due to the compatibility of microtiter plates, different antibacterial assays such as MIC tests, ATP bioluminescence assays, time-kill tests, fluorescence staining, and PCR haven been established in wells and produced reliable outcomes. [23, 38] Therefore, the throughput of screening in microtiter plates has been markedly increased comparing to the throughput of screening with agar plates. For example, Typas et al. used 384-well plates to conduct MIC tests to profile around 3,000 combinations of antibiotics, human-targeted drugs, and food additives to understand the interaction between drugs and find effective drug combinations against resistant microorganisms. [39]

Wu et al. combined HTS and drug repurposing to investigate antibacterial effect of 2,476 FDA approved drugs. They used 96-well plates to conduct optical density measurement with *P. aeruginosa* and demonstrated that 39 drugs were able to inhibit growth of bacteria or formation of biofilms. [40] Chen et al. carried out antibacterial screening in 96-well plates after they applied sunlight-photolyzed RAFT polymerization to synthesize glycopolymers in wells. [41] It showed the microtiter plates adapt to not only biological testing but also chemical synthesizing procedures.

Influences of parameters of microtiter plates such as surface properties, well-to-well contamination, microplate positional effects, etc. on drug screening have been discussed in another review, which provides information about correct selection of microplates for precise screening results. [33] As shown in Figure 3, formats commonly employed in most academic laboratories are 96- and 384-well plates. A high throughput of assays in industry can be achieved with 1,536-well plates, of which the working volume in each well is 3-10 µL. [42] The throughput can be increased further by miniaturization of wells, resulting in 2080-well plates, 3456-well plates, and 9600-well plates. The working volume decreases to as low as 25 nL in 20,000-well plates. Even though working volume of microplates is reduced, working with miniaturized microtiter plates faces difficulties including effective mixing, evaporation, adhesion of liquid to the wells´ side walls, pipetting, which need to be further solved. [42]

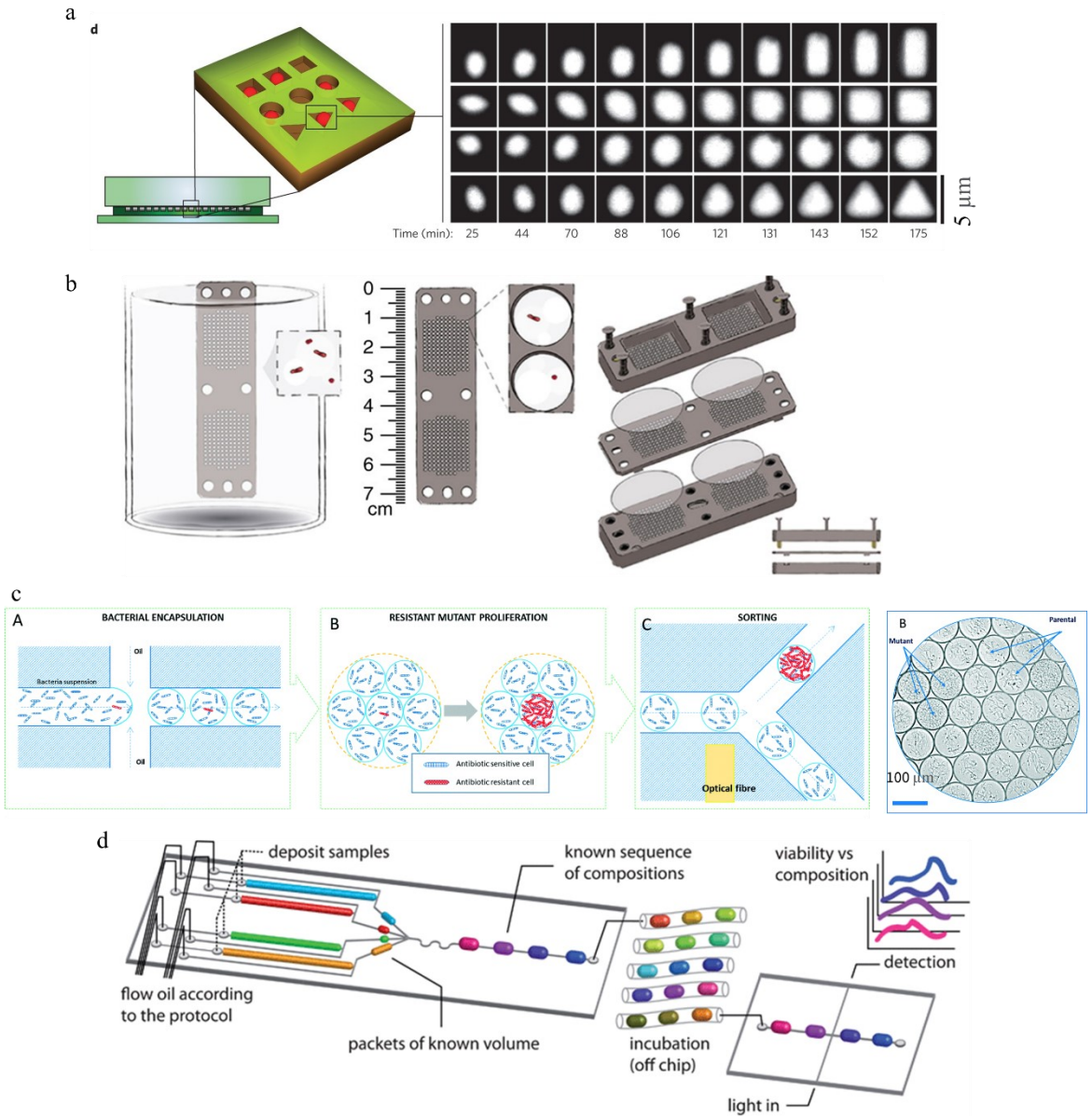

Figure 4. Microfluidic systems applied in antibacterial screening. (a) Left: Schematic illustration of the device to sculpt live bacteria. Right: Fluorescence images of bacteria growing into defined shapes. [43] (b) Schematic illustration of the 'ichip'. Holes on the device are able to culture single bacteria *in situ*. [44] (c) Left: Schematic illustration of the workflow of screening of resistant mutants using droplet microfluidics. Pico droplets containing a mixture of bacteria suspension and antibiotics are generated in a microfluidic device. Droplets containing only parental antibiotic sensitive bacteria and droplets containing resistant mutants are detected according to their different optical densities and then separated. Right: A microscope image of pico droplets containing parental bacteria and resistant mutant cells. [45] (d) A schematic of a microfluidic system for antibacterial

screening. Microdroplets of known volume from four channels are generated and merged into microdroplets with a defined composition of bacteria suspension and antibiotics. The merged droplets are stored in polyethylene tubing followed by off-chip incubation. The metabolism of bacteria in droplets is detected by measuring intensity of reagents, such as resazurin in individual samples. [46]

1.1.2.3 Microfluidics

The past decade has seen the rapid development of microfluidics in antimicrobial susceptibility assays. [45, 47, 48] Two essential elements in microfluidic systems are channels or reservoirs of various geometries of micrometer scale and the fluids flowing or preserved inside channels. Microfluidic systems provide microchamber arrays that are capable of separating and culturing bacteria. Soft lithography with materials such as PDMS, hydrogel or plastic are widely used to fabricate microfluidics. Dekker et al. reported a high throughput device made of PDMS that contains 10^5 reservoirs in defined shapes to culture bacteria and investigated the oscillation patterns of Min proteins in *E. coli*. (Figure 4a) [43] Lewis et al. used a device called 'isolation chip', which enables culture of microbes from soil in millimeter-sized separated spaces, to discover a new antibiotic termed teixobactin, without observing resistant mutant of *S. aureus* or *M. tuberculosis*. (Figure 4b) [49] As a benefit of booming developments in microengineering and manufacturing, antibacterial screenings can be miniaturized with various microfluidic platforms, leading to small working volumes (nano to picolitres) and small amount of reagents required in screening. [50] However, to increase the throughput of antibiotic screening using microfluidics is still challenging.

As a promising option, droplet microfluidics is one fascinating subset of microfluidics. [51] In droplet microfluidics, two immiscible phases including one continuous phase, which carries droplets, and one dispersed phase, which forms droplets, are required. Passive droplet generation strategies such as cross-flowing droplet formation, flow focusing droplet formation and co-flowing droplet formation are widely applied due to their simplicity. [52] The size of droplets depends on the

flow rate ratio of the two phases, interfacial tension between two phases, and the geometry of channels. [53] Owing to the rapid droplet generation, droplet microfluidics has been used in HTS of antibiotic resistance studies. [53] Smith et al. reported a microfluidic-based pico droplet platform to create picoliter droplets of bacteria suspension with antibiotics and use measurement of optical density to select resistant strains. This high throughput assessment enables isolation of antibiotic-resistant bacteria, for example strain HS 151 of *E. coli* in a label-free manner (Figure 4a). [45] Garstecki et al. applied a multi-channel microfluidic to prepare hundreds of droplets containing bacteria and antibiotics over a range of concentrations precisely in minutes. Therefore, rapid screening of toxicity of combinations of antibiotics and epistatic interactions between antibiotics can be achieved (Figure 4b). [46] Even though droplet microfluidics enable miniaturization of rapid antibacterial screening, further effort should be taken to enhance its capability to screen large libraries of potential antimicrobial reagents. [50]

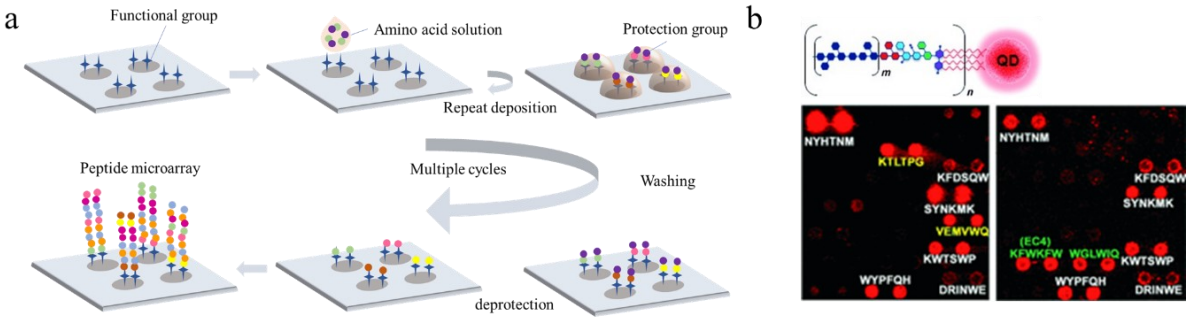

Figure 5. Peptide arrays in antibacterial screening. (a) Schematic illustration of fabrication of peptide arrays through the SPOT method. (b) Up: Schematic illustration of quantum dots-labeled lipopolysaccharides (LPS). Bottom: fluorescence images of LPS binding patterns on the peptide arrays incubated with LPS of: left) *P. aeruginosa* 10 and right) *E. coli* O111:B4. [54]

1.1.2.4 Peptide Array

Antimicrobial peptides (AMPs) produced by immune systems of almost all classes of life emerged as a promising class of antibiotics. AMPs are well known for their broad-spectrum capability against even multi-drug resistant bacteria including the

'ESKAPE'. [55] A peptide microarray refers to a collection of various amino acid sequences arranged in a spot array format on a solid substrate. Since a large number of different peptides are covalently bound to substrates in spots of relative small size, peptide arrays facilitate miniaturized screening of bioactivities of various peptides. [56]

Most manufacturing of peptide microarray is based on the principle of solid-phase synthesis of peptides developed in the 1960s by R. B. Merrifield. [57] In various manufacturing strategies, the SPOT-synthesis became commercialized and widely used due to its flexibility and reliability.[58] Small droplets containing amino acid derivatives are printed on a functionalized porous cellulose membrane in predefined pattern. Thereafter droplets are absorbed by the membrane and form circular spots, which serve as individual reactors. Then amino acid derivatives in respective droplets react with functionalized substrates by activating their C-terminus while protecting their N-terminus. Washing step can be easily applied to remove unreacted amino acids and by-products. Next, the α-amino groups of immobilized amino acids are deprotected, and the washing step is carried out again. By repeating the steps of deprotecting, reacting, and washing, peptides of desired sequences can be ensured (Figure 5a). However, there are still drawbacks of SPOT-synthesis. [59] For example, the spot size achieved in most cases is 1.0 mm in diameter, leading to a limited peptide density on substrates (approximately 25 spots/cm^2). The peptide spot is further miniaturized to increase peptide density by the particle-based synthesis (775 spots/cm^2) and lithographic method (10^6 spots/cm^2). [60, 61] The lithographic synthesis uses light to remove photo-sensitive protecting groups from tethered peptides at selected positions with photomasks. The particle-based synthesis applied a laser printer to dispense microparticles embedded with different amino acid derivatives on array substrates. Recently, further improvement of fabrication of peptide arrays have been made. For example, a combinatorial LIFT method and stochastic peptide microarrays have been reported by Nesterov-Mueller et al. [62, 63]

Benefiting from developments of techniques of peptide array fabrication, the produced libraries have been used to screen novel AMPs. Svarovsky et al. used a peptide array consisting of only 10,000 random sequences to screen bacterial lipopolysaccharides (LPS) and investigated the binding patterns of peptides and bacteria (Figure 5b). [54, 56] Arya et al. have synthesized a library containing 215 peptidic-aminosugars by solid phase synthesizing. The antibacterial effects and binding affinities to bacterial 16S ribosomal A-site RNA of the synthesized peptidic-aminosugars have been screened to find potential aminoglycoside antibiotics. [64] In another study, a new peptide named IDR-2009 (KWRLLIRWRIQK-NH_2) was discovered to possess enhanced antibiofilm activity against MRSA and *P. aeruginosa* based on SPOT strategy. [65]

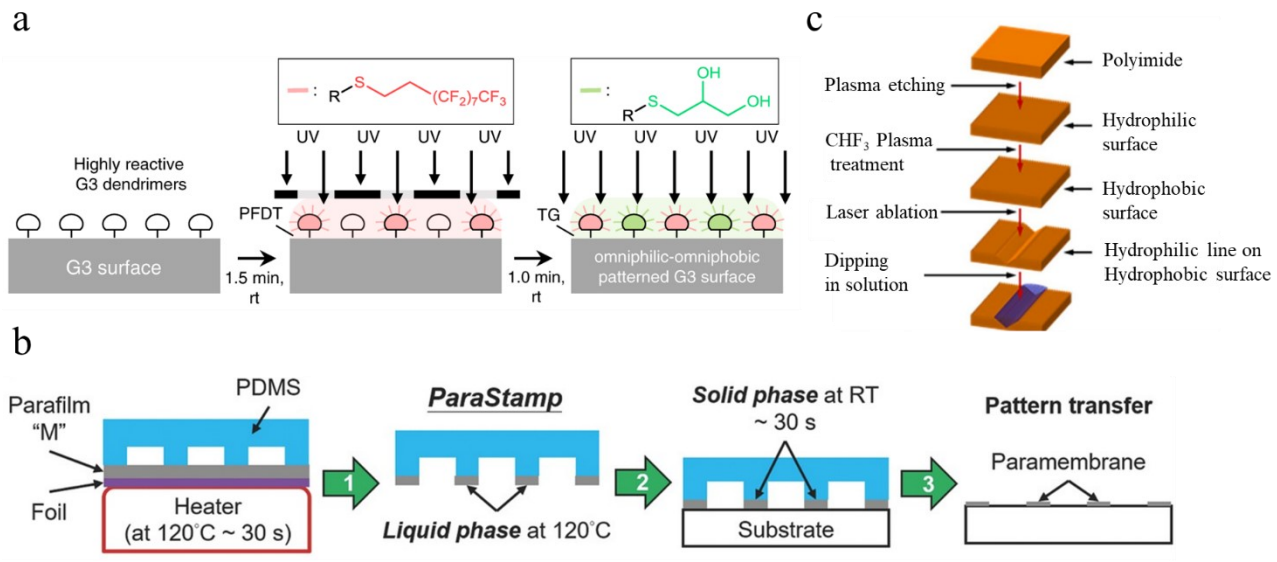

Figure 6. Examples of fabrication of patterned hydrophobic surfaces. (a) method: photolithography. [66] (b) method: soft-lithography. [67] (c) Method: laser ablation. [68]

1.1.2.5 Droplet Microarray (DMA) Platform

Since the first bio-microarray was developed by Langer et al., [69] 2D droplet microarrays have emerged as a versatile platform in cell-based HTS such as screening of single cells and 3D cell structures. [69-74] As an alternative of microtiter plates, droplet microarrays use chemical property of the flat surface instead of physical walls

to arrange a large number of droplets on solid substrates, in that case parallel reactions are confined to individual droplets to enable HTS. [71] Volume of droplets can be as low as 3 nL. [75] Owning to the open system, droplet microarrays eases the transferring of drug libraries in its system comparing to microfluidic systems.

Small volume of droplets on surfaces can be created by several methods including contact/non-contact dispensing, dip-pen nanolithography, and liquid deposition using patterned hydrophilic/hydrophobic surfaces. [76] In order to screen drug libraries with droplet microarray, combination of functionalized surfaces such as patterned hydrophobic surfaces and liquid dispensers is usually required. The differences of wettability of patterned hydrophobic surfaces enables formation of droplets by sliding or dragging a bulk droplet over the surface. Meanwhile test compounds can be added into droplets with liquid dispensers. [76]

Patterned hydrophobic surfaces can be achieved using photolithography, soft lithography, surface etching, etc. as shown in Figure 6. [74] In photolithography, a photomask is applied to allow or block light to control the reaction region. Therefore, a substrate patterned with hydrophilic or hydrophobic functional groups can be fabricated. Recently, our research group has developed the fabrication of droplet microarrays based on photolithography and demonstrated applications of droplet microarrays in biology assays.[77, 78] In order to prepare patterned hydrophobic surfaces, dendrimeric surface or porous polymer films (poly(2-hydroxyethyl methacrylate-co-ethylene dimethacrylate), HEMA-co-EDMA) modified with high-density alkene groups were applied as substrates, while hydrophilic molecule such as cysteamine hydrochloride or 1-thioglycerol and hydrophobic molecule 1*H*, 1*H*, 2*H*, 2*H*-perfluorodecanethiol (PFDT) are spatially functionalized to substrates via sequential UV-induced thiol-yne click reaction. [66, 79] In soft-lithography, PDMS with specific geometrical features is usually applied as templates to endow surfaces with hydrophilic/hydrophobic pattern. [80, 81] For example, Lee et al. used a PDMS master with micropatterns to stamp liquid phase paraffin on glasses, in order to prepare a patterned hydrophobic surface for further cell patterning and drug screening

applications. [67] Negative microcontact printing method using PDMS is demonstrated as well, which generates hydrophilic polydopamine (PDA) arrays on hydrophobic perfluorinated surfaces. [82] Surface treatments such as UV illumination, oxygen plasma treatment and laser ablation are widespread approaches to create patterned hydrophobic surfaces. For example, Dittrich et al. fabricated a microarray containing 2780 hydrophilic spots (720 µm center-to-center distance) surrounded by hydrophobic regions through laser ablation on a polysilazane-coated glass slide. A nanoscale liquid chromatography (nano-LC) was applied to separate a proteolytic digest and spotted the eluate on the prepared microarrays to screen protein phosphorylation. [83]

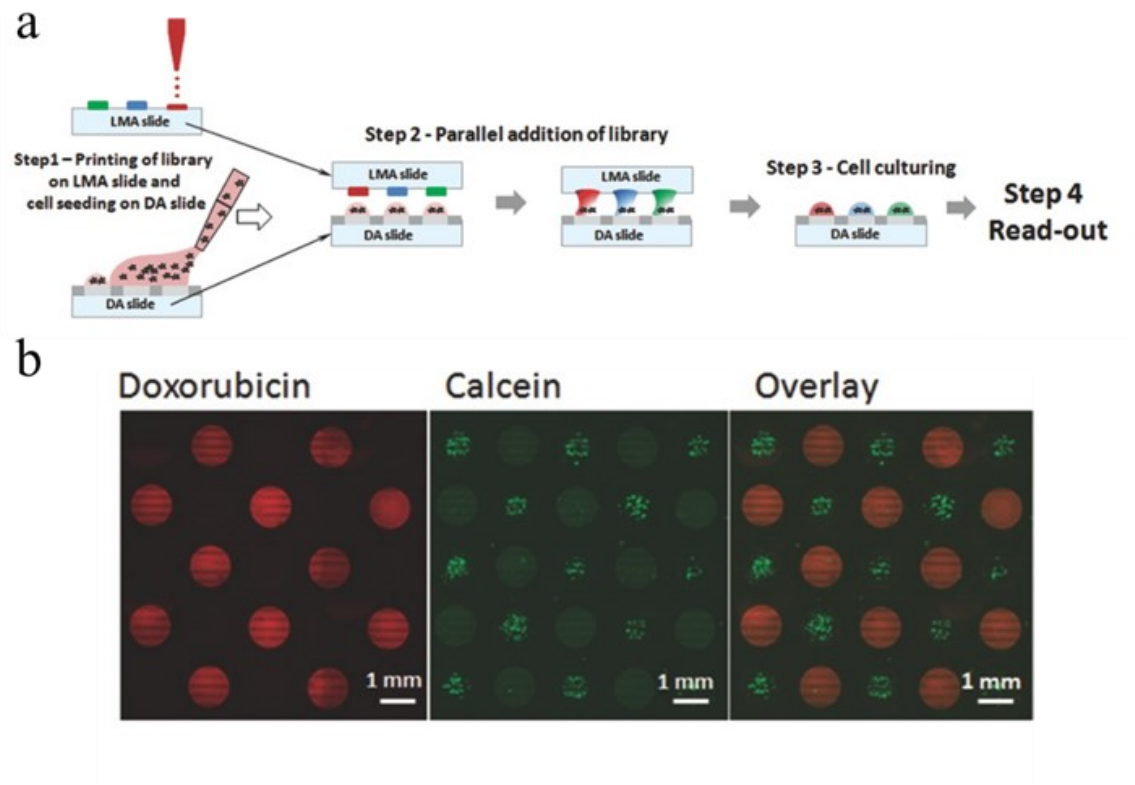

Figure 7. DMA in cell-based screening. (a) Schematic illustration of a workflow of cell-based screening using DMA and a sandwiching method. (b) Fluorescence images of HeLa cells on DMA slides after a treatment with doxorubicin. Left: Samples treated with doxorubicin in droplets showing red fluorescence. Middle: HeLa cells stained with calcein on the same DMA slide. Right: The overlay image. [77]

Our group has developed a sandwiching method to add libraries of testing drugs into droplets on DMA as shown in Figure 7. [77] With optimizing the DMA platform and HTS working line, DMA possesses great potential as a platform in multidrug-resistant (MDR) tests and HTS of antimicrobial compounds. Wang et al. applied a non-contact printer to create a lectin-hydrogel array affiniting bacteria, then 4 antibiotics were delivered to hydrogel spots. The inhibition efficiency of antibiotics to *S. aureus* was detected. [84] However, DMA as a miniaturization platform for antibacterial screening with compound libraries has not been investigated in detail by now.

1.1.3 Summary and Perspectives

Here, different platforms that have been exploited to conduct antibacterial screening are summarized. Currently, agar plates and microtiter plates are still the most widely used platforms due to their simplicity and compatibility to analytical laboratory techniques. As robust methodologies, the two platforms are applied to develop standards of drug sensitivity tests such as MIC tests and inhibition zone tests.

In order to reduce the consumption of reagents, miniaturization of antibacterial screening systems has been an increasing interest in recent years. A typical approach is to increase the density of microplates. By this manner the testing volume down to a few nanoliter can be achieved. Strategies based on microfluidic systems have been developed to screen antibacterial agents or drug-resistant mutants. Small droplets can be rapidly achieved using microfluidics. Nevertheless, there is still a great challenge to screen compound libraries with microfluidics, since automation of library addition into droplets is required. As an open system, peptide array has the advantage to combine synthesis of potential antimicrobial peptides and antibacterial screening on one surface. Mature techniques such as the SPOT method enable manufacturing of peptide libraries to investigate antibacterial effects of diverse sequences of amino acids.

Sessile droplets have been reported as an alternative to microwell plates. Working with droplets possesses the following advantages: (1) cost savings due to lower consumption of reagents and consumables used in small volumes; (2) eliminations of automation in laboratories; (3) improvement of limitations present in microplates, such as mixing and liquid adhesion. It is now well established that droplet microarray can be used in screening of eukaryotic cells even to form 3D cell spheroids. However, few studies have investigated applications of droplet microarray in drug sensitivity tests of bacteria. To adapt DMA to HTS of antibacterial compounds, the following issues should be considered including (1) the effect of small volume and high surface-to-volume ratio on bacteria growth in droplets; (2) the combination of compound libraries and droplets; (3) access of droplets for downstream analysis with existing techniques in microbiology. With clarification of these key points, DMA can contribute to the rapid discovery of agents combating multidrug-resistant bacteria.

1.2 Patterned Biofilms

1.2.1 Biofilms

As opposed to the planktonic state, bacteria in nature and industrial environments tend to adhere to surfaces of both synthetic and biological origin. Once bacteria adhere to surfaces and settle down, they will secrete extracellular polymeric substances (EPS) composed of polysaccharides, extracellular DNA, proteins, etc. Therefore, the living form of bacteria is changed from free living state to sessile communities (Figure 8). The adhered bacteria embedded in EPS are defined as biofilms, where EPS functions as 'glue' to maintain biofilms and possess other functions, for example, to protect bacteria from harsh environments. [85] Bacteria are different in many ways compared to planktonic ones such as metabolic activity, growth rate, transcriptions, and translations. [86] Bacteria in biofilms present 10-1000 times more antibiotic resistance than planktonic bacteria. In addition to the resistance mechanisms of planktonic bacteria such as target site alteration, efflux pumps, drug modifying enzymes, low cell wall permeability, resistance mechanisms of biofilms also include transferring of horizontal resistance genes, impeded penetration of antibiotics, emergence of slowly growing subpopulations such as persisters and viable but nonculturable (VBNC) bacteria. [86] Therefore, biofilms are extremely difficult to eradicate completely.

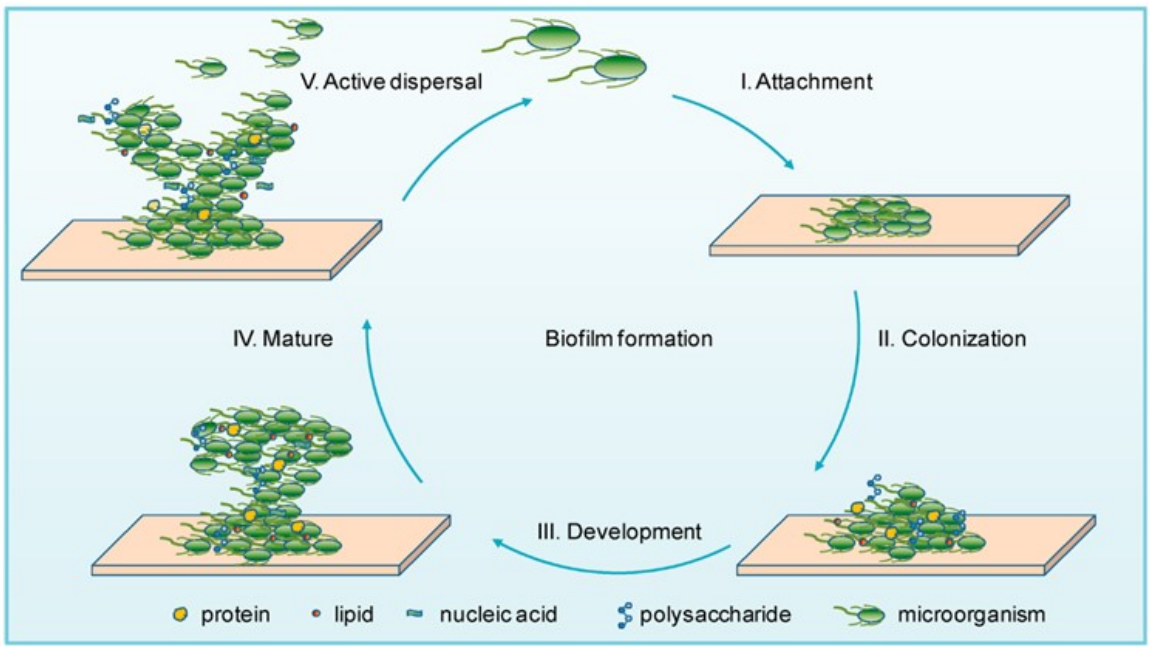

Figure 8. Schematic illustration of biofilm formation. [87]

It has been reported by the National Institute of Health (NIH) that biofilms are involved in approximately 80% of all microbial infections in the human body. There are in general two types of infections caused by biofilms. One is that biofilms form on surfaces of medical implant devices such as catheters, artificial heart valves, contact lenses, joint prosthesis, dental unit, etc. The dispersed bacteria from mature biofilms on those surfaces have a chance to cause urinary tract and bloodstream infections. [88] Typical treatment for biofilm associated infections on devices is surgical replacement of the contaminated device, which leads to financial loss and secondary injury to patients. Biofilms in host tissues often cause chronic infections, such as chronic lung infections, chronic prostatitis, chronic otitis media, chronic wounds, etc. [89]

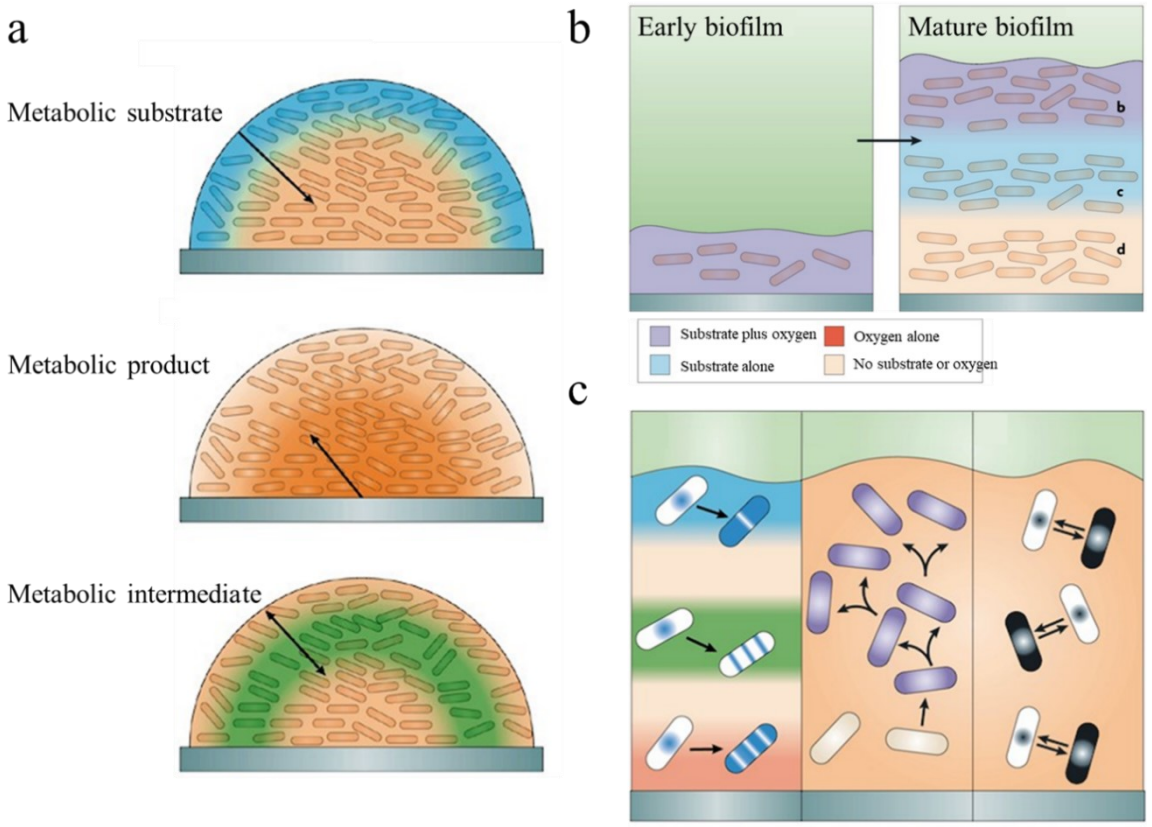

Figure 9. Heterogeneity within biofilms. (a) Chemical gradient in biofilms. (b) Physiological environment in early and mature biofilms. (c) Phenotypic diversification in biofilms. Left: Adaption to the physiological environment of bacteria. Middle: Mutations. Right: Stochastic gene switching. [90]

A major feature of biofilms is their biological heterogeneity, which means that bacteria of diverse phenotypes and genotypes coexist within a biofilm. Different from a nascent biofilm, where all cells inside are capable of obtaining substrate and oxygen due to rapid diffusive transport, mature biofilms possess chemical gradients inside. For example, cells in the upper layer of biofilms often respire oxygen actively, while the interior bacteria have no access to oxygen. [90] With increased depth into biofilms, the concentration of nutrients decreases, while the concentration of metabolic products of bacteria rises. For example, in biofilms of methanogenic bacteria, the methane concentration at the surface is only 10% of that measured in deep biofilms. [91]

To adapt to diverse chemical environments in mature biofilms, even in a single-species biofilm, bacteria could present at least three different states. Cells located at the interface of biofilm and fluid have access to both nutrients and oxygen, leading to aerobic metabolism and often rapid growth. Deeper in the area where oxygen is depleted, cells grow by aerobic metabolism. In the zone where both oxygen and nutrients are depleted, cells become inactive. There are more factors that contribute to the physiological heterogeneity such as different electron acceptors and donors and diverse metabolic capabilities of bacteria. [90] In mixed-species biofilms, there is a possibility for bacteria to distribute according to their species and chemical micro-niches, due to the capability of bacteria to sense and adapt to the environment. When bacteria confront anaerobiosis, starvation, pH alteration, oxidative stress, and antimicrobial treatments, the expression of corresponding gene will be finely regulated. Therefore, the adaptation of bacteria to diverse chemical environments contributes to physiological and biological heterogeneity in biofilms.

Genetic variation and stochastic gene expression result in genetic heterogeneity in biofilms. Genetic variation caused by mutation and recombination enables emergence of variant subpopulations. For example, Molin et al. reported mutations in the wapH homologue, which is associated with lipopolysaccharide biosynthesis, leads to a rapid evolution and better adaptability of *Pseudomonas putida* in a mixed biofilms with *Acinetobacter sp.* [92] In mixed-species biofilms, horizontal gene transfer between bacteria can be achieved by transformation, transduction or conjugation. The easy spread and share of resistance genes through horizontal gene transfer is one of the mechanisms that biofilms present high antibiotic resistance. Stochastic gene expression enables diverse phenotypes of bacteria in biofilms, which does not depend on the local environment. For example, Baty et al. demonstrated that even under identical chemical environments, the expression level of a chitinase gene (chiA) in a *Pseudoalteromonas* species is different. [90, 93]

Hence, biofilms are highly heterogeneous at micrometer scale. Such heterogeneity brings challenges to investigate changes of fine structures in biofilms cultured in bulk,

such as biofilms on agar or in flasks. However, the delicate structure is critical to understand the structure-function relationship in biofilms. In addition, the heterogeneity of biofilms reduces reproducibility of biofilm-involved experiments in different laboratories, which leads to different experiment results in different conditions. Therefore, techniques enabling spatial control of biofilms are urgent to help make progress in understanding of the process of biofilm formation and spreading. [94]

1.2.2 Strategies to Form Biofilm Patterns

To control the biofilms spatially with high resolution is important to investigate the heterogeneity, architecture, functions, and collective phenomenon of biofilms on the micrometer scale. Therefore, reliable approaches to create biofilm patterns are needed. Formation of biofilms comprises five steps including reversible attachment, irreversible attachment, formation of micro-colonies, maturation, and dispersion. [95] During the initial attachment, bacteria overcome long-range repulsive forces and motion close to surfaces, meanwhile bacteria can still be easily removed from the surface by the shear force of fluid. In this process, surface property such as topography, roughness, charge, hydrophobicity, stiffness, etc. influence the attachment. [96-99] Therefore, strategies including using surfaces with various property to promote/inhibit bacteria attachment, different printing approaches to locate bacteria on preset regions on surfaces and combination of techniques from optics and genetics to enable light-controlled attachment of bacteria have been developed. [100]

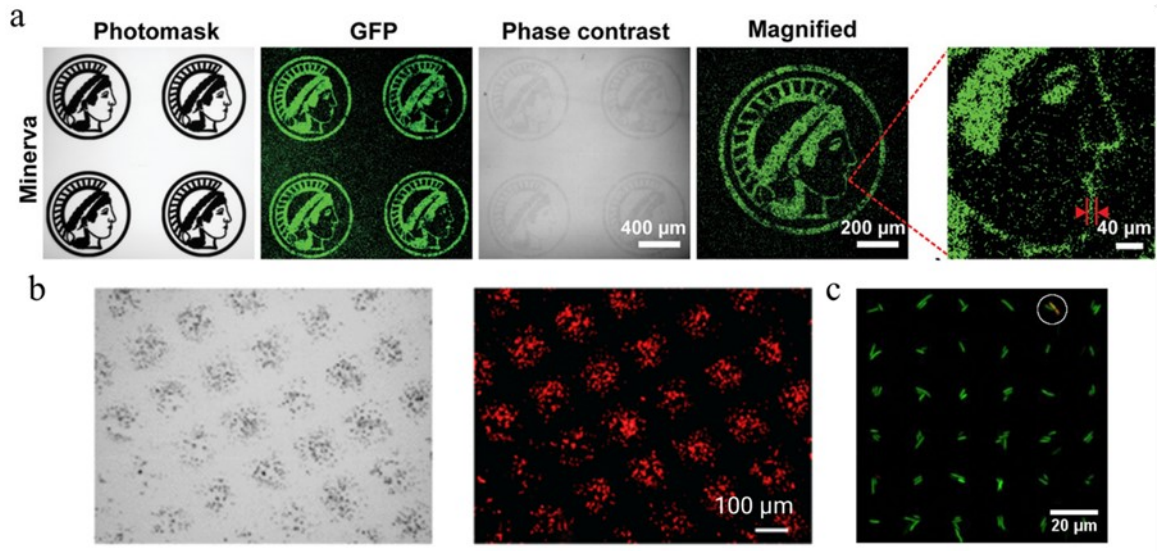

Figure 10. Microscope images of patterned bacteria on chemically modified surfaces. (a) PEG-coated glass surfaces were modified α-D-mannoside, a bacteria adhesin, through a photocleavable 2-nitrobenzyl linker. UV light was used to remove α-D-mannoside to expose non-adhesive area to *E. coli*. [101] (b) Engineered *E. coli* expressing pMag proteins on their surface adhered to nMag protein modified surfaces under blue light. The bacteria were labeled with mCherry for imaging. [102] (c) *Pseudomonas putida* immobilized on polydopamine microarrays on a PEG coated glass surface. [103]

1.2.2.1 Surface Guided Patterning

By using patterned surfaces containing both bacteria-repellent regions and bacteria-adhesive regions, spatially controlled attachment of bacteria can be obtained. Bacterial adhesins such as antibodies and poly-L-lysine have been employed to attract bacteria, while PEG has been used to shelter bacteria. [102, 104-106] For example, Wegner et al. applied photolithography to construct α-D-mannoside modified areas on non-fouling PEG coatings. Due to the recognition of α-D-mannoside by FimH receptor locating on surfaces of *E. coli*, bacteria were patterned with a resolution down to 10 μm (Figure 10a). [101] With photolithography method, Feringa et al. used UV light to cleave fluoroquinolone antibiotic from agar surfaces and created bacteria-friendly area to form arrays of mixture of *E. coli* and *Micrococcus luteus*.[107] When specific selectivity is not required, simple

modification of surfaces could be applied. Sletmoen et al. created micrometer size polydopamine (PD) patterns on PEG coated glass slides through microcontact printing. It was demonstrated that *Pseudomonas putida* KT2440 attached to strip shape PD regions and constrained to PD arrays after 5 min incubation with bacteria (Figure 10c). [103] Amphiphilic block copolymers have been patterned on polystyrene surfaces via UV crosslinking, leading to increased hydrophilicity of determined regions. Therefore, *S. aureus* was allowed to bind to modified hydrophilic areas with a resolution down to a few micrometers, while bacteria tended to form clusters. [108]

Despite the versatile method by chemical modification of surfaces to form patterned bacteria clusters even single bacteria, it is still hard to persistently resist bacteria over time to mantain the spatially control of distribution of bacteria on surfaces. Inspired by nature, topographical features of surfaces have entered the field of vision of researchers. [109] Wang et al. classified ordered topographies into three groups according to the size of patterns and bacteria. The surfaces with pattern of size smaller than bacteria tend to have bactericidal effect, while surfaces with pattern size comparable to bacteria or larger have potential capabilities to control the attachment of bacteria to surfaces. [100] Aizenberg et al. employed arrays of high-aspect ratio (HAR) polymer posts of nanometer size to culture rod shape *P. aeruginosa*. They found that by adjusting post pitch ((0.9 - 4 μm), bacteria have altered their attachment from lying along the substrate to oriented to the substrate and fit into pitches. Then an array of standing up bacteria could be achieved (Figure 11a). [110] The same research group further reported that *P. aeruginosa* were capable of aggregating from a disordered state into an ordered state on the surface with arrays of orthogonal double-gradient nano-size posts. [109] Leng et al. fabricated honeycomb-like patterns on silicon wafers through deep reactive-ion etching. They found that sphere-shape *S. aureus* are able to spontaneously attach to the edge of the honeycomb-like structure of 10 μm and form arrays. While this phenomenon did not happen with rod shape *E. coli* or with patterns of smaller or larger size (Figure 11b). [111]

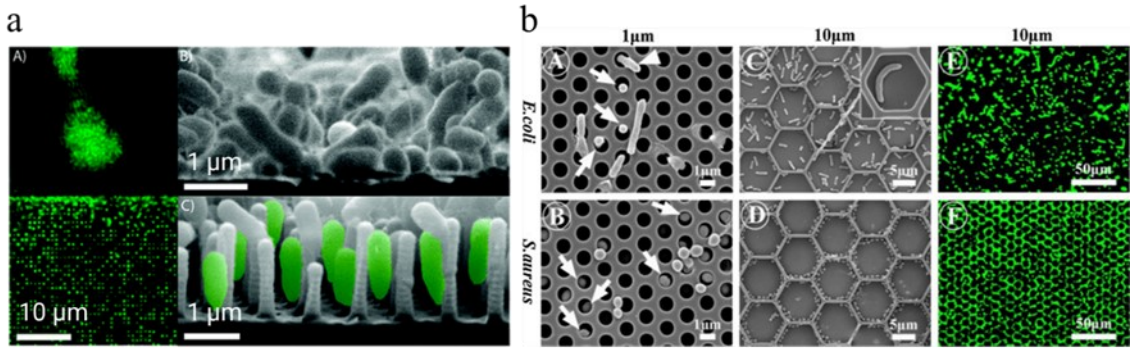

Figure 11. Bacteria pattern on nano- and micro-structured surfaces. (a) Fluorescence and SEM images show that rod-shape *P. aeruginosa* formed patterns on periodic nanostructure arrays of high-aspect ratio polymer posts. [110] (b) Fluorescence and SEM images show that sphere shape *S. aureus* patterned on honeycomb-like structured surfaces of silicon wafers, meanwhile no pattern of rod shape *E. coli* was observed. [111]

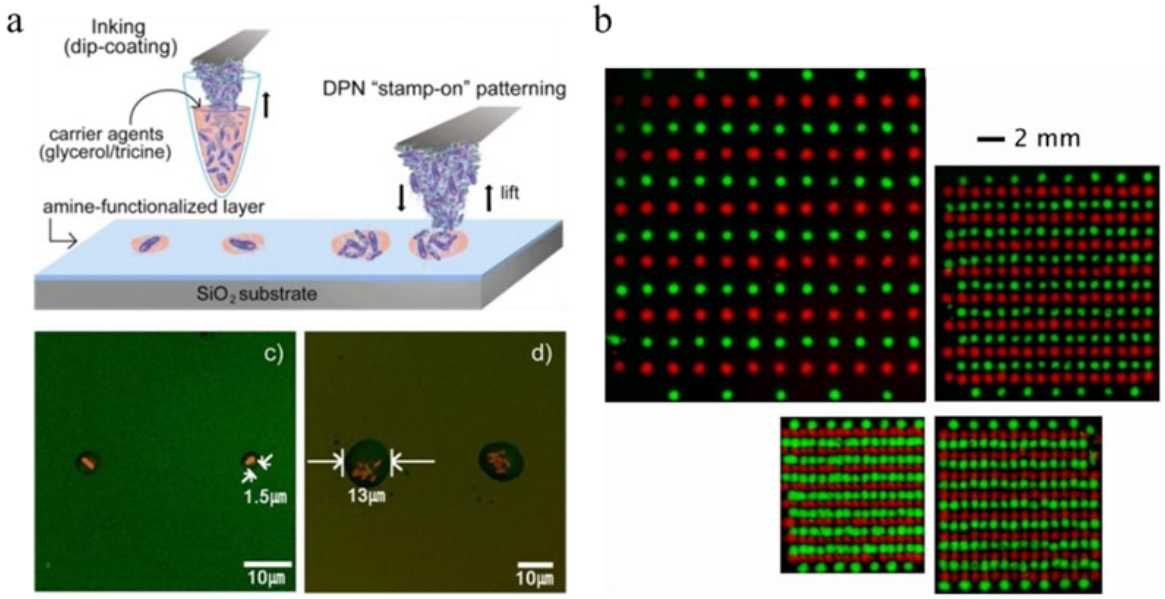

Figure 12. Bacteria patterns on surfaces by direct printing. (a) Up: Schematic illustration of "Stamp-on" dip-pen nanolithography to print bacteria on functionalized substrates. Bottom: Fluorescence images of a pattern of individual *E. coli* printed with bacterial suspension of different bacteria density. [112] (b) Inkjet printers produced colony arrays using *E. coli* strains labeled with red and green fluorescence proteins. [113]

1.2.2.2 Direct Printing

Instead of using chemically or physically modified surfaces to guide bacteria to self-assemble into patterns, a more straightforward approach is to deposit bacteria to predetermined regions, which benefits the control of later biofilm formation. Various printing methods such as microcontact printing (μCP), inkject printing, dip-pen nanolithography and 3D printing have been developed to enable bacteria patterning. [114, 115]

In μCP, a master polydimethylsiloxane (PDMS) stamp with relief pattern is often used to first impregnate with ink, followed by drying process and stamping on substrates to leave ink patterns. By this principle, *E. coli* were printed on agarose substrates as arrays and grew into bulk culture. [116] Whitesides et al. used agarose hydrogel as stamps instead of PDMS to print bacteria. The compatibility and liquid absorbing property of agarose facilitate the inking process. [117] The emergence of inkject-printing based arrangement of bacteria on surfaces overcomes the limitation of μCP to print multiple species bacteria. [113] A commercial ink-jet printer (HP Desktop 550C printer) has been used to print suspension of *E. coli* on agarose surfaces and generate complex patterns. [118] Dip-pen nanolithography, which uses an inked atomic force microscope (AFM) tip to create patterns on a surface, has been employed to generate single bacteria cell arrays on agarose surfaces (Figure 12a). In order to deliver large size ink materials such as bacteria, the tip was coated by nanostructured poly(2-methyl-2-oxazoline) (PMeOx) and combined with glycerol and tricine as carrier inks to keep bacteria from drying and increase the viscosity of the ink. [112]

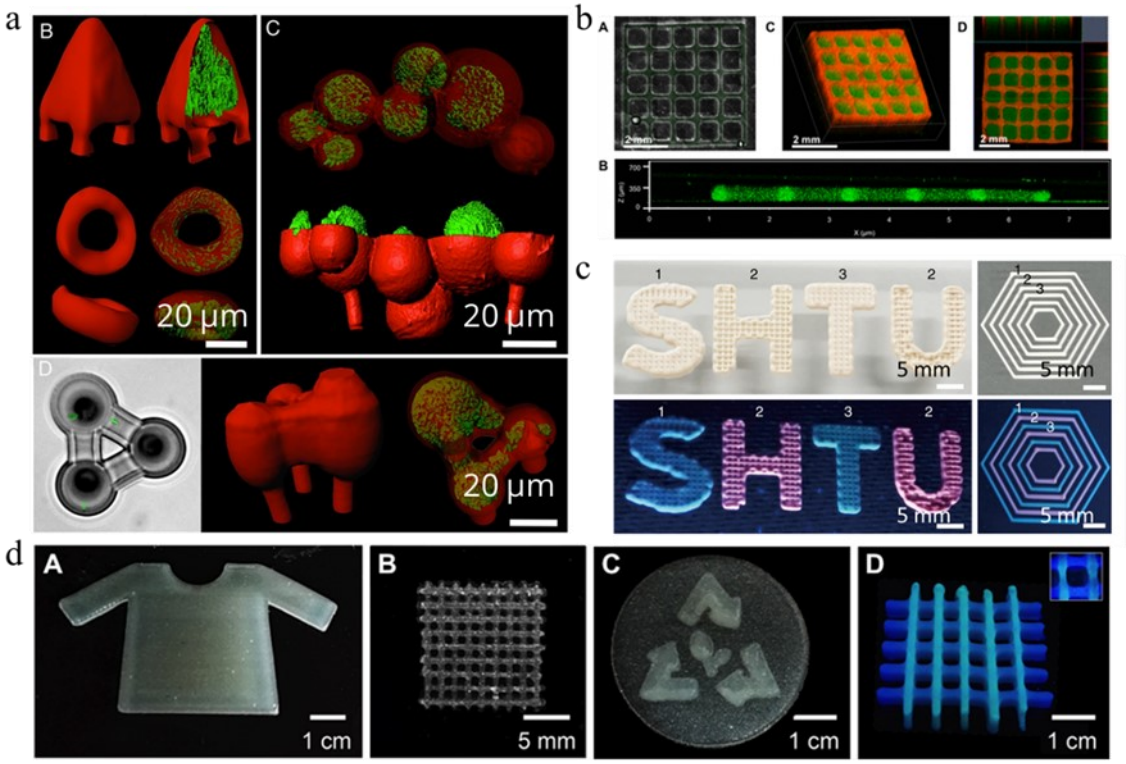

Figure 13. 3D printed bacteria colonies. (a) Multiphoton lithography-based 3D printing of *P. aeruginosa* microcolonies in gelatin gel. [119] (b) Top view and side view of confocal z-stack images of printed *E. coli* expressing GFP (A and B) by PµSL. Confocal z-stacks of printed *E. coli* expressing either GFP or mCherry (C and D). [120] (c) Digital photographs of 3D complex printed biofilms of TasA-HisTag *Bacillus subtilis* and inorganic NPs. Up: normal light. Bottom: under UV light. [121] (d) Different geometries of printed bacteria in Flink hydrogels (A to C). Two species including *B. subtilis* (green) and *P. putida* (blue) were printed into orthogonal lines (D). [122]

Recently, three-dimensional printing (3D printing) of bacteria has become a promising area to control distribution of bacteria and biofilms, which meanwhile provides new perspectives to culture bacteria, investigate interactions in biofilms and use engineered biofilms as live materials (Figure 13). [122-125] In order to obtain 3D bacterial communities, Shear et al. mixed bacteria in a warm solution containing gelatin, bovine serum albumin (BSA) and photosensitizer. Multiphoton lithography (MPL) technique was used to print the prepared gelatin gel into desired shape. By this method, different bacteria populations were able to be assembled in a core-shell

structure, with the viability of bacteria remained. They showed that in the 3D printed complex communities, antibiotic-resistant pathogen *P. aeruginosa* facilitates the survival of *S. aureus* during antibiotic treatments. [119] To provide a feasible and time-saving approach to generate 3D microbial-laden structures, Hynes et al. applied projection microstereolithography (PμSL) to create various 3D geometries containing different species. By printing engineered *Caulobacter crescentus*, which are able to bind lanthanide, into predetermined shapes, they demonstrated that such bacterial structure can be used to adsorpt neodymium and sense uranium in liquid. [120] Mannoor et al. applied a syringe extrusion-based 3D printer (Fab@Home) to successfully print electronic ink containing graphene nanoribbons (GNRs) and another bio-ink containing cyanobacterial onto pileus of mushrooms and formed intersected patterns. They demonstrated that the 3D printing enables generation of densely packed, anisotropic cyanobacterial cells on mushrooms to realize synergic operation. The photosynthesis of cyanobacterial could generate photocurrent transferred through GNRS as a power supply. [126] The research group of Anne S. Meyer has developed 3D biofilm printing not only with commercially available extrusion based 3D printers but also with printers assembled with K'NEX parts, a modular toy construction system. The printed *E. coli* were able to express a curli fiber protein, CsgA, to allow the formation of biofilms in later incubation after the printing process. [127, 128] With the same extrusion-based printing method, biofilms of *Bacillus subtilis* were directly used as ink to achieve 3D geometries showing self-regeneration capacity, engineerable viscoelastic properties and templated assembly of inorganic nanoparticles via engineering of biofilms with variants of *Bacillus subtilis* TasA amyloid machinery. [121]

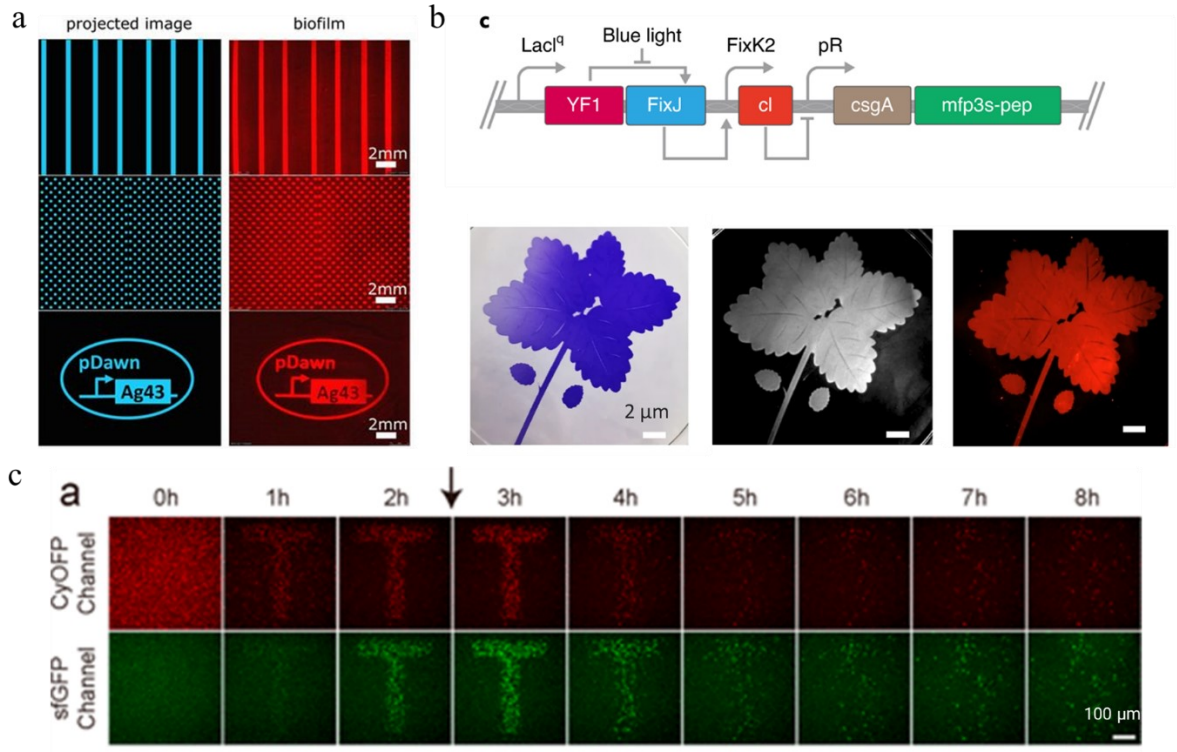

Figure 14. Bacteria patterns on surfaces generated by optogenetic methods. (a) Fluorescence images of *E. coli* patterns. In *E. coli*, a light-activated transcriptional promoter (pDawn) was inserted upstream of the gene of an adhesin, Ag43. Control of attachment of *E. coli* was achieved with projected blue light. [129] (b) Up: Schematic illustration showing that biofilms can be functionalized by fusing sequences encoding the CsgA protein and Mfp3S-pep, which promote bacteria attachment to surfaces and biofilm formation. Both genes are located downstream of the light-sensitive pDawn transcriptional promoter. Bottom: Patterned biofilms stained with crystal violet (left); bright field image showing mineralized composite (middle); bacteria in patterned biofilms showing induced fluorescence, indicating the bacteria were still alive. [130] (c) Fluorescent images showing the formation and disappearance of T shape biofilm patterns regulated by two lights. The level of c-di-GMP, which promotes biofilm formation, was regulated by near-infrared light and blue light. [131]

1.2.2.3 Optogenetic Methods

By gene manipulation, biofilm formation can be spatially and temporally controlled by light illumination. Riedel-Kruse et al. inserted the ribosomal binding site and the coding sequence of Ag43, a cell membrane protein promoting bacteria-surfaces interaction, to the downstream of transcriptional elements of pDawn, which are

regulated by blue light. Then *E. coli* transformed with pDawn-Ag43 construction formed biofilms of various patterns on polystyrene surfaces under illumination by a projector. The formed patterned biofilms remained stable in liquid culture medium over three days. [129] In another study, a high resolution of patterned biofilms (approximately 10 μm) was achieved by dual-color illumination of blue and near-infrared light on *P. aeruginosa* to decrease or increase the level of c-di-GMP molecules that are critical to regulate EPS and biofilm formation. [131] As major biofilm protein components, which assemble into amyloid fibers on cell walls of *E. coli*, CsgA have been used to change the live state of *E. coli* from planktonic to biofilms under light by fusing sequences encoding the CsgA protein downstream of the light-sensitive transcriptional control element. This principle has been employed to pattern biofilms of *E. coli* onto various surfaces including textiles, plastic and mica. [132] Zhong et al. used *E. coli* engineered with CsgA–Mfp fusion proteins to have light-inducible biofilms, which promotes the process of hydroxyapatite mineralization. [130] Optogenetic approaches possess many advantages in patterning biofilms such as reversible and temporally control, and access to multifunction of patterned biofilms. Given such advances, one can have a view of a future in which bacteria can be integrated into various materials to enable new applications in fields of bio-sensors, wearable devices, live materials, etc.

1.2.2.4 Other Methods

Approaches to realize biofilm patterning are not limited to the above discussed methods. Xia et al. found that surface waves strongly affect biofilm formation. They applied deterministic waves and stochastic waves to generate different motion of fluid in bacteria suspension. Strong biofilms were observed under the wave antinodes while bacteria only settled but not attached to surfaces under nodal points. Therefore, patterned biofilms were achieved with determined wave patterns. [133] Using micropatterned PDMS with pillars, Mofrad et al. created patterned micro-colonies of *S. aureus*. They first cultured biofilms on top of PDMS micropillars with bacteria not filling between pillars. Then by aspirating liquid, patterned biostrings were achieved

and the pattern could be controlled by the direction of liquid retraction. They demonstrated that both biological activity of bacteria and wetting properties of PDMS contribute to biostring formation. [134] Furthermore, droplet evaporation and meniscus-layer-driven liquid motion were used to control bacteria assembly on surfaces. [135, 136]

1.2.3 Patterned Liquid Infused Surfaces (pLISs)

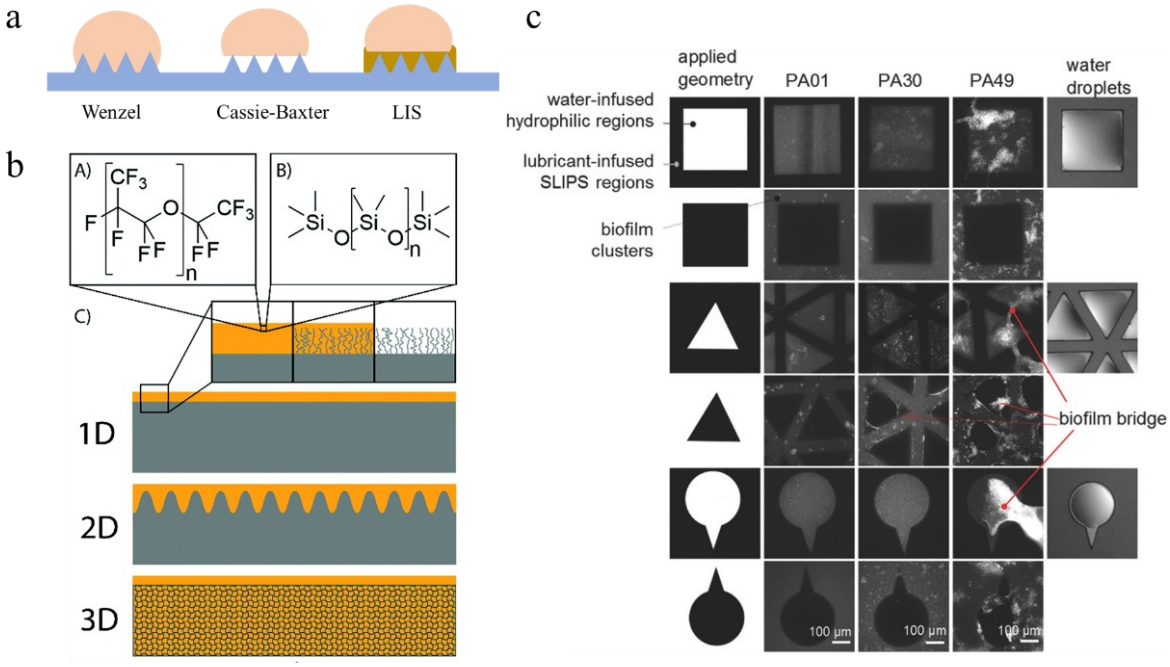

Figure 15. Liquid infused surfaces in biofilm patterning. (a) Three states of water droplets on hydrophobic surfaces. (b) Classification of LISs. [137] (c) Fluorescence images of biofilm patterns of various geometries formed on pLISs and biofilm bridges. [138]

Inspired by Nepenthes pitcher plants, liquid infused surfaces have been well-known for their liquid-repelling property since 2011. [139] The system of LISs usually includes a solid substrate and a class of liquid trapped by the substrate as lubricant. To achieve a stable LIS, three principles should be followed: (i) the chosen lubricant and testing liquid should be immiscible; (ii) the lubricant should spread and wet on the substrate; (iii) the solid substrate should possess higher affinity with the lubricant than with the testing liquid. Due to the liquid-like, defect-free, and hydrophobic

properties of LISs, they have been widely used as anti-adhesive surfaces to cells, bacteria, and biofilms in many applications. [137, 140]

The manufacturing techniques have been described in detail in recent reviews. [137, 141] Neto et al. categorized LISs into three classes including: (i) LISs with lubricants infused within a layer of perfluorinated molecules grafted onto solid substrates, or LISs with covalently attached long-chain molecules to substrates, as they termed 1-dimensional LISs; (ii) LISs with lubricants infused into nano/micro-porous structures by capillary action, as they termed 2-dimensional LISs; (iii) LISs with lubricants infused within 3D molecular networks, as termed 3-dimensional LISs (Figure 15b). [137] The selections of lubricants and substrates depend on the required applications. Lubricants of various molecular weights, vapor pressure, viscosity, refractive indexes are available in fabrication of LISs. [141]

Combination of LISs and patterned surfaces leads to new surface properties and applications. For example, patterned LISs shows discontinues wetting property and have been used for patterning aqueous solutions, cells, and blood samples, and for directing droplets. [142, 143] Recently, Xie et al. used microcontact printing (μCP) to transfer dopamine droplets onto linear poly(dimethylsiloxane) grafted surfaces to allow patterning of polydopamine (PDA) on 1-dimensional LISs. They used the versatile properties of PDA to immobilize biomolecules, grow perovskite microcrystal and quantum dots thin films in patterned regions. [144] Our group applied a patterned 2D LIS with patterned hydrophilic-superhydrophobic porous polymer as substrates and Krytox 103, a fluorinated synthetic oil, as the lubricant to form arrays of biofilms. Geometries of biofilm clusters can be controlled by using predetermined micropatterns. [138] A new structure, termed ‘biofilm bridges’, connecting biofilm clusters has been discovered. Since natural biofilms possess various structures, for example, the string-like structure called ‘streamers’ that benefits the spread of biofilms in environments, this new artificial structure might enhance our understanding of formation and spread of biofilms. Therefore, further efforts should be made to clarify the mechanism of formation of biofilm bridges.

1.2.4 Summary and Perspectives

Biofilms are an important living state of bacteria required to survive in harsh environments. Bacteria in biofilms possess different features compared to planktonic bacteria, such as high tolerance of treatments by antimicrobial agents. Chemical and biological heterogeneity in biofilms hamper understanding of cell signaling in biofilms, mechanisms of biofilm formation, drug resistance of biofilms, etc. Traditional studies of biofilms use bulk culture in microtiter plates or on agar plates, leading to possibilities of overlooking of small-scale interactions among bacteria and undesirable low reproducibility of experiments. The significance of biofilms has motivated numerous studies to develop techniques for spatial control of biofilms. Currently, patterned surfaces, printing methods and optogenetic methods are most widely used approaches to achieve patterned biofilms, with high resolution down to a few micrometers. Patterned biofilms can be achieved both in liquid medium and on agar surfaces.

Despite the progress made in this field, there are still challenges in this research area that need to be overcome. Up to now, far too little attention has been paid to employ the patterned biofilm created in laboratories to study diseases caused by biofilms in clinics. Another challenge is the integration of patterned biofilms with more functions, to realize applications in various fields including environmental monitoring, drug screening, medical diagnosis, and living materials.

2 Work Objectives

i) Droplet-microarray: a miniaturized high throughput screening platform of antimicrobial compounds

Multidrug resistant bacteria have been severe threats to human health globally. Compared to the rapid development of drug resistance of bacteria, the discovery of new antimicrobial compounds is quite slow, leading to a dangerous situation in future that no effective treatments available to infections caused by multiresistant bacteria. [5] Factors that keep antibiotic discovery away from ordinary laboratories and pharmaceutical enterprises include the high cost of compound libraries and high-level requirements of equipment. Therefore, various miniaturized HTS platforms have been exploited by researchers, such as high-density microplates, microfluidics, peptide arrays, etc. [145, 146] However, there are still challenges. For example, automatic equipment is still essential for the screening with microplates. Few studies have been reported that microfluidics were used to screen big compound libraries.

Droplet microarrays (DMA) is a promising miniaturized HTS platform in drug development. [75] Due to the discontinuous wetting property of the patterned superhydrophobic-hydrophilic surfaces of DMA, hundreds of aqueous droplets of nanoliter volume can be formed in seconds by sliding or dragging aqueous liquids across on DMA. In this way, automation of pipetting is not necessary. With about hundreds of reduction of testing volume compared to microplates (DMA: ~ 100 nL per spot, 384-well plates: ~ 40 µL per well), the cost of testing libraries would decrease.

One of the work objectives of this thesis is to apply DMA in HTS of antimicrobial substances. The stated aim has defined the following project objectives:

1. Establishments of culture conditions of bacteria in droplets

The process to generate droplets containing bacteria, growth of bacteria in small volume, viability of bacteria after overnight incubation should be investigated, to ensure the following drug susceptibility tests in droplets.

2. Developments of approaches to transfer library compounds into droplets
   In order to use DMA for large libraries, the delivery of testing chemicals to droplets is a critical step. In this research, two approaches including a sandwiching method and direct dispensing method will be tested. Successful delivery of chemicals into droplets without any contamination is required.
3. Developments of readout methods of inhibition of bacteria proliferation
   Readout methods compatible with HTS and laboratory equipment should be established.
4. Application of DMA to discover novel antimicrobial compounds against multidrug resistant bacteria
   With validation of the DMA-based HTS working line, this platform should be used to identify antimicrobial substances from compound libraries to combat drug-resistant bacteria such as multidrug resistant *P. aeruginosa* and carbapenem resistant *K. pneumoniae*, which are important pathogens involved in infectious diseases.

(ii) Formation of biofilm bridges with controlled geometries on patterned LISs

Biofilms is a major living form of bacteria in nature as well as in medical surroundings including wound- and catheter-related infections or dental plaques. Biological heterogeneity is an important feature of biofilms. This heterogeneity is caused by many factors, such as chemical heterogeneity within biofilms, adaptation of bacteria to environments, mutants and genetic regulations of biofilm bacteria. [90] Very high heterogeneity of biofilm populations is a big hindrance in this research field, as spatial variations in cell behavior, cell density and gene expression often cause low reproducibility of experiments conducted in different laboratories. [138] Fine structures in biofilms are difficult to detect and investigate in bulk culture. Therefore, controlling biofilm formation is essential to study mechanisms of biofilm

formation and spreading. By now, various approaches including patterned surfaces, direct printing and optogenetic methods have been employed to fabricate patterned biofilms.

Recently, a special structure termed ‘biofilm bridges’ has been discovered between biofilm arrays formed on pLISs. However, the mechanism of formation of biofilm bridges has not been demonstrated. Here, the aim of this research is to investigate the fine structure of biofilm bridges on pLIS and reveal the formation process of biofilm bridges. The stated aim has defined the following project objectives:

1. Investigation of ubiquity of biofilm bridges using different Gram-positive and Gram-negative bacteria.
2. Development of staining methods to observe biofilm bridges.
3. Clarification of formation of biofilm bridges.
4. Developments of methods to spatially control biofilm bridges on pLISs.

3 Results and Discussion

3.1 Droplet-microarray for High-Throughput Screening of Antimicrobial Compounds*

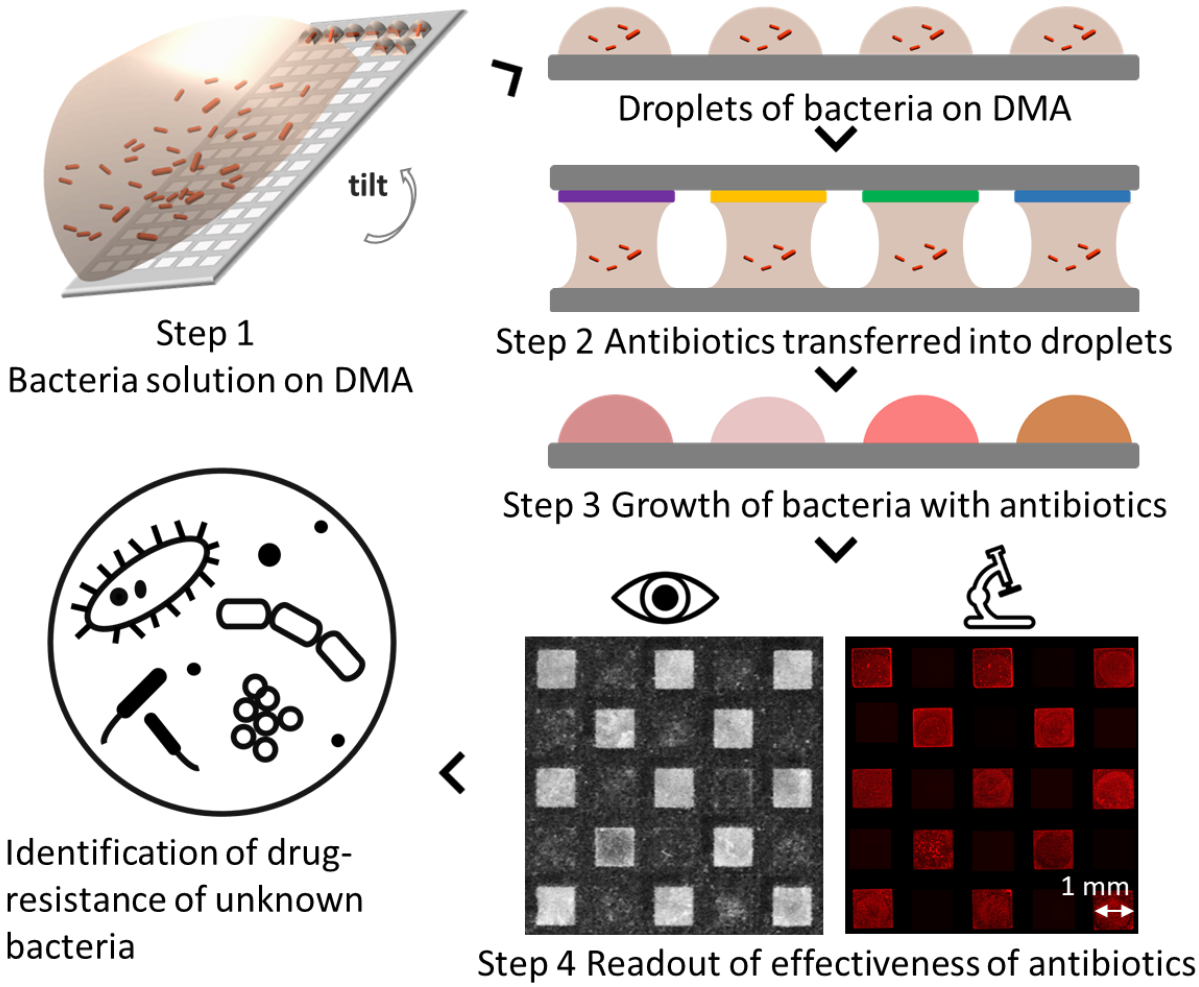

*This chapter and associated sections were published previously:
Lei, W., Demir, K., Overhage, J., Grunze, M., Schwartz, T., & Levkin, P. A. (**2020**). *Advanced Biosystems*, 4(10), 2000073. [1]

3.1.1 Introduction

The increasing incidence of antimicrobial resistance in bacteria and the lack of new antibiotics that can be used to treat drug-resistant bacterial infections has become a major threat to human health worldwide. [147-149] The development of antibiotic resistance among various bacteria belonging to the "ESKAPE" group of human facultative pathogenic bacteria is a particular cause for concern. The ESKAPE group of bacteria comprises *Enterococcus faecium*, *Staphylococcus aureus*, *Klebsiella pneumoniae, Acinetobacter baumannii*, *Pseudomonas aeruginosa,* and *Enterobacter spp*., which are known causes of serious hospital-acquired infections. [148] Several of these clinically relevant bacteria have developed resistance to most currently available antibiotics. [147] It is estimated that during the last decade the direct cost caused by antimicrobial-resistant bacteria is €1.5 billion per year in the EU, Iceland and Norway. [150] Consequently, novel agents that control the growth of these human pathogens are urgently required. [28, 151, 152] Evaluation of the synergistic effects of existing drugs and investigation of the inhibitory activity of numerous naturally occurring compounds against pathogenic bacteria are also regarded as important approaches in the search for novel treatment options.

The currently available high-throughput screening methods based on multi-well microplates are time-consuming and costly, requiring expensive robotics for plate handling and pipetting. [153-158] Furthermore, this type of screening requires relatively large amounts of expensive reagents, and microtiter plates. Most antibiotic resistance analyses are based on defined protocols for routine testing, and the cost of the modifications required to screen newly identified natural compounds and synergistic effects with other compounds are prohibitive for many research and development (R&D) laboratories.

Alternative methods have been developed for specific applications. Choi et al. developed a paper-based array to screen the electricity-producing bacteria. [159] In another study, a growth chip with a porous aluminum oxide layer containing small cavities was used to culture and screen microorganisms. With a cavity size of 7 × 7

µm and up to one million cavities per chip, this method offers the capacity for very high-throughput screening although single cavities cannot be used to assess the effectiveness of antimicrobial substances. [160] Despite the advantages of these alternative techniques, the difficulties associated with production and high cost remain.

Recently, we introduced the droplet-microarray platform (DMA) with precisely separated superhydrophobic and hydrophilic areas. [2, 78, 161, 162] By wetting the DMA with aqueous solutions, we can create an array of small (90 nL), spatially separated droplets. These micro-reservoirs contain sufficient liquid to provide an appropriate environment for the growth of eukaryotic cells and prevent cross contamination, with the additional advantages of ease of handling and few pipetting steps. The DMA platform also facilitates the simultaneous analysis of a library of substances in parallel by sandwiching compound printed glass slides with DMA slides. [77] Thus, the DMA platform represents a simple, rapid, and highly cost-effective method of screening the antibacterial effects of a variety of substances.

Here, we present the DMA platform as a novel and cost-effective technology for performing miniaturized high-throughput screening of bacteria to accelerate the detection of antibiotic-resistant microbes in samples from patients and environments. In this study, we used *Pseudomonas aeruginosa* as a target strain since this opportunistic Gram-negative human facultative pathogenic bacterium is known to cause a plethora of hospital infections, including respiratory, urinary tract, and wound infections. [163, 164] Moreover, this pathogen is well-known for its high intrinsic resistance against a variety of different antibiotics and disinfectants. [165, 166] Therefore, due to the extensive use of antibiotics in hospitals, acquired multidrug-resistance among *P. aeruginosa* is a major concern. [167, 168] Thus, in this study, we validated the DMA screening platform using clinically applied antibiotics to investigate the antibiotic-resistance of the multi-drug resistant *P. aeruginosa* PA49 isolate.

3.1.2 Results and Discussion

Growth of *P. aeruginosa* PAO1 GFP on DMA

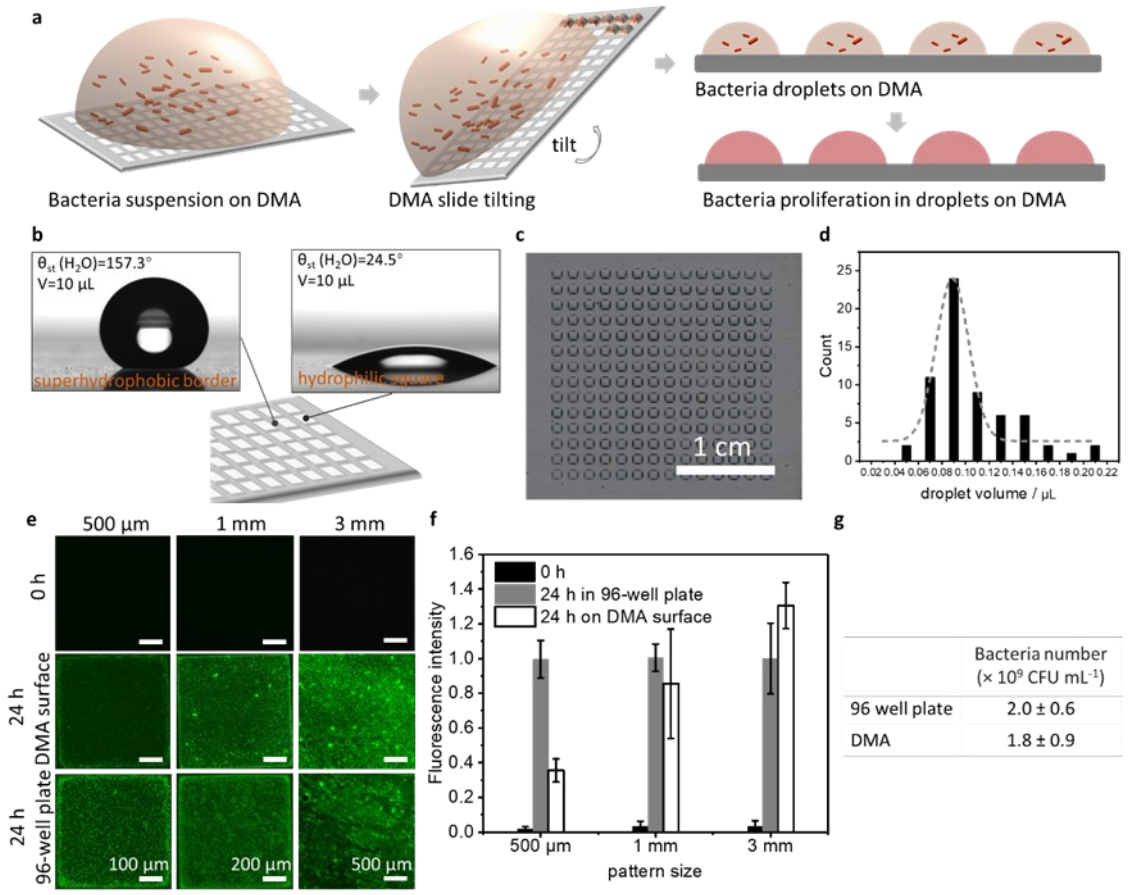

Figure 16. Growth of *P. aeruginosa* PAO1 on a DMA slide. (a) Scheme of bacteria seeding on DMA. (b) Photographs of droplets of water on the hydrophobic border (left) and hydrophilic square (right) of the DMA surface with the corresponding static water contact angle. (c) Digital image of DMA after droplets of BM2 medium formed. (d) Distribution of droplet volume on DMA slides. (e) Fluorescence images of *P. aeruginosa* PAO1 GFP incubated for 24 h on the DMA slide and in a 96-well plate. 500 µm, 1mm, 3mm are the edge lengths of hydrophilic squares. (f) Growth of *P. aeruginosa* PAO1 GFP strain in 96-well plates and on DMA surfaces detected by measuring mean fluorescent intensity per pixel of cultured bacteria. All fluorescence intensity values were normalized against *P. aeruginosa* PAO1 GFP cultured for 24 in 96-well plates. (g) Bacterial density in 96-well plate and on DMA surfaces after incubation for 24 h.

A schematic representation of bacterial seeding and proliferation on DMA slides is shown in Figure 16a. Aqueous solutions applied onto this slide spontaneously form an array of separated microdroplets due to the difference in wettability of the hydrophilic square and the superhydrophobic borders (Figure 16b, Table S1). 1.5 mL of droplet of bacterial suspension was placed onto the superhydrophobic-hydrophilic array for 30 s before the slide was tilted to form microdroplets containing bacteria. Each DMA slide (7.5 × 2.5 cm) contains three microarray pattern compartments containing 196 hydrophilic squares (Figure 16c). With one DMA slide, 588 droplets in one second were formed, where each droplet representing an individual compartment for subsequent antimicrobial testing.

The distributed volume of droplets on DMA slides were evaluated with a pattern size of 1 mm. Figure 16d shows a Gaussian distribution of the droplet volume, with the volumes of more than 80% of the droplets ranging from 70 nL to 130 nL. Based on this information, single droplets of 90 nL were used in the subsequent experiments. The distribution of the radius and height of the droplets were shown in Figure S1.

Firstly, *P. aeruginosa* PAO1 expressing GFP (*P. aeruginosa* PAO1 GFP) was used to evaluate the growth of bacteria after seeding on DMA slides since expression of this protein facilitates direct microscopic monitoring of bacterial persistence or growth. The distribution of initial bacteria number in each droplet after seeding was shown in Figure S2a. There were 109 ± 54 bacteria in each droplet on average. Figure S2b shows that the high humidity in the box could prevent the evaporation of droplets on DMA slides. The mass of droplets on DMA slides placed in air was decreased from 0.066 ± 0.001 g to 0.001±0.001 g in 25 min at room temperature. While the mass of droplets on DMA slides placed in the humidity box was decreased from 0.069 ± 0.003 g to 0.060±0.003 g in 15 min and didn't change much in the next 2 h. The mass change of droplets incubated in the humidity box over 24 h at 37 ℃ was measured as well. It shows that more than 77% of the volume of droplets remained on the DMA after incubation.

To investigate the effect of pattern size on bacterial growth, three hydrophilic square pattern sides were applied to DMA slides. Bacteria on DMA slides with hydrophilic spots of 1 mm and 3 mm showed both bright green fluorescence after incubation for 24 h, which was visually comparable with the fluorescence of bacteria grown in 96-well plates (Figure 16e). Digital images of the bacterial spots were quantified for the fluorescence intensity using Axioplan software ImageJ. Here, the fluorescence intensity of all spots was normalized to the fluorescence intensity of bacteria grown in 96-well plates after 24 h incubation to investigate whether growth of bacteria would be affected in small volume. The fluorescence intensity of bacteria on DMA slides with hydrophilic spots of 0.5 mm was 0.35 ± 0.06 fluorescence units, which was much lower than the fluorescence intensity of the bacteria in 96-well plates. This result suggested that the small volumes of the 0.5 mm hydrophilic spots contained not enough cells of *P. aeruginosa* PAO1 for fluorescence signal evaluation. Therefore, the 1 mm spot patterns were used to form droplets on one DMA slide for further applications, rather than the 3 mm pattern for DMA production. The density of bacteria on the DMA slide was $1.8 \times 10^9 \pm 0.9 \times 10^9$ CFU mL^{-1}, which was close to the density of bacteria ($2.0 \times 10^9 \pm 0.6 \times 10^9$ CFU mL^{-1}) incubated in 96-well plates (Figure 16g, Table S1). Both fluorescence imaging and bacterial density results confirmed that the DMA slides with hydrophilic spots of 1 mm support the persistence and growth of bacteria in individual microdroplets.

DMA as a screening platform

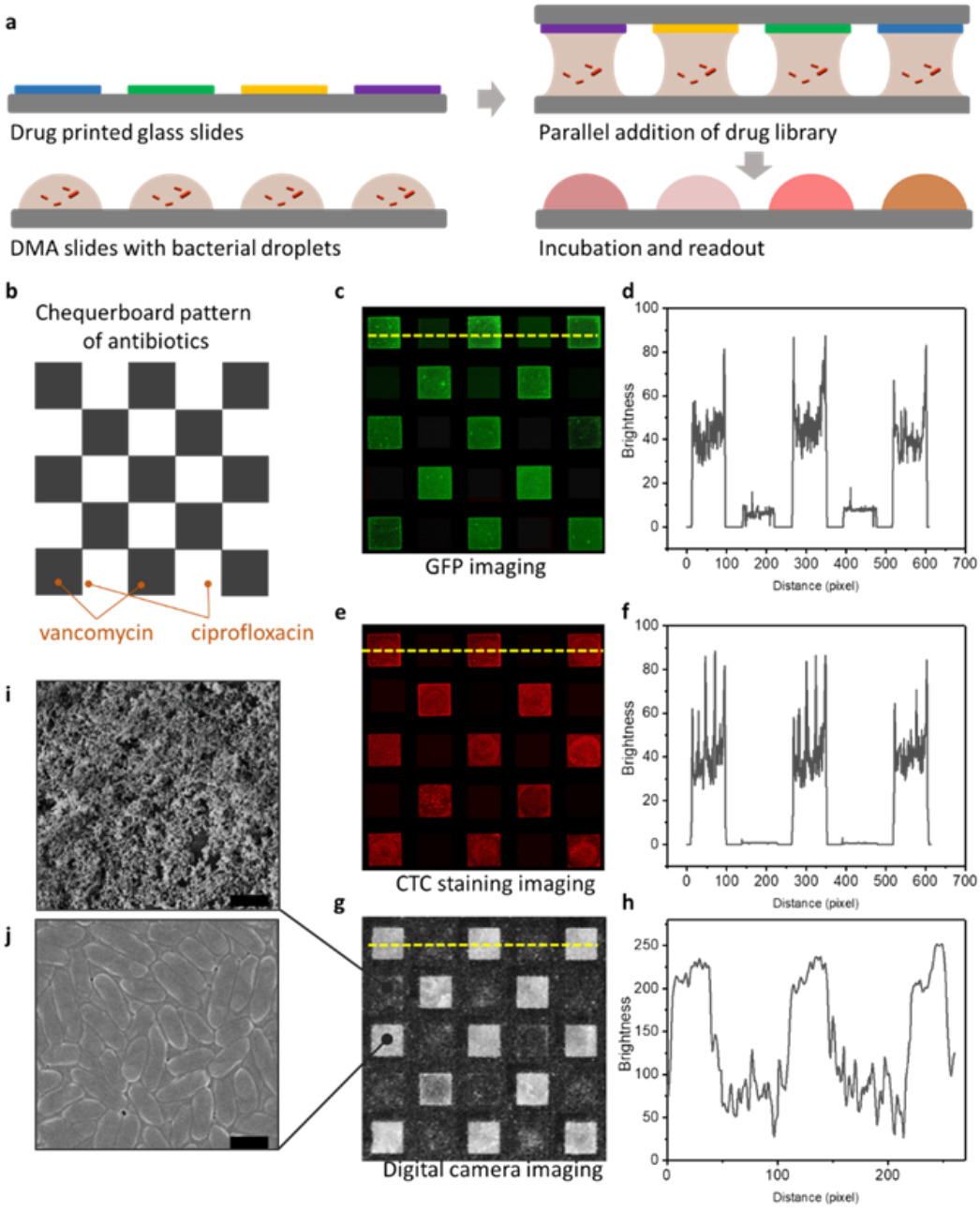

Figure 17. Droplet microarray as a screening platform. (a) Scheme of the sandwiching process for screening antibiotics. (b) Predesigned pattern of printed antibiotics on fluorinated glass slides. (c) Image of green fluorescence of the bacteria on DMA with 25 (5 × 5) spots treated sequentially with vancomycin (13.5 µM) or ciprofloxacin (40 µM). (d) Scan of fluorescence intensity across the yellow line shown in (c). (e) Image of red fluorescence of active bacteria on DMA with 25 (5 × 5) spots treated sequentially with

vancomycin (13.5 µM) or ciprofloxacin (40 µM), and stained with CTC using the sandwiching method. (f) Scan of fluorescence intensity across the yellow line shown in (e). (g) Digital image of DMA surface of the bacteria on DMA with 25 (5 × 5) spots treated sequentially with vancomycin (13.5 µM) or ciprofloxacin (40 µM)). The DMA slide was placed on black color paper. (h) Grayscale scan of the yellow line shown in (g). (i) SEM image of the transparent hydrophilic spots on the DMA surface in (g). (j) SEM image of opaque hydrophilic spots of DMA surface in (g).

Aiming on a single step screening approach, the sandwiching process was evaluated using nano-liter amounts of antibiotics being transferred into individual bacterial droplets. Antibiotics were preprinted onto a fluorinated glass slide with the I-DOT instrument and then accurately placed into contact with the bacterial droplets on DMA slides using the CSC (Figure 17a, 17b, Figure S1). Figure 17c–h shows the results of the test using vancomycin at 13.5 µM (ineffective for inhibition of *P. aeruginosa* PAO1 growth) and ciprofloxacin at 40 µM (effective for inhibition of *P. aeruginosa* PAO1 growth) printed in on the DMA in a chequerboard pattern. Figure 17c confirms the absence of cross-contamination during the sandwiching process between the droplets containing ciprofloxacin (no strong green fluorescence) and the neighboring droplets containing vancomycin (bright green fluorescence). A scan of the fluorescence intensity of each droplet is shown in Figure 17d. Furthermore, we used this sandwiching method to stain the droplets with CTC, which is converted to the red fluorescent molecule CTC-formazan by metabolically active cells. A shown in Figure 17e and 17f, the bacteria showed bright red fluorescence in droplets containing vancomycin, which was not observed in droplets containing ciprofloxacin being directed against the sensitive strain of *P. aeruginosa*. The growth of bacteria can also be visually evaluated, with droplets containing actively dividing bacteria appearing opaque after drying, while the droplets without high density bacteria appear transparent (Figure 17g). We speculate that the difference in transparency is caused by the deposition of living bacteria and as well as the formation of a biofilm on the DMA surface since the printed vancomycin was not able to prevent the multiply of bacteria. Then the layer of bacteria reflects light leading to a brighter,

opaquer surface (Figure 17g). This hypothesis was supported by the SEM images shown in Figure 17i and 17j. A layer of bacteria was observed on the white spots, while there was no such bacterial film on the transparent spots. This visually detectable readout of bacterial growth on DMA surfaces has the advantage over the other approaches that no expensive device is required.

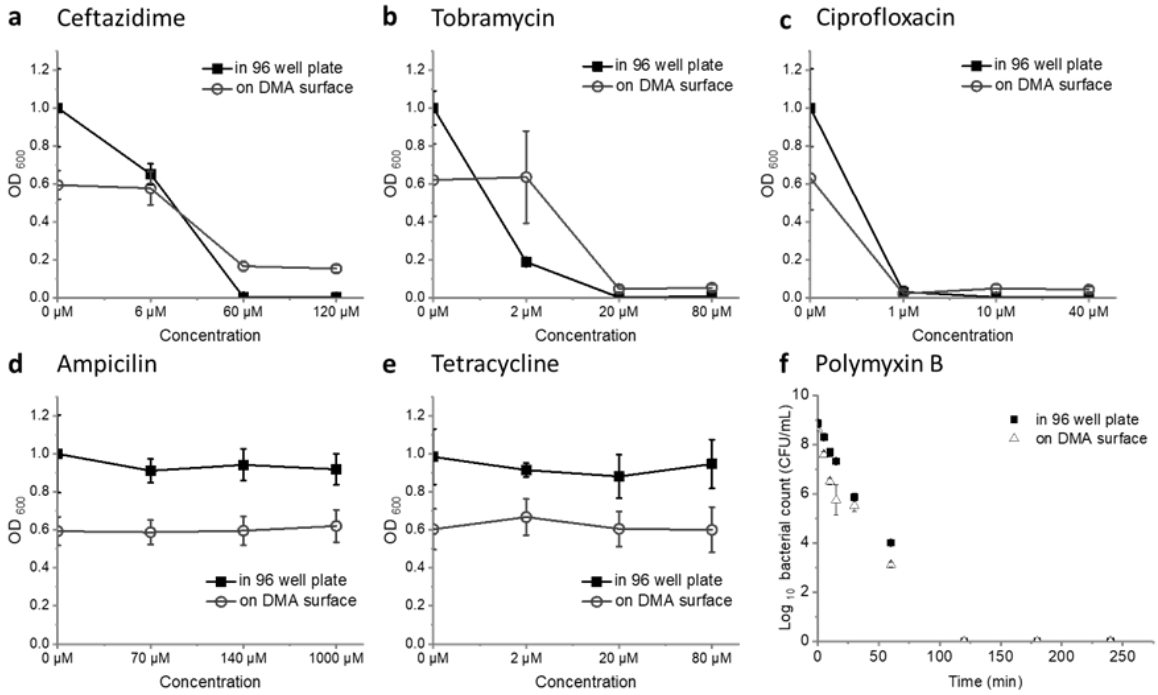

Figure 18. Comparison of 96-well plates with DMA. (a–e) MIC of ciprofloxacin, ceftazidime, tobramycin, ampicillin, and tetracycline for *P. aeruginosa* PAO1 GFP assayed in 96-well plates and on DMA surfaces (DMA slides: readout by fluorescence intensity and the intensities were converted into OD values (Figure S2); 96-well plates: readout by OD measurement). All results were normalized to a blank control (0 µM in 96-well plates). (f) Time-course assay of the antibacterial activity of polymyxin B on *P. aeruginosa* PAO1 on DMA slides.

As an antibiotic screening platform, the DMA should give comparable results to those obtained using a microtiter plate-based method. Hence, the MIC (Minimal Inhibition Concentration) of five antibiotics were investigated with *P. aeruginosa* PAO1 GFP assayed on DMA surfaces and in 96-well plates. The MIC is the lowest concentration of an antimicrobial compounds that is able to inhibit the growth of

bacteria in an overnight assay based on determination of the OD_{600} value. As shown in Figure 18, the MIC values of ceftazidime on DMA slides and in 96-well plates were both in the range of 6–60 μM. The MIC values of ciprofloxacin on DMA slides and in 96-well plates were both in the 0–1 μM range. The MIC value of tobramycin on DMA slides was in the 2–20 μM range, while the MIC was in the 0–2 μM range in 96-well plate, although values were consistent with the range of MIC values listed in EUCAST database (0–68 μM). Ampicillin and tetracycline were shown to be ineffective antibiotics for *P. aeruginosa* PAO1 in both the DMA slide and 96-well plate assays. The time dependence of the antimicrobial effect of polymyxin B was also investigated on DMA slides and in the 96-well plate. As shown in Figure 18f, the number of living bacteria was reduced by exposure to polymyxin B in a time-dependent manner inactivating all bacteria on the DMA slides and in the 96-well plates in the first 2 h incubation. These observations confirm that the small volume of the droplet on a DMA slide does not influence the kinetics of the antibacterial effect of polymyxin B on *P. aeruginosa* PAO1.

Antibiotic resistance study of *P. aeruginosa* PA49 on DMA slides

As a new methodology, the DMA platform shows promising potential in facilitating and advancing antibiotic resistance studies of bacteria derived from patients or the environment. We investigated the ability of 18 antibiotics at two concentrations to inhibit growth of *P. aeruginosa* PA49 on DMA slides and in a 96-well plate as a proof of principle to identify antibiotic resistance. *P. aeruginosa* PA49 were isolated from clinical waste-water from the sewer close to the surgery department and from the clinical wastewater collection pipes in Germany. [169] Berditsch et al. reported that *P. aeruginosa* PA49 are resistant to gentamicin, ciprofloxacin, imipenem, ceftazidime, amikacin, azlocillin and piperacillin-tazobactam with using disk diffusion assay. [170] Here, a number of 18 antibiotics have been chosen of various categories of antibiotic; include β-lactam antibiotic (cephalosporins, ceftazidime, imipenem, meropenem, amoxicillin, carbenicillin, ampicillin, methicillin), quinolone antibiotic (ciprofloxacin), antimicrobial peptides (polymyxin B), macrolide antibiotic

(erythromycin), tetracycline antibiotics (tetracycline), aminoglycoside antibiotic (kanamycin sulfate, streptomycin, tobramycin), sulfonamides (sulfamethoxazole), chloramphenicol antibiotic (chloramphenicol) and combinations (piperacillin - tazobactam). We used the MIC concentration obtained from the EUCAST database of *P. aeruginosa* as reference (Table S2). We also tested 10-fold MIC concentrations to reveal the sensitivity of *P. aeruginosa* PA49 to these antibiotics. The antibiotics were transferred into *P. aeruginosa* PA49 droplets using the sandwiching method. After incubation for 24 h, the DMA slides were dried in air. Opaque spots (bacterial growth has not been inhibited) indicated the lack of antibiotic effectiveness, while transparent (bacterial growth has been inhibited) spots revealed that the antibiotic was effective. In 96-well plates, wells with high turbidity suggested the lack of antibiotic effectiveness, while low turbidity transparency suggested that the antibiotic was effective. All the results were read out visually. Figure 19a shows that, except for ceftazidime and polymyxin B, *P. aeruginosa* PA49 was not sensitive to the chosen MIC concentrations of antibiotics. However, piperacillin-tazobactam, cefotaxime, amoxicillin, carbenicillin, and ampicillin inhibited the growth of *P. aeruginosa* PA49 at the high concentration (10× MIC). According to the universal definition of drug-resistance, *Pseudomonas* bacteria are defined as multidrug-resistant bacteria if the strain is resistant to some of antimicrobial agents from the following four categories: penicillins + β-lactamase inhibitors, cephalosporins, carbapenems, and fluoroquinolones. [171] As shown in Figure 19b, *P. aeruginosa* PA49 isolated from waste-water was identified as a multidrug-resistant bacterial strain.

a

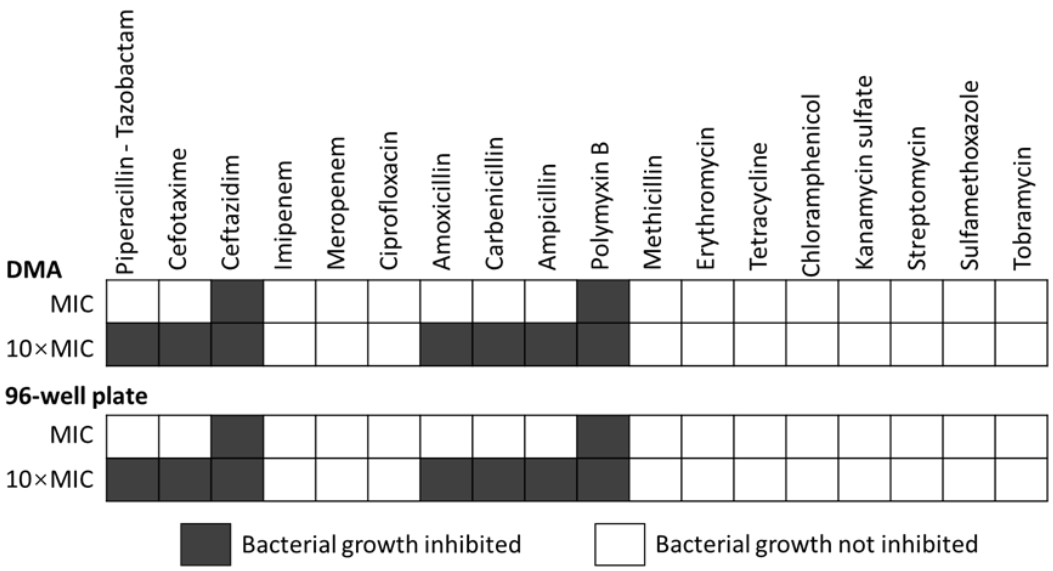

b

Antimicrobial category	Antimicrobial agent	Result of antimicrobial susceptibility testing	
		DMA	96-well plate
β-lactamase inhibitors	Piperacillin-tazobactam	NS	NS
Cephalosporins	Ceftazidime	S	S
	Cefotaxim	NS	NS
Carbapenems	Imipenem	NS	NS
	Meropenem	NS	NS
Fluoroquinolones	Ciprofloxacin	NS	NS

Figure 19. Screening result of antibiotic effectiveness against *P. aeruginosa* PA49 on a DMA surface and in a 96-well plate. Two concentrations of antibiotics were tested. The MIC value of antibiotics was obtained from the EUCAST database. In the 96-well plate, antibiotics were transferred into the bacterial suspension (100 µL per well). On DMA surfaces, antibiotics were transferred into droplets of bacterial solution using the sandwiching method. Initial bacterial density: OD_{600} = 0.001. The bacteria were incubated with antibiotics for 24 h at 37°C. The antibiotic activity was evaluated by visual inspection of the transparency of the wells or droplets (opacity indicates live bacteria). Three experiments with 10 repeats (10 wells and 10 spots) of each concentration of antibiotics

were performed. The antibiotic was defined as effective when there were ≥ 8 wells or spots were transparent. S is sensitive; NS is not sensitive.

3.1.3 Summary

A novel platform for culturing bacteria in spatially separated micro-reservoirs filled with medium was established. This DMA platform can be used for screening the efficiency of clinically used antibiotics against bacterial pathogens. The advantages of the DMA platform are ease of handling, almost no pipetting steps in creating hundreds of micro-reservoirs, and parallel testing of chemical compounds in minute amounts for screening full drug libraries. This platform offers the ability to investigate drug-resistance of bacteria isolated from patients and the environment with minimal cost and effort. As a proof of principle *P. aeruginosa* PAO1 as well as the multi-drug resistant *P. aeruginosa* PA49 isolate could be grown successfully on the DMA surfaces within 24 h. Here, the different categories of antibiotics were applied by sandwiching a fluorinated glass slide preprinted with the drugs to the DMA containing bacteria using the CSC technology. The growth of the bacterial culture on DMA slides can be visualized by microscopy using a GFP expressing strain PAO1::GFP or applying a staining method. Furthermore, bacterial growth can be detected and evaluated by visual examination of the turbidity/transparency of the hydrophilic spots. In parallel and as a control, the obtained DMA screening results were comparable to those using a conventional 96-well plate assay against a multi-drug resistant *Pseudomonas aeruginosa* strain.

In further studies, the DMA platform will be used to identify potential natural or synthetic drug candidates for the treatment of bacterial infections. In extension, this DMA platform opens the opportunity to study synergetic effects of combinatorial drug treatment.

3.2 DMA-based HTS of a Library of 608 Compounds with Carbapenem-Resistant *Klebsiella pneumoniae*

3.2.1 Introduction

In Chapter 4.1, Droplet microarray (DMA) has been demonstrated as a potential miniaturized platform for HTS of antimicrobial compounds by our group. [1] Due to the discontinuous wetting probability of DMA, hundreds of aqueous droplets of around 100 nL can be generated in patterned hydrophilic regions by simply sliding a big droplet across the slide. A sandwiching method has been applied to adding reagents into droplets parallelly. [77] DMA platform has been used to successfully identify the drug resistance of *P. aeruginosa* PA49 by screening of a small library containing 18 antibiotics. [1]

In this section, we aim to optimize the HTS working line with DMA to screen compounds able to inhibit growth of a very important pathogen, *Klebsiella pneumoniae* ATCC BAA-2146, a Gram-negative bacteria producing New Delhi metallo-β-lactamase (NDM-1) that is resistant against almost all beta-lactam antibiotics including the intravenous antibiotic carbapenem. *K. pneumoniae* ATCC BAA-2146 belongs to the family carbapenem-resistant Enterobacteriaceae (CRE), which is listed as an 'urgent threat' to public health in the report of *Antibiotic Resistance Threats in The United States 2019*. To treat infections caused by *K. pneumoniae*, double or triple antibiotic combinations are required. [172]

In order to identify compounds inhibiting *K. pneumoniae* to provide new therapies, over 3,000 synthetic compounds from Compound Platform (ComPlat) are screened using DMA. The classes of compounds include benzofuran-2,3-diones, 2-pyrones, 5-aminopent-2-enoates, polyamine adducts, etc. The molecular weight of most compounds is in a range of 157 - 502 Da. The octanol-water partition coefficients (log *P*) of most compounds are in a range of 0.01 – 6.01. Meanwhile the topological polar surface area (TPSA) of most compounds is lower than 90 $Å^2$. According to the

druglikeness and Lipinski's rule of five (RO5), the compounds show potential druglikeness.

Non-contact liquid dispensers are used to dispense bacteria suspension onto DMA and afterwards add compounds into droplets containing bacteria. A simple colorimetric readout method using Cell Counting Kit-8 is optimized with the DMA platform. Then the growth of bacteria in droplets on DMA after overnight culture can be detected by simply scanning the DMA slide in minutes with a paper scanner. The details of the screening process can be found in Chapter 5.3. After validation of the working line, this platform paves the way for HTS of compounds against multidrug resistant bacteria.

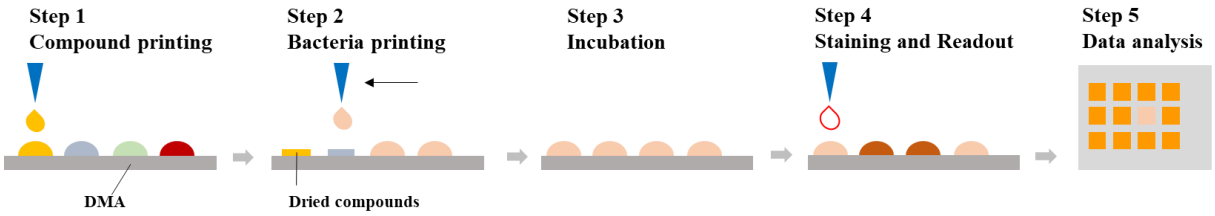

Figure 20. Schematic illustration of the workflow of HTS of antibacterial compounds using DMA.

3.2.2 Result and Discussion

Distribution and growth of *K. pneumoniae* in droplets

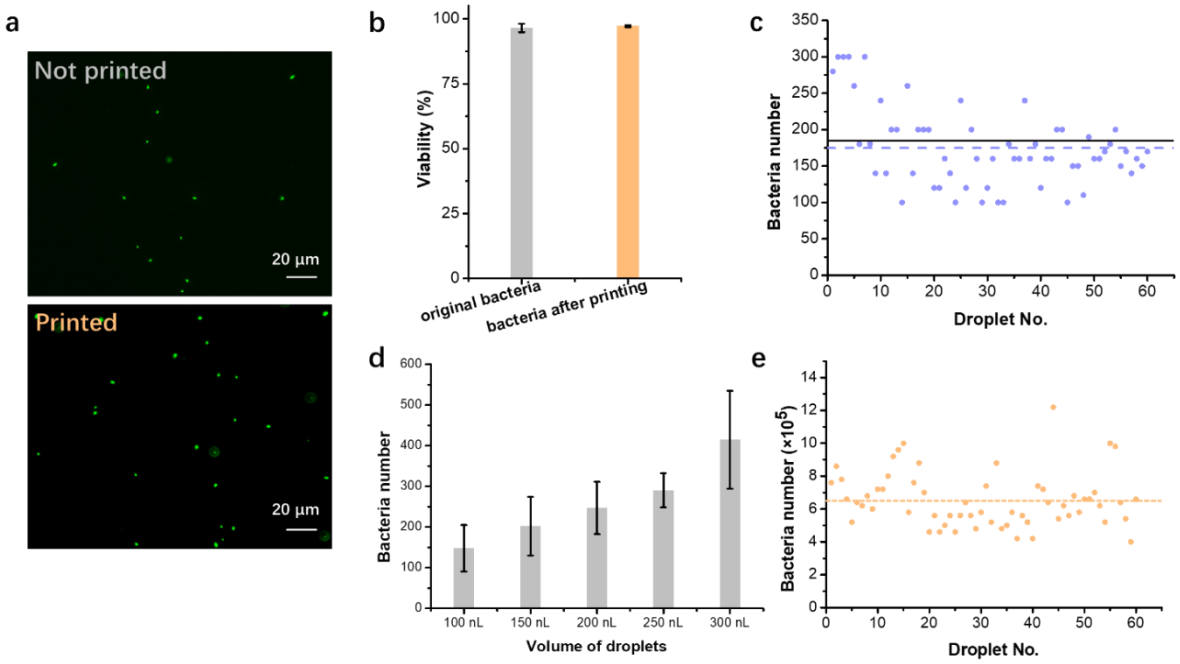

Figure 21. Distribution and growth of *K. pneumoniae* culture in droplets. (a) Fluorescence images of not printed and printed *K. pneumoniae* stained with LIVE/DEAD BacLight™ Bacterial Viability Kit. (b) Viability of not printed and printed *K. pneumoniae*. The ratio of live bacteria/dead bacteria was determined by counting the number of bacteria presenting red fluorescence and number of the total bacteria after LIVE/DEAD staining. (c) Bacteria number in droplets of 150 nL after printing, estimated by colony counting experiments. The horizontal black solid line shows the average number of bacteria in single droplets estimated according to initial bacteria density. The blue dash line shows the average number of bacteria in single droplets obtained from experimental data. (d) Bacteria number in droplets of different printing volume. (e) Bacteria number in 150 nL droplets after 18 h incubation, estimated by colony counting experiments. The yellow dash line shows the average number of bacteria in single droplets obtained from experimental data. Data were presented as mean ± SD of three experiments with three repeats each time.

DMA slides patterned with an array of hydrophilic spots separated with superhydrophobic borders have been used in this research. The DMA slides are with

a dimension of 7.5 × 2.5 cm containing 588 individual hydrophilic spots (1 mm side length of square spots). Due to the precise dimension of spots and stable borders, homogeneous bacterial droplet arrays can be generated by printing bacteria suspensions directly into each individual spot using a non-contact liquid dispenser. As shown in Figure 20, solutions of compounds in DMSO are firstly printed onto DMA slides with a liquid dispenser. Slides are dried in a desiccator overnight afterwards. Then 150 nL bacteria suspension of *K. pneumoniae* is printed onto each hydrophilic spot to form droplets. Bacteria are incubated with the compounds in droplets overnight. Then droplets are stained with Cell Counting Kit-8, which allows spots containing high density of live bacteria to present a visible orange color. Therefore, inhibition of growth of bacteria in droplets can be detected visibly. With a cheap paper scanner, the whole DMA slide can be scanned in a few minutes to further obtain the value of color depth of each droplet by data analysis.

In order to investigate the influence of printing process on viability of *K. pneumoniae* in suspension, LIVE/DEAD assay was applied to detect any dead bacteria in droplets after printing, which are supposed to present red fluorescence due to stained propidium iodide. As shown in Figure 21a, no dead bacteria was observed either in initial bacteria suspension or in bacteria suspension collected from printed droplets on DMA. The viability of bacteria in printed droplets measured from LIVE/DEAD assay was 97.2 ± 0.3%, close to the viability of bacteria in initial bacteria suspension, which was 96.5 ± 1.6% (Figure 21b). The result indicates that the printing process caused no obvious destruction to bacteria. In order to investigate the number of bacteria in droplets, 60 droplets of bacteria suspension from three DMA slides were collected and a colony counting method was used to estimate bacteria number. As shown in Figure 21c, there were 100 to 300 bacteria in each droplet. The average bacteria number in droplets was 174.8± 57.8, which is close to the bacteria number (185.0 ± 8.6 bacteria per droplet) calculated according to the bacteria density of initial suspension and printing volume. This confirms that the printing process is not harmful to *K. pneumoniae*. Due to the precise printing by the liquid dispenser,

bacteria number in droplets could be adjusted by altering printing volume as shown in Figure 21d. With the colony counting method, bacteria number in droplets after overnight incubation was estimated. Figure 21e shows that bacteria proliferated in droplets and reached a high bacteria density of 6.5 ± 1.7 $\times 10^5$ bacteria per droplet. Therefore, by printing with a liquid dispenser, droplets containing a certain number of live bacteria can be created. The droplets are generally homogeneous, since no obvious difference of bacteria number in droplets before and after incubation was detected.

Colorimetric readout on DMA using Cell Counting Kit-8

In order to read the screening result in a convenient, rapid, and cost-saving manner, a colorimetric readout method has been developed. Cell Counting Kit-8 solution is widely used in quantitation of viable cell numbers in proliferation and cytotoxicity assays. Water-soluble tetrazolium salts 8 in Cell Counting Kit-8 solution, as termed WST-8, is reduced by live cells to produce a strong orange dye. Therefore, cell number can be estimated by the formation of dyes and their light absorbance. [173] Droplets of 150 nL containing different bacteria numbers were generated on DMA. Then a staining solution of 100 nL was added into droplets and droplets were incubated for 1 h. Figure 22a and b show the scan images and corresponding color depth value of stained droplets. A color change of the droplets was observed, from bright orange to almost transparent with the decrease of bacteria number in droplets. The droplets containing bacteria of low density (650 bacteria per droplet), which was close to the density of initial bacteria suspension, can be easily distinguished from the droplets containing bacteria of high density, which was the same density of overnight cultured droplets (6.5 ± 1.7 ×105 bacteria per droplet). The detection limitation of growth inhibition of bacteria was 99.9%, and this method was not sensitive to detect very low numbers of bacteria in droplets. Figure 22c and d show that printed DMSO on DMA did not influence the growth of *K. pneumoniae*, indicating the use of DMSO as solvent for compounds will not cause any false positive result. DMSO was then applied as negative controls in the following

screening experiments. When 5.7 μM colistin were printed onto DMA spots, the growth of bacteria was inhibited with stained droplets showing no orange color. The color depth was down to 0.01 ± 0.02, much lower than the color depth of bank samples (0.27 ± 0.02) and negative controls (0.28 ± 0.02). Therefore, spots printed with 5.7 μM colistin were used as positive controls in the screening. The images showed that antibacterial screening on DMA shows the 'Yes' and 'No' of antibacterial effects of testing compounds, with effective compounds presenting almost transparent color and very low color depth value. Figure 22e shows that there was no contamination between droplets incubated with and without colistin.

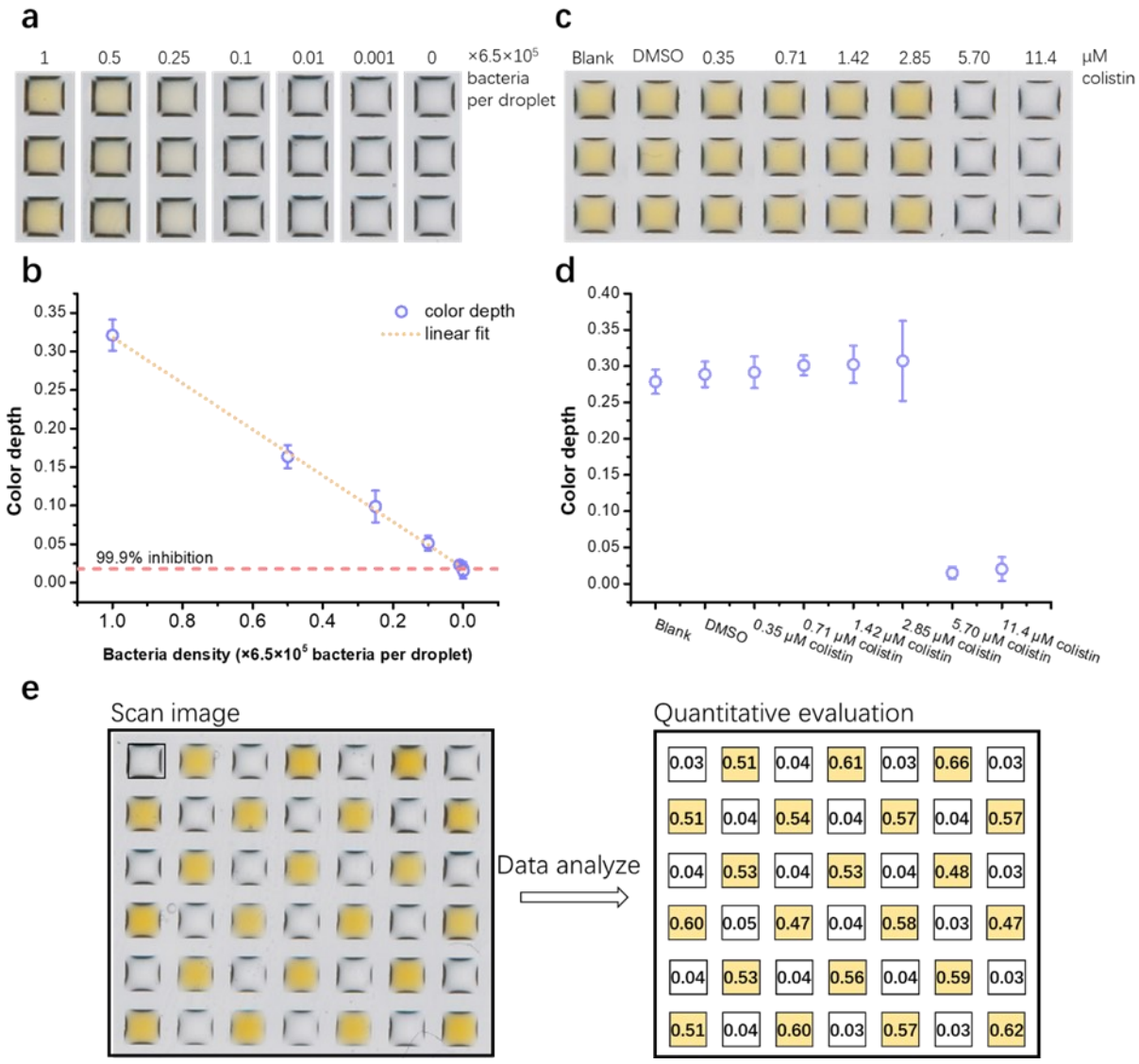

Figure 22. Colorimetric readout method to evaluate growth of bacteria in droplets using Cell Counting Kit-8. (a) Scan images of droplets containing different numbers of bacteria stained with Cell Counting Kit-8 solution. (b) Color depth of stained droplets shown in (a). (c) Scan images of droplets containing overnight incubated bacteria on DMA, which were printed with DMSO and colistin. (d) Color depth of stained droplets shown in (c). Data were presented as mean ± SD of three experiments with three repeats each time. (e) Left: A scan image of stained droplets containing bacteria on DMA. A checkerboard pattern of colistin

was printed on DMA before the printing of bacteria. Right: Color depth of droplets shown in the scan image.

Influence of solubility of compounds in screening

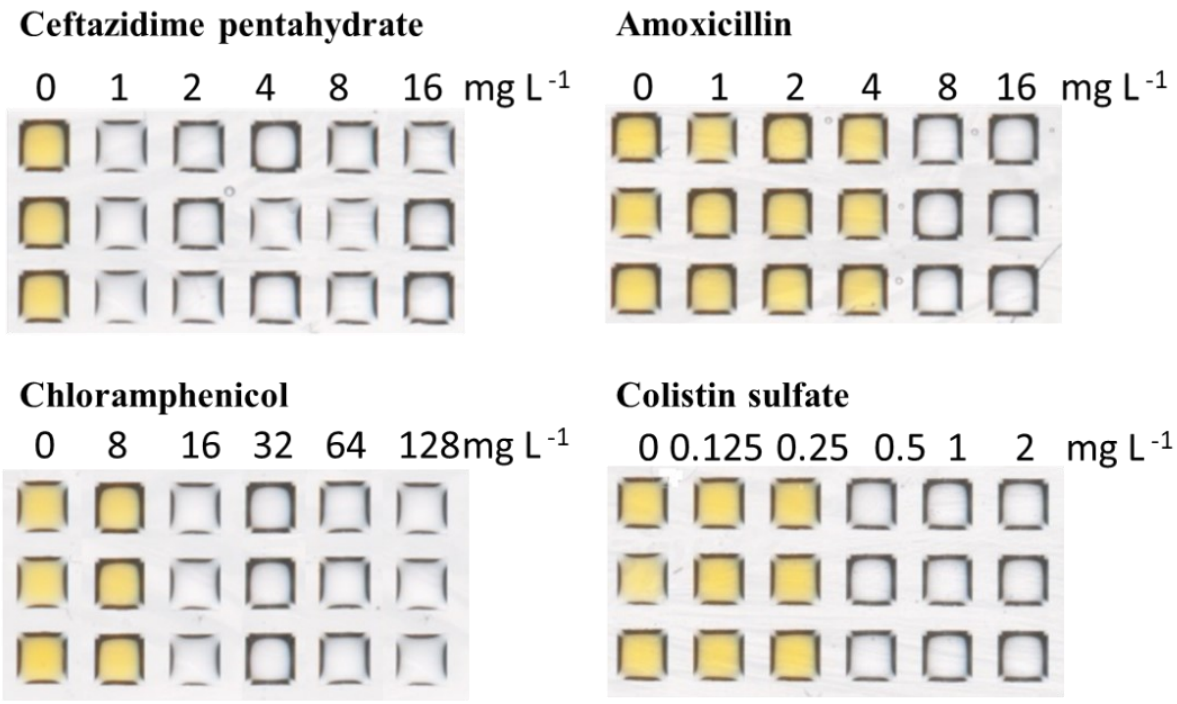

Figure 23. Scan images of stained droplets containing bacteria incubated overnight on DMA printed with antibiotics.

Given that the testing compounds possess a wide range of water solubility and printed compounds are firstly dried out on DMA, it is necessary to ensure the hydrophobic antibacterial compounds can be screened with DMA platform. Four antibiotics ceftazidime pentahydrate (solubility: 0.028 mg mL^{-1}, data from DrugBank Online), amoxicillin (solubility: 4.7 mg mL^{-1}), chloramphenicol (solubility: 2.5 mg mL^{-1}, data from DrugBank Online), and colistin sulfate (solubility: freely soluble in water, data from product description of Merck) were selected to investigate their antibacterial ability against *E. coli* K12. [174] Figure 23 shows that the minimum inhibition concentration of ceftazidime pentahydrate, amoxicillin, chloramphenicol and colistin sulfate measured with DMA were 1 mg ml^{-1}, 4 mg ml^{-1}, 8 mg ml^{-1} and 0.25 mg ml^{-1},

respectively, indicating that even hydrophobic compounds can be screened for their antibacterial property with DMA.

Preliminary screening of 608 compounds from ComPlat

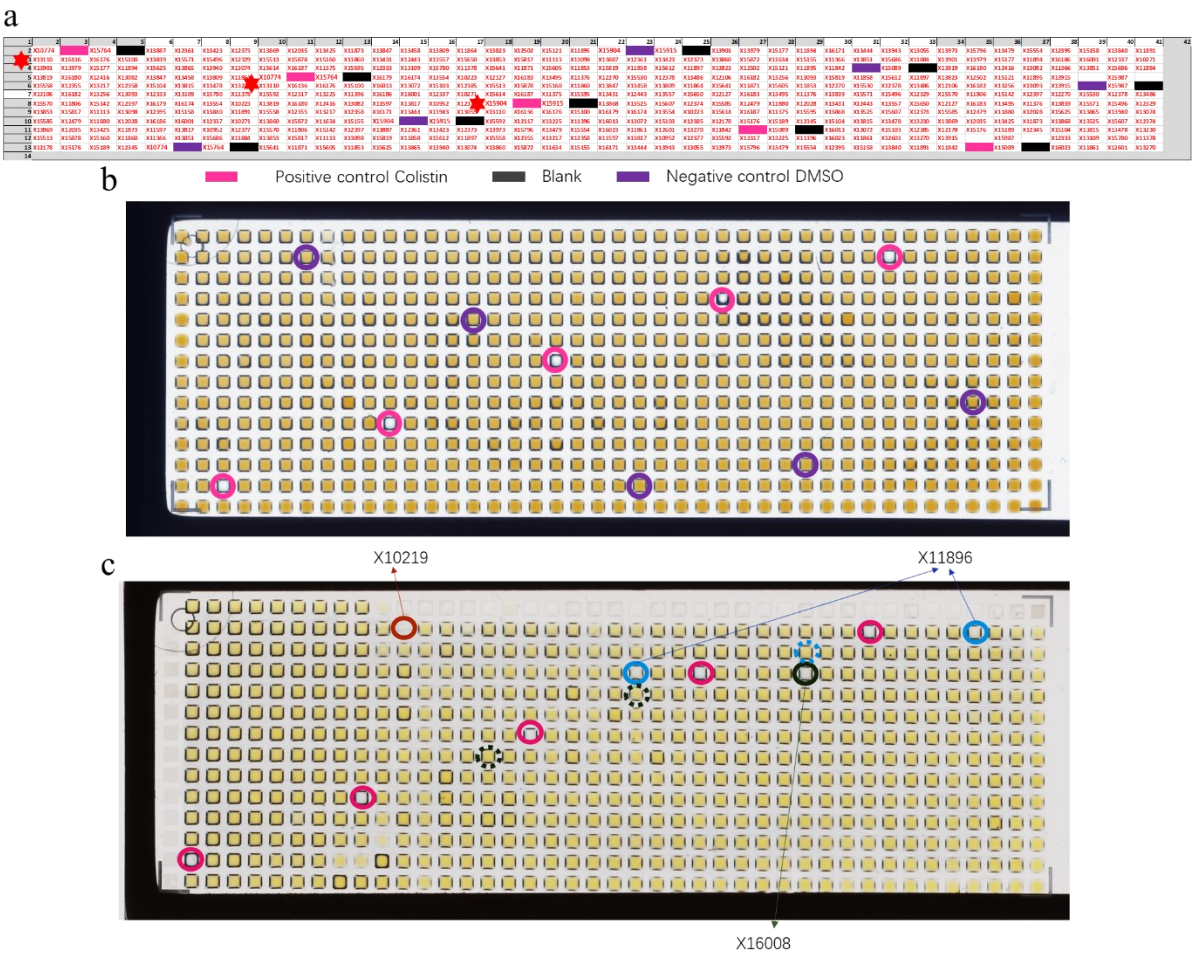

Figure 24. Examples of DMA slides used in antibacterial screening of 608 compounds from the ComPlat library. (a) The layout of 152 compounds on a DMA slide. Each compound has three repeats. The distribution of compounds was shown with an example with red star mark. (b) A scan image of stained droplets containing bacteria incubated on DMA printed with compounds from the ComPlat library as shown in (a). Droplets as positive controls are shown in pink circles. Droplets as negative controls are shown in purple circles. (c) A scan image of stained droplets. Droplets showing positive results are shown in solid circles. Repeats of the compounds showing positive results are shown in dashed circles. Droplets are on 1 × 1 mm spots.

An example of a DMA slide in the HTS process is shown. 152 compounds from the ComPlat library were printed on a DMA slide. The layout of compounds is shown in Figure 24a. Five positive controls, five negative controls and 10 blank controls were set up on the slide. Three repeats of each compound are distributed to different regions of DMA to prevent any artifacts. Figure 24b shows the scan image of the DMA slide after the screening process. Droplets as positive controls were transparent, while negative controls and blank controls showed orange color as expected, suggesting the validity of the screening process using DMA. The value of color depth of droplets on the slide are shown in Supporting Information Figure S1. All droplets except for positive controls presented orange color, implying that no hits have been found from the screened 152 compounds.

As shown in Figure 24 c, on another DMA slide, there were three compounds that presented positive results in the preliminary screening. The three compounds include X10219, X11896, and X16008. The structures of the three compounds are shown in Supporting Information Figure 2. X10219, X11896 and X16008 will be listed as candidates, which will be validated for their antibacterial effects in the next step after the screening of 3,000 compounds from ComPlat.

3.2.3 Summary

In this study, the work flow of HTS of antimicrobial compounds using DMA has been established and validated. It is demonstrated that cell printers can be applied to generate homogeneous droplets containing a certain number of bacteria. *K. pneumoniae* grew from ~ 170 bacteria per droplet to ~ 6 $\times 10^5$ bacteria per droplet in droplets. A simple colorimetric readout method was developed. Droplets containing hit compounds, which lead to inhibition of bacteria growth, could be easily distinguished visibly. With an ordinary paper scanner, a DMA slide with 588 droplets (152 testing compounds) can be screened in several minutes to provide quantitative data of color depth of stained droplets. Finally, 152 compounds from the ComPlat library were screened using a DMA slide.

The aim of this project is to screen 3,000 compounds from the ComPlat library. Current experiments and results build a solid foundation for the next screening. The HTS working line developed in this research opens opportunities to identify antimicrobial agents from other libraries to provide new therapies to treat drug resistant infections.

3.3 Biofilm Bridges Forming Structural Networks on Patterned LIS (pLIS) *

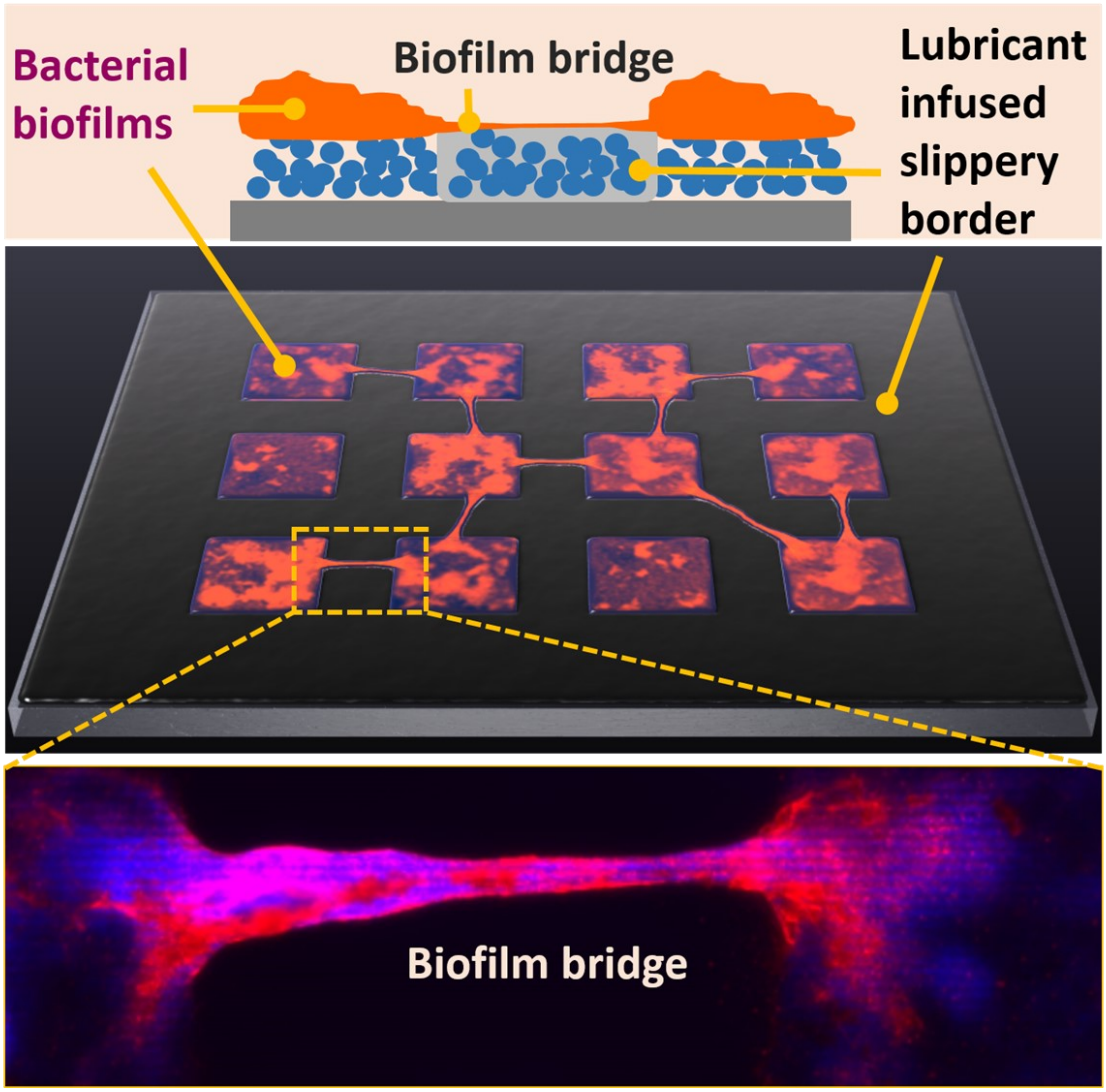

*This chapter and the associated section were published previously:
Lei, W., Bruchmann, J., Rüping, J. L., Levkin, P. A., & Schwartz, T. (**2019**). *Advanced Science*, 6(13), 1900519. [2]

3.3.1 Introduction

Biofilms on surfaces is the predominant form of bacterial lifestyle not only in technical settings and nature but also in 80% of all infections in medicine. [175, 176] Such sessile bacterial communities work as a team through varies interaction and communication such as horizontal gene transfer, protein exchange and quorum sensing. [177, 178] Despite a lot of research, internal organizations, interactions within biofilms, mechanics and details behind biofilm development often remain to be determined. Reasons for this lie in the heterogeneity of biofilms, which leads to high variances in the gene expression, stress response and behavior of different subpopulations. [90] The lack of understanding of biofilm spreading is especially important in clinical settings, where the host immune system, drug administration or other factors can influence biofilm expansion and may result in severe conditions. [179, 180] Furthermore, biofilm removal or manipulation is a major cost intensive factor in technical systems as high consumptions of toxic biocides or mechanical efforts are performed to avoid biofilm formation (water condition and distribution). Biofilms play a significant role in medicine since high numbers of infections originate from biofilm contaminations, e.g., at implants. These biofilms are much more insensitive against antibiotics than planktonic pathogens especially in case of multi-resistance against antibiotic drugs. Hence, there is an urgent need to design models aiding us to investigate structure, interconnectivity, diversity, and dynamics in biofilm in a controllable way.

Biofilms are highly heterogeneous due to their spatial partitions in larger structures (landscape), which leads to the inability to investigate fine structural changes of biofilm communities as a function of various relevant factors. Hence, fine changes, which are often critical in understanding structure-function relationships in biofilms, are often overlooked in case of such bulk analyses. In addition, every laboratory uses a different method for biofilm investigations, which might have a significant influence on biofilm behavior, e.g., medium composition, construction of flow cells, fluidic versus static culturing etc. Biofilm cannot be considered as a simple sum of

individual bacterial cells, but as a complex differentiated community with a heterogeneous 3D structure. [181] Biofilms represent organized communities encased in a matrix of extracellular polymeric substances (EPS) that hold microbial cells together to a surface. [182] EPS is composed mainly of biomolecules, exopolysaccharides, extracellular DNA (eDNA), and polypeptides that form a highly hydrated polar mixture that contributes to the overall structural scaffold and architecture of the biofilm. [181] Depending on the bacterial species or strains and the nutritional conditions, different biofilm phenotypes can be developed starting with a reversible attachment to surface, followed by irreversible colonization with formation of micro-colonies in EPS-matrix. Bacterial micro-colonies expand and a more structured phenotype with channels and voids is developed during biofilm maturation. Finally, bacteria disperse from biofilm structures and spread to downstream areas forming new biofilms. One of the special structural assemblies in biofilm are biofilm streamers, which occur under flow conditions along the fluidic direction. [183, 184] These filamentous structural streamers of e.g., *Pseudomonas aeruginosa* are networks of biofilm filaments consisting of EPS and bacteria. By catching cells flowing through the gaps between them, streamers are able to connect bacterial clusters and promote spreading of biofilm. [185] Revealing structure-function relationship in biofilms might help us to prevent biofilm spreading and invasion in all kinds of medical and technical system. However, suitable assays for analysis of biofilm spreading are still missing.

Bioinspired “slippery” lubricant-infused porous surfaces (LIS) have been exploited in various applications, including prevention of eukaryotic cell and biofilm adhesion. [139, 186, 187] Due to the liquid-like properties and the defect-free nature of LIS, it is difficult for mammalian cells and bacteria to attach onto them irreversibly. [140] It is reported that LIS were able to decrease the biofilm occupation on surfaces. [188-190] Recently, we demonstrated a method to form arrays of biofilm clusters with defined 2D geometries by using patterned LIS. To our surprise, on lubricant-infused bacteria repellent regions, biofilm bridges were formed spontaneously between

neighboring clusters of *Pseudomonas aeruginosa* separated by LIS regions in the range of 50 to 500 μm. [138]

Here we apply patterned LIS to create spatially separated biofilm clusters to investigate the phenomenon of biofilm bridging. Patterned LIS is a useful tool to study biofilm bridging, as it builds up physical "walls" between biofilm clusters, while allowing transport of signals, nutrients, and bacteria between them. We used both Gram-negative species including *Pseudomonas aeruginosa*, *Stenotrophomonas maltophilia* and Gram-positive species *Staphylococcus aureus* to investigate biofilm bridges. Fine structure of bridges and metabolic activity were studied with fluorescence microscopy. Fluorescence In - Situ Hybridization (FISH) demonstrated the structural organization of bridges consisting of two species mixed populations.

3.3.2 Results and Discussion

P. aeruginosa PA49 form string-like structure on pLIS

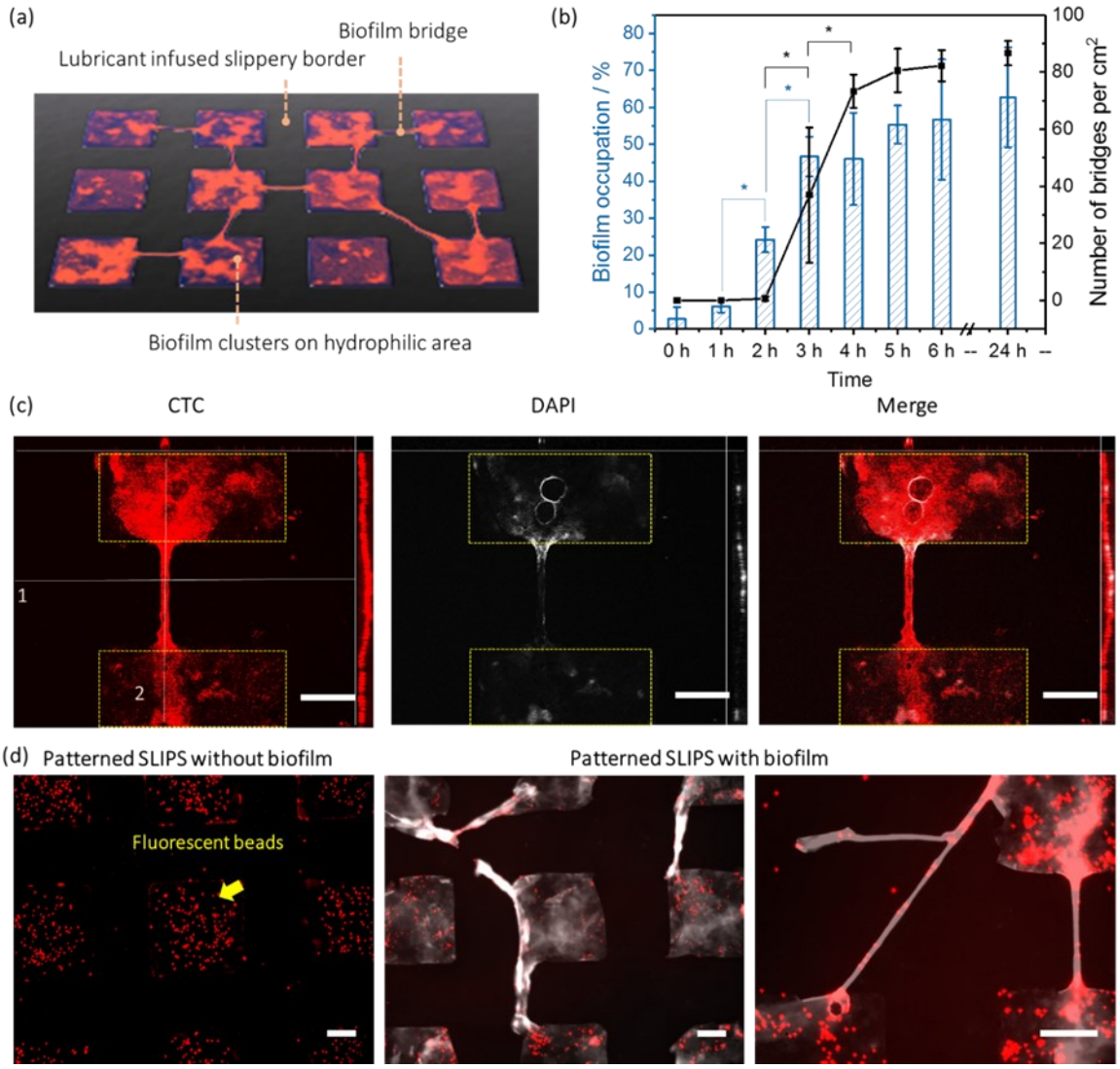

Figure 25. Biofilm bridges of *P. aeruginosa* PA49 on pLIS. a) Scheme of biofilm bridges formation of *P. aeruginosa* PA49 on patterned LIS. (b) Numbers of bridges and biofilm occupation of *P. aeruginosa* PA49 on patterned LIS after certain time points in bacterial suspension of BM2 medium. DAPI staining coverage of hydrophilic area calculated from fluorescence images with ImageJ software is presented as biofilm occupation. (c) Z-stack images of biofilm bridges. (Left: CTC staining. Middle: DAPI staining. Left: merge. For each image, up: cross section, corresponding line1; right: cross section, corresponding line 2, middle: top view). Patterned LIS were incubated with *P. aeruginosa* PA49 for 24 h. Then

samples were stained with CTC (red color) and DAPI (white color). The thickness of the z-stack is 40 μm. (d) Fluorescence microscope images of patterned LIS after deposition of microbeads labeled with red dye: (left) without biofilm and (right two) with *P. aeruginosa* PA49 biofilm formed during 24 h. Both samples were stained with DAPI (white color), followed by 10 min incubation with the microbeads (1 μm) for 10 min and washing with water. The scale bars: 100 μm.

In order to investigate the phenomenon of biofilm bridges, we first formed an array of bacteria adhesive hydrophilic squares with side length of 350 μm separated by 200 μm lubricant infused biofilm repellent regions. Perfluorinated polypropyleneoxide (Krytox GPL 103) was used as the lubricant. SEM image shows the porous structure of the surface (Figure S1), which is required to lock lubricant and form a stable lubricant layer. Water contact angles and sliding angles of patterned surfaces with and without lubricant were shown in Table S1. The sliding angles of lubricant infused surfaces were 1.6°± 0.2°, while the advancing water contact angles were 100.4°± 5° and receding water contact angles were 95.5°± 2°, indicating the slippery property of the surfaces. Patterned slides were incubated in *P. aeruginosa* PA49 strain suspension under shaking to grow biofilm clusters on hydrophilic spots (Figure 25a). We used 4′, 6-diamidino-2-phenylindole (DAPI) to stain both intracellular DNA in bacteria and DNA in extracellular polymeric substances (EPS) of biofilms. The first biofilm bridges were observed on surfaces after 3 h incubation (Figure 25b), which increased up to 82.2 ± 5.4 bridges per cm^2 after 6 h of incubation. Each hydrophilic square showed 0.24 biofilm bridges on average after 24 h incubation. The occupation of biofilm in hydrophilic spots increased with longer incubation time as well, from 6.1 ± 1.6% after 1h incubation to more than 56.6 ± 16.3% of the hydrophilic area of each cluster after 6 h incubation. These observations suggested that the biofilms formed on the hydrophilic spots already after 1 h of incubation, while the first bridges were detected only after 3 h. String-like structure of biofilm was demonstrated before. Z. Jahed et al. used dewetting properties of poly (dimethyl siloxane) micropillars to fabricate “biostrings” of *S. aureus* after liquid retracting process. [134]

To demonstrate the scale of the bridge structure, we analyzed Z- stack images of the bridge of *P. aeruginosa* PA49 after 24 h incubation in BM2 medium. As shown in Figure 25c, the bridge did not attach to the substrate surface such as the biofilm grown in hydrophilic spots but rather formed an arc above the substrate's plane. The distance between the highest part of the bridge and the substrate was 20.4 μm. This distance should be caused by the existence of lubricant, making the LIS plane higher than that of the hydrophilic area. To prove this further, we used 1 μm microbeads labeled with red dye to incubate with patterned LIS with and without *P. aeruginosa* PA49 biofilm formed. All samples were incubated in BM2 medium for 24 h, stained with DAPI and incubated with the fluorescent beads for 10 min. As shown in Figure 25d (left), on the patterned LIS without bacteria, the beads only aggregate in the hydrophilic spots, suggesting that beads tend to sediment and bind to the hydrophilic areas. Figure 25d (right) showed that there was an overlay of beads and bridges, confirming that bridges were exposed to the medium enabling their interaction with the fluorescent beads. The specificity of this microbead attachment to biofilm and bridge structures illustrates that the bridges are located on top of the lubricant area and not covered by the oil.

Formation of biofilm bridges by different bacteria species

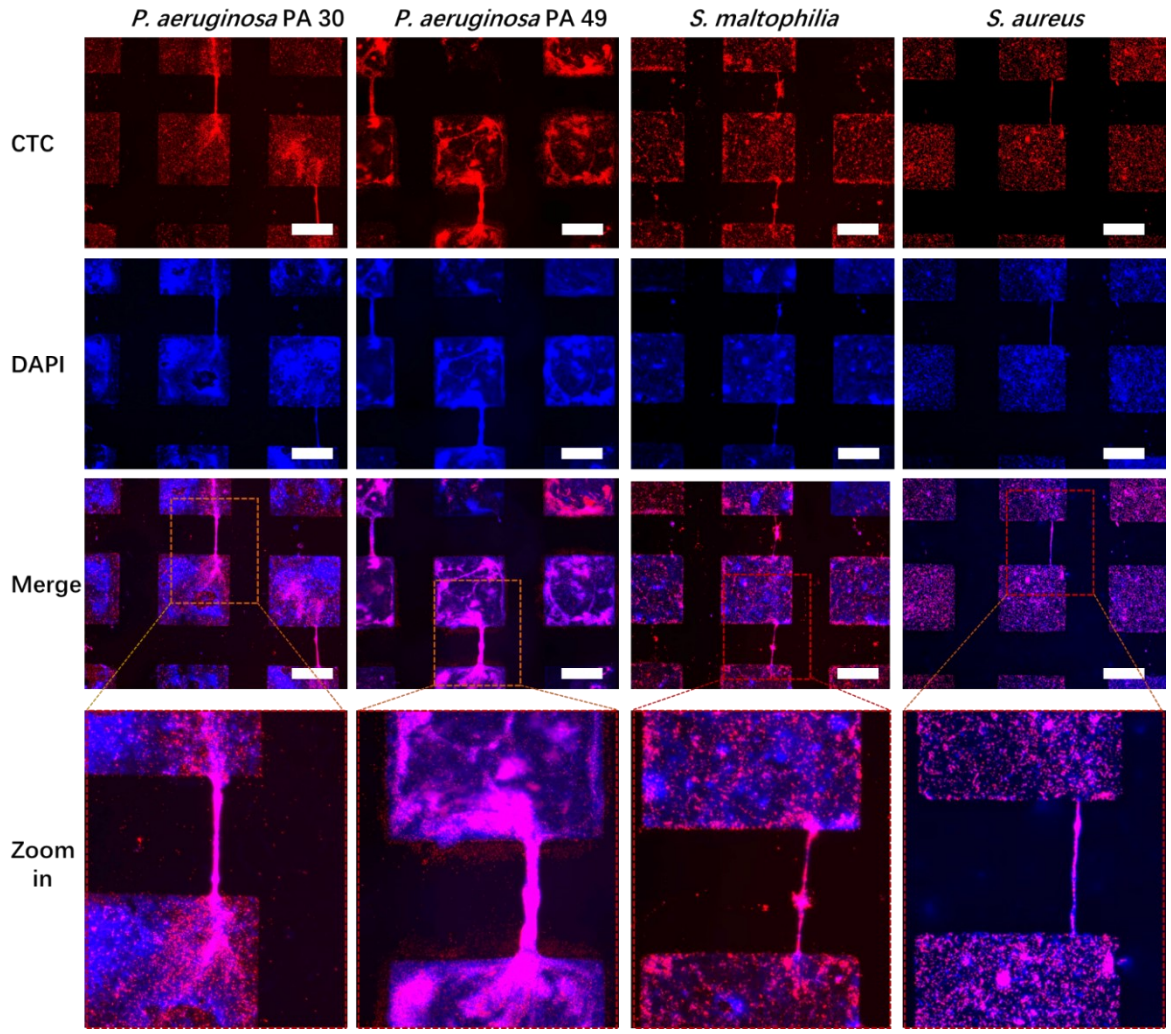

Figure 26. Fluorescence microscope images of biofilms of different species on patterned LIS. *P. aeruginosa* PA30, PA49, *S. maltophilia*, and *S. aureus* after 1 day incubation in BH1 1:4 medium. Biofilms were stained with CTC for 3 h then with DAPI for 10 min before images were produced. Red color represents active bacteria from CTC staining and blue color represents DNA (external + inside of bacteria). The microscope observations were completed by ImageJ software. The scale bar is 200 µm.

In order to understand whether the biofilm bridge formation is a ubiquitous phenomenon during biofilm growth in the bacterial world, four different bacterial species were selected. Two strains of *P. aeruginosa*, PA30 and PA49, as well as *S. maltophilia* were used as Gram-negative species, which occur in lung infection and urinary tract infection. [191, 192] In addition, we used *S. aureus*, a Gram-positive

pathogenic bacteria involved in broad clinical infections such as infective endocarditis and osteoarthritis. [193] These facultative-pathogenic bacteria are frequently associated with nosocomial infections and tend to form multi-resistances against clinically relevant antibiotics, which can hardly become medically treated in case of infections. [194, 195]

After incubation with bacterial solution for 24 h, LIS samples were removed from the petri dishes and stained with CTC and DAPI. As shown in Figure 2, for all species biofilms were formed on hydrophilic areas. Actively respiring, CTC-positive bacteria (red fluorescence) could be observed in hydrophilic squares and only a few attached aggregates of bacteria were detected on hydrophobic slippery areas. The blue fluorescence from DAPI, staining intra- and extra-cellular DNA, was also found predominantly in the hydrophilic bacteria-adhesive squares with only a few biofilm colonies in the lubricant-infused regions. The biofilm bridges were clearly observed for all species under investigation (Figure 26). Biofilm bridges represented thin biofilm strings showing active metabolism (CTC-positive) and presence of intra and extra-cellular DNA (DAPI-positive) and connecting adjacent biofilm clusters formed in the hydrophilic squares. Interestingly, the CTC-staining of the bridges was brighter than that of the biofilm main clusters, indicating presence of highly active bacteria in the bridges. The shape of the bridges depended on the bacteria strain. For *P. aeruginosa* PA30 and PA49, the bridges were dense, uniform, with bright fluorescence of respiring bacteria, and total DNA, indicating a possible interaction of active bacteria and extracellular polymeric substances (EPS). Bridge formation by *S. maltophilia* performed differently compared to the other two bacteria types. This indicates that bridge formation is species dependent.

Figure 27a shows the time-dependent formation of biofilm bridges for all species studied. The density of bridges for *P. aeruginosa* PA49 was the highest among all species. It was 56.9 ± 30.4 bridges per cm^2 (0.2 ± 0.1 bridges per hydrophilic square), which is almost 4 times more than *P. aeruginosa* PA30 (13.2 ± 0.3 per cm^2, 0.1 bridges per a hydrophilic square) after 24 h incubation. *S. maltophilia* and *S. aureus*

developed only 1.7 ± 1.6 and 1.8 ± 2.2 bridges per cm^2, respectively (0.01 and 0.01 bridges per a hydrophilic square, respectively), much less than the both *P. aeruginosa* strains PA30 and PA49. The number of bridges increased for *P. aeruginosa* PA30 to 43.1 ± 7.9 per cm^2 after 48 h with refreshing the nutrient medium after 24 h. This increase was not observed with *P. aeruginosa* PA49 with similar experimental conditions. Similar results were obtained with *S. maltophilia* and *S. aureus* with an unchanged number of bridges after 24 h incubation. More generally, the density of bridges of all species did not increase significantly after 48 h incubation.

The width of bridges ranged from a few micrometers to more than 70 µm, depending on the species and incubation times (Figure 27b). The width of bridges changed with the incubation time especially for *P. aeruginosa* PA49, which increased from 9.4 ± 5.0 µm to 36.4 µm and the broadest bridges could reach 79.4 µm after 48 h incubation. Nevertheless, this increase did not continue in the next 24 h incubation. For *P. aeruginosa* PA30, the width of bridges increased from 8.5 ± 4.1 µm after 24 h incubation to the broadest 34.1 µm after 48 h incubation**.** There were no obvious changes in width of bridges for other species with time, as most were in a range of dimension from 2 to 20 µm. The distance between hydrophilic squares was 200 µm, therefore the length of bridges for all bacterial species was around 200 µm. For half bridges, which were connected with only one biofilm cluster, the length was shorter than 200 µm (Figure 27c). In some cases, biofilm bridges longer than the side-to-side distance between hydrophilic squares were observed. For example, connecting two corners from two biofilm squares diagonally resulted in bridges of around 280 µm. As previously described, *P. aeruginosa* PA49 is known to possess an increased biofilm formation capacity compared to *P. aeruginosa* PA30. [196] This higher biofilm forming potential could contribute to the increased bridge development especially during the first 24 h of incubation. Either the increase of bridge width of *P. aeruginosa* PA49 could be responsible for a possible start of biofilm spreading on the biofilm repellent slippery area. Bridge formation by *S. maltophilia* performed differently comparing to the other two bacteria types indicate that bridge formation is species dependent.

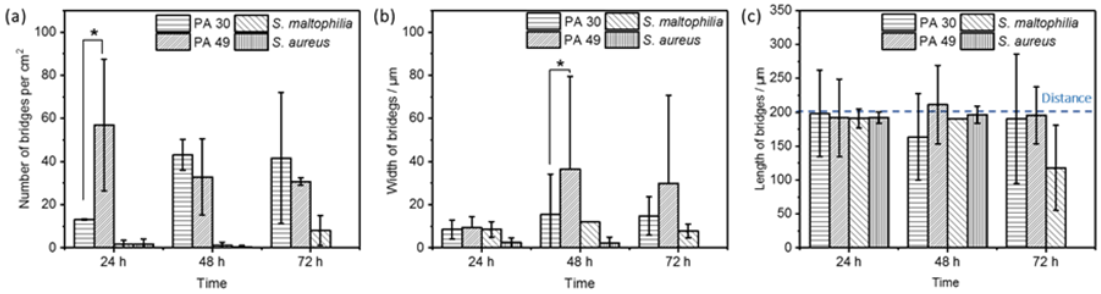

Figure 27. Formation of biofilm bridges for *P. aeruginosa* (PA30, PA49), *S. maltophilia* and *S. aureus*. (a) Number of bridges per area (cm^2), (b) width of bridges at the middle of a bridge (b), and (c) length of bridges. Biofilm bridges were analyzed on patterned LIS after 1, 2, and 3 days incubation in BHI 1:4 medium and stained with CTC and DAPI. The dotted line in (c) represents the closest distance between neighboring hydrophilic spots (200 µm).

Composition and structure of biofilm bridges

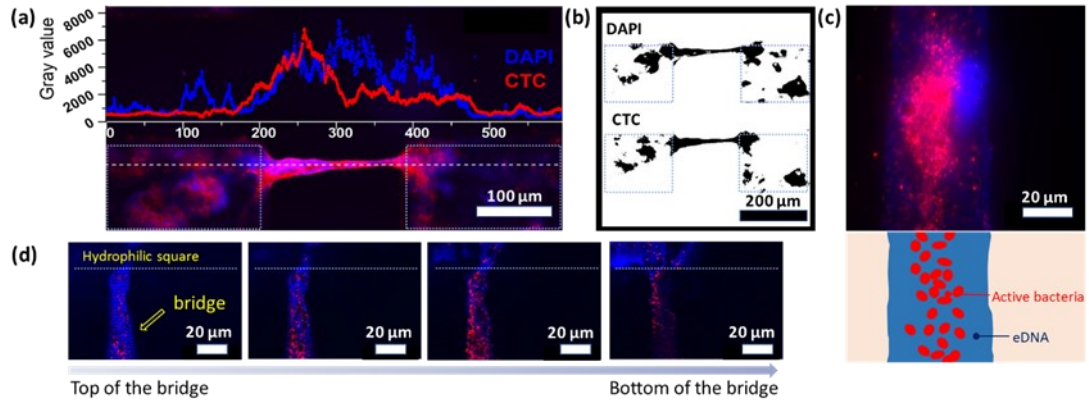

Figure 28. Fluorescence microscope images of bridges of *P. aeruginosa* PA49 after 24 h biofilm formation stained with CTC (metabolically active cells, red) and DAPI (DNA as total biomass indicator, blue). (a) Fluorescence intensity of CTC and DAPI staining of the line (white dot line) along a biofilm bridge connecting two biofilm clusters. (b) Images of the biofilm bridge after threshold adjustment. (c) Fluorescence microscope image of a biofilm bridge at a higher magnification showing active bacteria and extracellular structural DNA (top). Corresponding schematic (bottom). (d) Z-stacks images of a biofilm bridge. Images from left to right represent features of bridges at different Z-positions from the top to the bottom of the bridge.

To investigate the structure and composition of biofilm bridges, high magnification fluorescence microscopy was used. Figure 28a shows both CTC and DAPI fluorescence intensities plots along a single *P. aeruginosa* PA49 biofilm bridge formed after 24 h incubation. The fluorescence intensity corresponding to the metabolically active bacteria in the bridge (5000~6000 gray unit) was about 3 times higher than the fluorescence intensity of the biofilm located in the neighboring hydrophilic spots (1500~2000 gray unit). Interestingly, both the CTC and DAPI fluorescence increased not only in the bridge but also in the areas adjacent to the ends of bridges, where bridges attached to the main biofilm clusters (Figure 28a, b). Such bright fluorescence demonstrated an aggregation of actively respiring bacteria and eDNA in the bridge structures including the attachment points of the bridges. There is a clear overlap of both signals indicating the co-existence of active bacteria and eDNA inside the bridge.

Figure 28c showed respiratory active bacteria were surrounded with a layer of nucleic acids (eDNA) as part of the EPS or non-active bacteria. Z-stacks scanning was also used to analyze the bridges in more detail. Figure 28d showed from the top of the bridge, fluorescence from DAPI staining was firstly presented, revealing that it is eDNA components of the EPS but not respiratory active bacteria exposed directly to the environment. Such a structure was described in Figure 28c. As commonly known, EPS plays a critical role in biofilm formation and contributes to some crucial features of biofilms, such as antibiotic-resistance, high tolerance of environmental stress and difficult eradication in biofilm bridges, EPS occurs as a protective shell for inner respiratory active bacteria, indicating the role of EPS is necessary for biofilm bridges formation and stability. [197, 198]

Biofilm bridges of mixed species

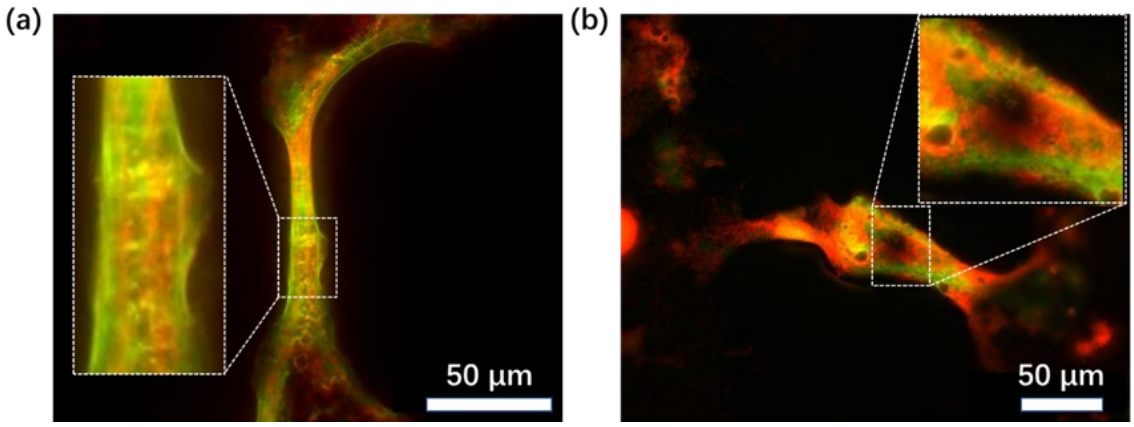

Figure 29. Images of biofilm bridges of mixed species of (a) *S. maltophilia* and *P. aeruginosa* PA49. (b) *S. maltophilia* and *P. aeruginosa* PA30 after FISH hybridization.

Here we used FISH analysis with the fluorescently labelled gene probes targeting specific sequences of the 16S rRNA of different bacteria types cultured on patterned LIS samples, aiming to deeper understand the composition of bridges and the spatial distribution of the cells in bridges. The oligo-nucleotide for *S. maltophilia* was labeled with a red fluorescence dye (ATTO550), whereas *P. aeruginosa* PA30 and PA49 were labeled with a green fluorescence dye (AT488). Although both bacterial species were found in the same biofilm bridge, the fluorescence images in Figure 29a, 29b and S3 show a spatial segregation of the two different investigated bacterial species in the biofilm bridges. The two bacteria types in the bridges did not mix homogeneously but at the same time utilized this structural element of the biofilm. Both red and green fluorescent "strings" corresponding to each bacterial species were a few micrometers thick and went along the whole length of the bridge, which was clearly visible inside individual mixed population biofilm bridges (Figure 29). This observation may indicate the importance of the bridges as a functional unit of biofilm and shows the use of such elements by different bacterial species together, which in turn may be beneficial for the overall survival of biofilms.

To the best of our knowledge, this core-shell structure was not reported before. The co-existence of *P. aeruginosa* and *S. maltophilia* in the biofilm bridges would be the

result of coaggregation interaction, which is caused by protein adhesions on bacteria surfaces, and other structural biofilm relevant factors. [199] The segregation and specific spatial organization of *P. aeruginosa* and *S. maltophilia* in the bridges are one of typical characteristics of co-operative interactions in multiple species biofilms, which is beneficial for efficient diffusion path for organic compounds such as nutrients and signaling molecules. [199]

3.3.3 Summary

With the help of micro-cluster analyses being fundamental to study biofilm structures and stimuli dependent reactions of biofilms. It was possible to describe a novel important phenomenon: the biofilm bridging. This biofilm bridging might have implications in biofilm development, spreading and surpassing adverse surface conditions. It was shown that this bridge strucutre is common to different Gram-negative and Gram-positive bacteria in species-dependent manner. Organisms' distribution and organization in bridges of multi-species biofilm were demonstrated. Hence, the biofilm bridges are important to bring deeper understanding of biofilm complex 3D structure. By manipulating incubation environment, formation of networks composed of bridges between biofilm clusters and spreading over multiple biofilm clusters were discovered. Thus, biofilm bridge formation is an important novel phenomenon, which can be useful to reveal more details about the dynamics and communication within biofilm communities as well as to understand the relations of subpopulations, stress responses including virulence regulations and biofilm spreading.

3.4 Controlling Geometry and Flow Through Bacterial Bridges on pLIS*

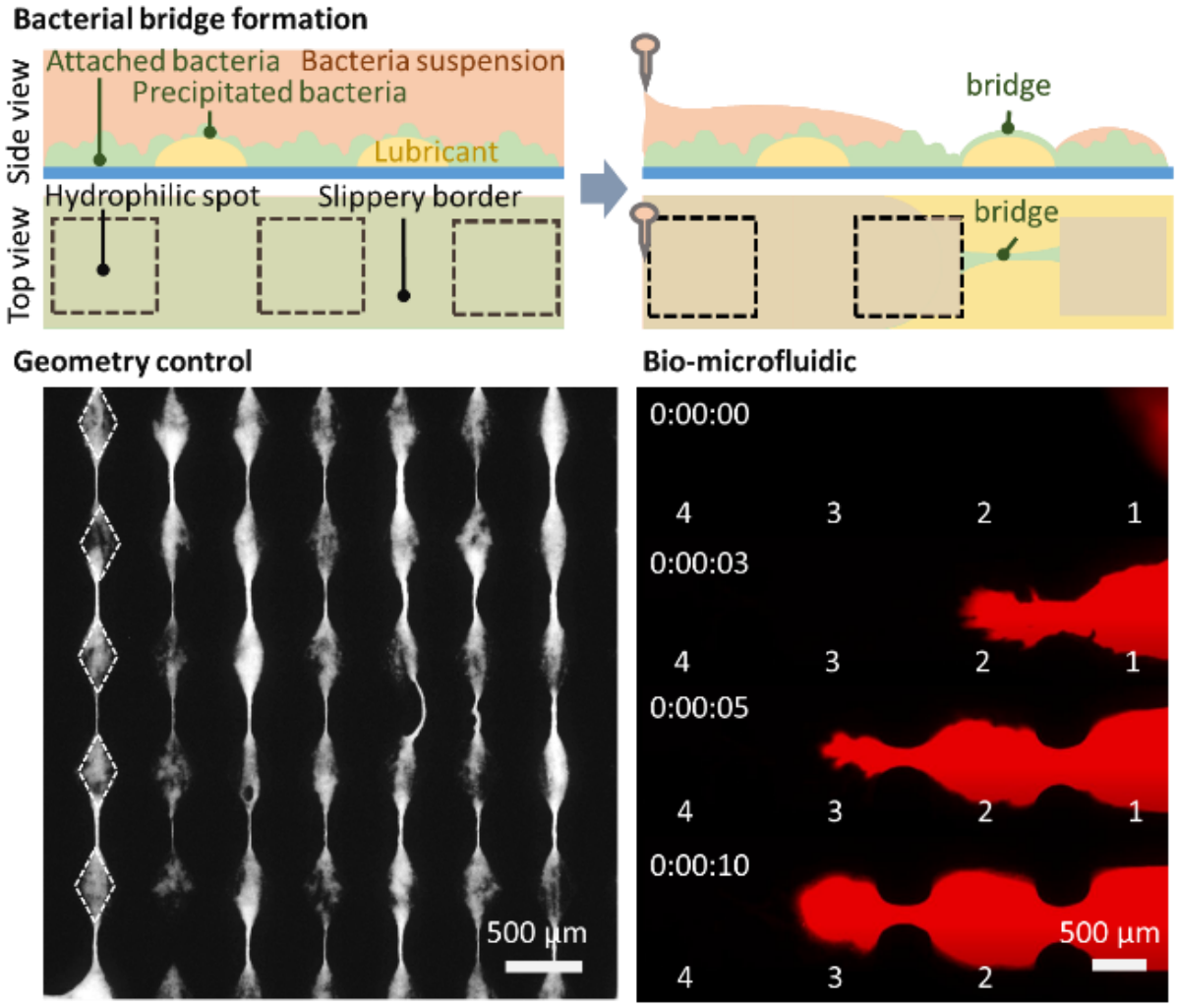

This chapter and associated sections were published previously:
Lei, W., Krolla, P., Schwartz, T., & Levkin, P. A. (**2020**). *Small*, 16(52), 2004575. [3]

3.4.1 Introduction

Gram-negative bacteria such as *Acinetobacter spp.*, *Pseudomonas aeruginosa*, *Escherichia coli*, *Enterobacter spp.* widely spread in natural and artificial environments. [200] The facultative pathogenic *Pseudomonas aeruginosa* is a major cause of chronic infections strongly involved in cystic fibrosis patients and immunocompromised individuals. [201] Various mechanisms including active efflux of antibiotics in bacteria, membrane permeability barrier, enzymatic inactivation/modification of drugs, and/or antibiotic target changes/protection contribute to the high resistance of gram-negative bacteria. [8, 202, 203] Except for its high level of intrinsic resistance, Gram-negative bacteria such as *P. aeruginosa* are able to achieve adaptive antibiotic resistance by living together as biofilms. [204]

Bridge or string-like structures of bacteria colonies were reported in biofilm studies previously. Thus, Jahed et al. used used micropatterned poly(dimethyl siloxane) (PDMS) to form 3D nanostring of microcolonies of *Staphylococcus aureus*.[134] Drescher et al. demonstrated that *Pseudomonas aeruginosa* flowing through microfluidic channels made from PDMS form streamer structure, causing clogging. [185] In our previous study, we used patterned liquid-infused surfaces (LIS) to form arrays of homogeneous biofilm microclusters and observed string-like connections between biofilm patches. [205] Since the string-like structure is observed under highly controlled conditions, it indicates that this phenomenon might be common in nature. The phenomenon of bacterial bridges could help better understand biofilms, complex 3D biofilm structures, functions, or factors that can affect biofilm formation, and the removal of biofilms. It is not clear, how far micro-structures contribute to the formation and adaptation of biofilms.

Bioinspired liquid-infused surfaces (LIS) have been introduced as an antifouling material. [141, 186, 206-211] The solid porous surface of LIS provides its mechanical stability and also stabilizes impregnating oil or lubricant. [139] Due to the liquid nature and smoothness of the liquid-liquid interface at the LIS' surface, bacteria cannot strongly and irreversibly attach to it. [188, 212]

In previous study, detailed structure of biofilm bridges of *P. aeruginosa* was investigated and we showed a spatial distribution of bacteria and biomass in the bridges. [2] It was proposed that the biofilm bridges formed due to the migration or growth of bacteria on the hydrophobic repellent LIS regions. Nevertheless, the mechanism of the bridge formation was not known.

In this study, the pLIS are used to investigate the mechanism of biofilm bridge formation of *P. aeruginosa*. We hypothesize that with the correct understanding of the formation of biofilm bridges, we could control the geometry and distribution of bridges by using preset hydrophilic-superhydrophobic patterns. Such controlled biofilm bridge formation and structuring could be used to understand the biofilm formation and function both in vitro and in vivo. Potentially such bridges could be used for bio-microfluidic applications to study the transfer phenomena through the bridges or in biofilm-involved infections.

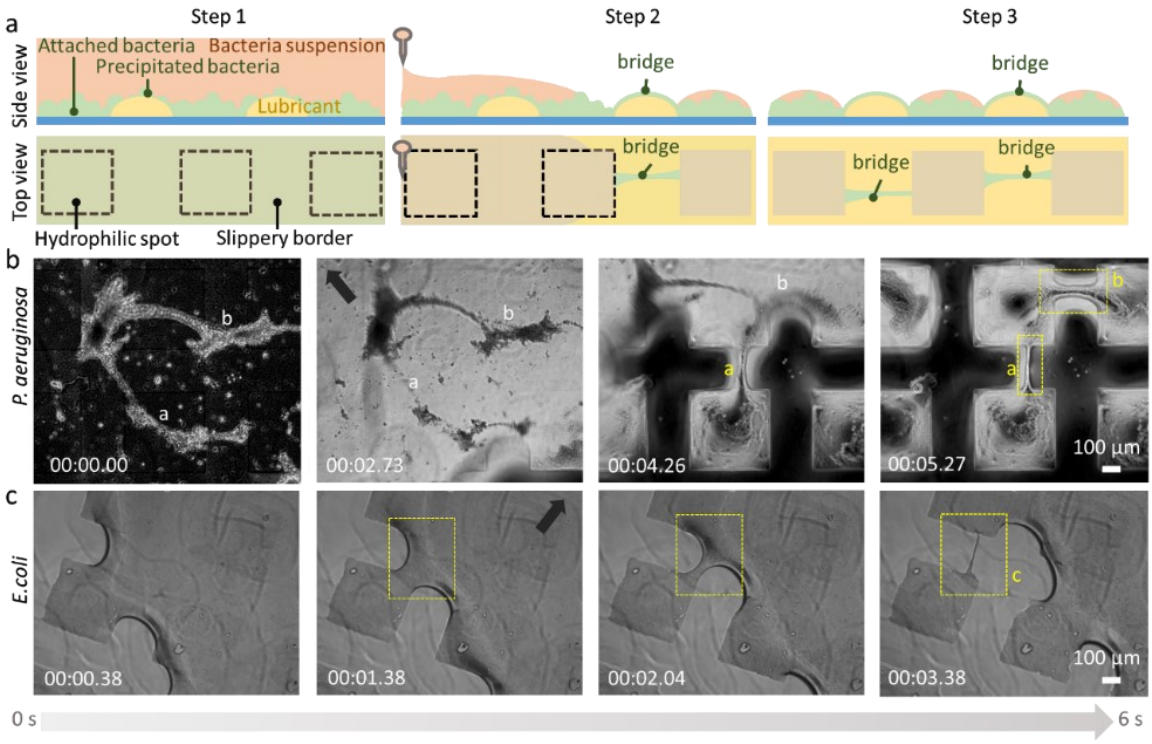

Figure 30. Bacterial bridges form during the dewetting process. (a) Schematic showing the bridge formation during the dewetting process on patterned LIS. (b) Formation of bridges between *P. aeruginosa* PA49 attached to hydrophilic spots over lubricant infused borders. 3D filamentous structure of *P. aeruginosa* PA49 in suspension is marked with "a" and "b" in white. The bridges formed are marked with "a" and "b" in yellow. (c) Formation of bridges between *E. coli* attached to hydrophilic spots over lubricant infused borders. Bridges formed in the area indicated by yellow dashed lines. The bridges formed are marked with "c" in yellow. Direction of liquid retraction from the surface was indicated by black arrows.

3.4.2 Results and Discussion

Formation of biofilm bridges of *P. aeruginosa* and *E. coli* on pLIS

Patterned superhydrophobic–hydrophilic glass slides were used to prepare patterned LIS. The patterned glass slides were firstly immersed into water to form water droplets on hydrophilic spots, and then perfluoropolyether (Krytox GPL 103) was used to spread on the surface to form the lubricant infused borders between the water occupied hydrophilic spots. The excess of the lubricant was removed by dipping the slides into water and flushing the slides with a stream of water until all hydrophilic

spots were exposed to air. The porous structure of the surface, water contact angles and sliding angles of the patterned LIS have been shown in a previous study. [2] Multidrug resistant *P. aeruginosa* PA49 previously isolated from wastewater and *E.coli* DSM1116 were used in this research. [169] Table S1 shows the height of LIS borders is around 10 µm. Previously we showed that string-like biofilm structures were observed between *P. aeruginosa* PA49 attached hydrophilic spots after 3 h incubation in bacteria suspension (Basal Medium 2, BM2). Therefore, incubated surfaces for 3 h were used in this study instead of 24 h. [2] As shown in Figure 30a, there are three steps to achieve bridges on patterned LIS. Firstly, the surfaces were incubated in bacteria suspension for 3 h at 37°C with gentle shaking. During this 3 h, bacteria attached onto the hydrophilic spots. At the same time, bacteria precipitated onto the lubricant infused areas, but they were not able to attached to the lubricant infused borders due to their antifouling property (Figure 30a step 1). Next, the bacteria suspension was aspirated using a peristaltic pump, resulting in the dewetting of the liquid from the LIS areas exposing them to air and at the same time leading to the formation of biofilm bridges connecting bacteria clusters formed in the hydrophilic (adhesive) regions (Figure 30a step 2). Surprisingly, after the supernatant with bacterial suspension was completely gone, bridges remained on the lubricant infused borders (Figure 30a step 3).

Figure 30b and Video S1 show the bridge formation of *P. aeruginosa* PA49 on the surfaces. On the surface incubated with *P. aeruginosa* PA49 for 3 h, the precipitated bacteria layer was found to be heterogeneous with not only small bacterial clusters randomly growing on the surface, but also revealing 3D filamentous bacteria structures stemming from the surface into bacteria suspension (Figure S1, Figure 30b, white a and b). Some of these filamentous structures remained on the surface during the dewetting process, forming bridges (Figure 30b, marked with yellow color a and b). After the bridge formed, a needle was used to break the bridge. As shown in Figure S2a and Video S3, the precipitated bacteria in the bridge were not attached to the LIS border, since the broken bridge shrank towards the hydrophilic area but not remained

still on the LIS border. Figure S2b and Video S4 show that the bridge was not attached to the LIS border after 24 h incubation in air.

E. coli was used in order to investigate the formation of the bacterial bridges using other Gram-negative bacteria. *E. coli* formed a more homogeneous layer on the surface after incubation (Figure 30c, Video S2). When the bacteria suspension was removed, bacteria attached on the hydrophilic squares remained and the bacteria precipitating on the lubricant infused borders were removed, with some of the bacteria left on the surface to form bridges. Even though the precipitated *P. aeruginosa* and *E. coli* layers showed different structure and morphology, bridges formed in both cases during the dewetting procedure.

Figure S2a shows that the bacteria number of initial *P. aeruginosa* PA49 suspension was 4.5×10^7 CFU mL^{-1}. The bacteria number of the supernatant of the bacteria suspension after 3 h incubation decreased to 0.7×10^7 CFU mL^{-1}. After mixing the medium above the surface, the bacteria number of the suspension increased to 3.8×10^7 CFU mL^{-1}. This indicates that a large number of bacteria precipitated on the surface during 3 h incubation. Interestingly, as shown in Figure S2b, there were no bridges formed when the surfaces were incubated vertically in bacteria suspension. It only showed attached bacteria on hydrophilic spots. This suggests that there are two requirements to form bacterial bridges. First, the surface should provide attachable regions for bacteria. Only with LIS itself no bridge could be formed due to its antifouling property. [188] The second requirement is that a certain number of bacteria precipitating on the surfaces is necessary to form bridges. Thus, the formation of biofilm bridges seems to be a consequence of the dewetting process on patterned LIS covered with attached and precipitated bacteria and not due to the growth of biofilm bridges between adhesive clusters as was hypothesized in our previous study. [2]

To understand better the biofilm bridge formation and function, it is important to investigate factors that influence its formation. Thus, we studied how nutrients

present in the bacterial growth medium influence the bridge formation. As shown in Figure S3, no bridge was formed on the surfaces incubated in glucose-free medium, while only few bacteria colonies were observed on the hydrophilic spots. Glucose is important to form extracellular polymeric substances (EPS). [213, 214] Absence of glucose in the medium could affect the filamentous bacteria structures as shown in Figure S3c, leading to less bridge formation. There was no significant difference in the bridge number on the surfaces between samples incubated with or without DNase despite that secreted nucleic acids have been found inside biofilm bridges.[2] With lower bacteria density of the initial cell suspension (10^6 CFU mL^{-1}) no bridges were formed (Figure S3). Thus, it seems that the density of *P. aeruginosa* bacteria at the interface increased by precipitation or because of the initial high concentration increases the ability of bacteria to form such bridges. As we discussed, bacteria attached to hydrophilic areas and precipitated on the surface both contribute to the formation of bridges, thus, we assumed that a certain number of bacteria are required from the initial bacteria suspension to form bridges.

Distance-depended formation of bridges on pLIS

In order to investigate the distance-dependent formation of *P. aeruginosa* PA49 bridges, we cultured bacteria on patterned LIS with variable widths of the lubricant infused regions from 50 µm up to 1 mm keeping the hydrophilic adhesive spots identical (350 µm). Examples of biofilm bridges of up to 700 µm long can be seen (Figure 31), however the number of bridges per square drops significantly from about one bridge per biofilm spot for 50 µm gaps down to about 1 bridge per 20 hydrophilic spots for 700 µm gaps (Figure 31f). With 350 µm hydrophilic spots, 700 µm lubricant infused borders is the limit for the formation of bridges using *P. aeruginosa* PA49. In case of hydrophilic squares (length of square edge = 50, 200, 350, 500 µm) separated by lubricant infused borders of a constant width (200 µm), the bridge number increased from 0.1 per square to 0.7 per square with the increase of the size of hydrophilic squares. Therefore, bridges tend to form over short lubricant infused

border with large adhesive areas. This can be useful for predicting the bridge distribution on patterned surfaces.

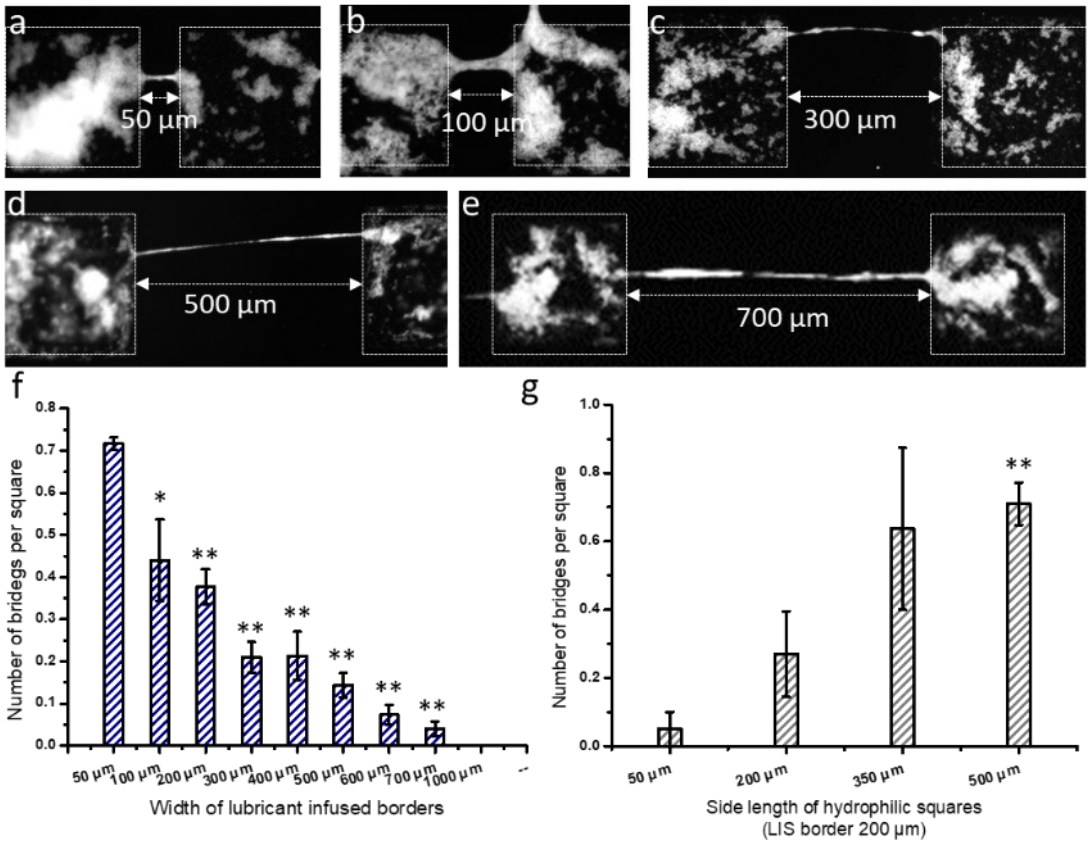

Figure 31. (a-e) Fluorescence images of CTC stained bridges of *P. aeruginosa* PA49 over lubricant infused borders of various widths (from 50 µm up to 1 mm). Side length of hydrophilic bacteria adhesive squares is 350 µm (indicated by white dashed lines). CTC was added into bacteria suspension from the beginning of the incubation. Images were taken after the medium was removed from the surfaces and bridges were formed due to the dewetting of lubricant infused regions. (f) Number of bridges of *P. aeruginosa* PA49 over lubricant infused borders of different widths. Side length of the hydrophilic square is 350 µm. (g) Number of bridges of *P. aeruginosa* PA49 on surfaces with hydrophilic squares of different sizes, while keeping the width of lubricant infused borders the same (200 µm). Data were presented as mean ± SD of three experiments with three repeats each time. The statistical significance of the experimental data was determined with a two-tailed Student t -test (* p -value < 0.05, ** p -value < 0.001).

Control of bridge pattern

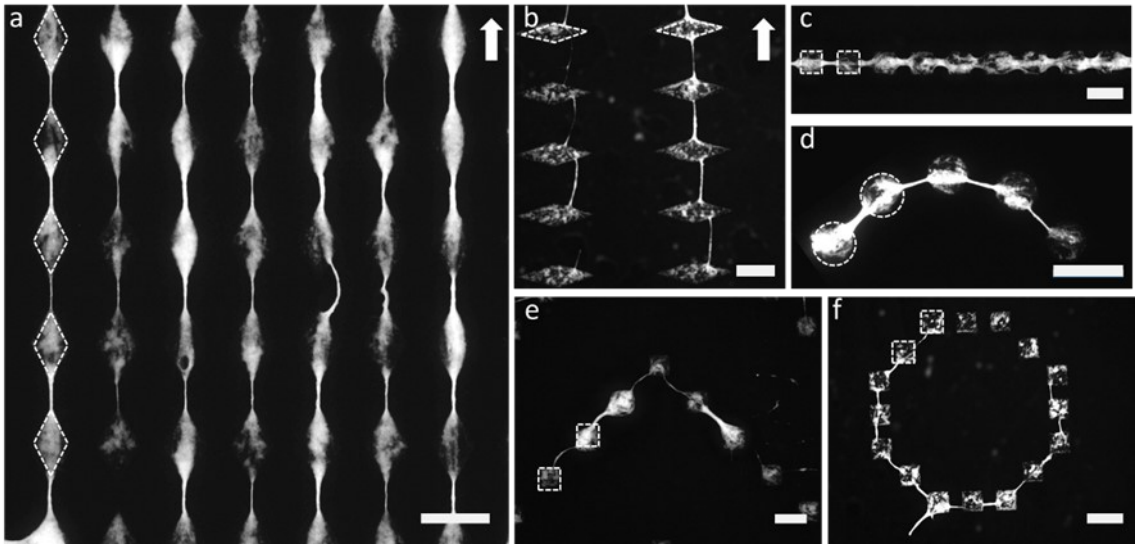

Figure 32. Creating biofilm bridge micropatterns of defined geometry. Fluorescence images of CTC stained bacterial bridges formed by *P. aeruginosa* PA49 on surfaces with predesigned hydrophilic-LIS patterns. Hydrophilic spots are indicated by white dashed lines. CTC was added into bacteria suspension from the beginning of the incubation to facilitate imaging. Images were taken after the medium was removed from the surfaces. White arrows in (a) and (b) indicate the direction of liquid retraction from the surface. Scale bars: 500 μm.

Understanding the mechanism of the formation of biofilm bridges using the geometry of patterned hydrophilic-LIS structures allows us to create complex interconnected structures of biofilm bridges (Figure 32). Since discontinuous dewetting of patterned hydrophilic-LIS surfaces covered with a preincubated layer of bacteria is responsible for the formation of biofilm bridges between the adhesive regions, positioning hydrophilic spots closer to each other enables preferential bridge formation between these structures during the dewetting process (Figure 32a). In addition, since direction of liquid retraction is important for the dewetting process, it could be used to align biofilm bridges to form networks of biofilm bridges with aligned parallel lines along different directions (Figure 32). Figures 32c-f demonstrate the possibility to create single biofilm bridge lines of defined geometry by positioning multiple

hydrophilic spots into a certain pattern on a lubricant infused background. Such architectures might be useful to study biofilm organization and various signaling or transport phenomena within biofilms.

Bacterial bridges as bio-microfluidic channels

In order to investigate continuity of the biofilm bridges, we utilized 1 mm hydrophilic spots (square side length 1 mm, lubricant infused border between squares 500 μm) (Figure 33a). Bacterial bridges were formed by the incubation of patterned LIS with *P. aeruginosa* PA49 for 3 h, followed by removing the medium to form the bridges and either leaving the structures under air (Figure 33b, c) or covering the biofilm bridges with a fluorinated lubricant (Figure 33d, e). 1 μL Rhodamine B solution was added to the first hydrophilic spot (spot 1) and the spreading of the dye solution through the bridges was monitored over time (Figure 33c). Figures clearly demonstrate that the dye is spread through the bridges and does not escape from the bridges´ walls. No fluorescence was observed on the lubricant infused surface outside the bridge structures. This suggests strong hydrophilicity of the bridges and their confinement. The dye reached spot 2 and 3 within a few seconds and covered spot 3 within 2 min. Then the spreading of the dye slowed down and it was observed in spot 4 only after 1 h (Figure 33c). The mechanism of spreading in this case is related to wetting of the hydrophilic bridges with the aqueous dye solution. Then, we also investigated the diffusion of the dye through the bridges confined under an oil. In this case, a layer of lubricant was spread to cover the bacterial bridges as well as biofilm clusters attached to the hydrophilic squares, while keeping one hydrophilic spot exposed to air to be able to add the dye solution (Figure 33d). In this case, the spreading of the dye was significantly slower than in the open system and the dye took 2 h and 24 h to reach and cover spots 2 and 3, respectively. Nevertheless, the spreading clearly demonstrated the continuity of the biofilm bridges connecting hydrophilic spots indicating its potential application to study various transfer phenomena through the bridges or bridges´ functionality in vivo. The average width of the bacterial bridges was 99.4 μm while the smallest width was 18.4 μm (Figure

S4). These microchannels are composed of biomass and bacteria from the bacteria suspension, which makes them fully biological microfluidic channels (bio-microfluidic channels). Here we define "bio-microfluidic channels" as microstructures made of bacterial colonies, which are able to transport fluids.

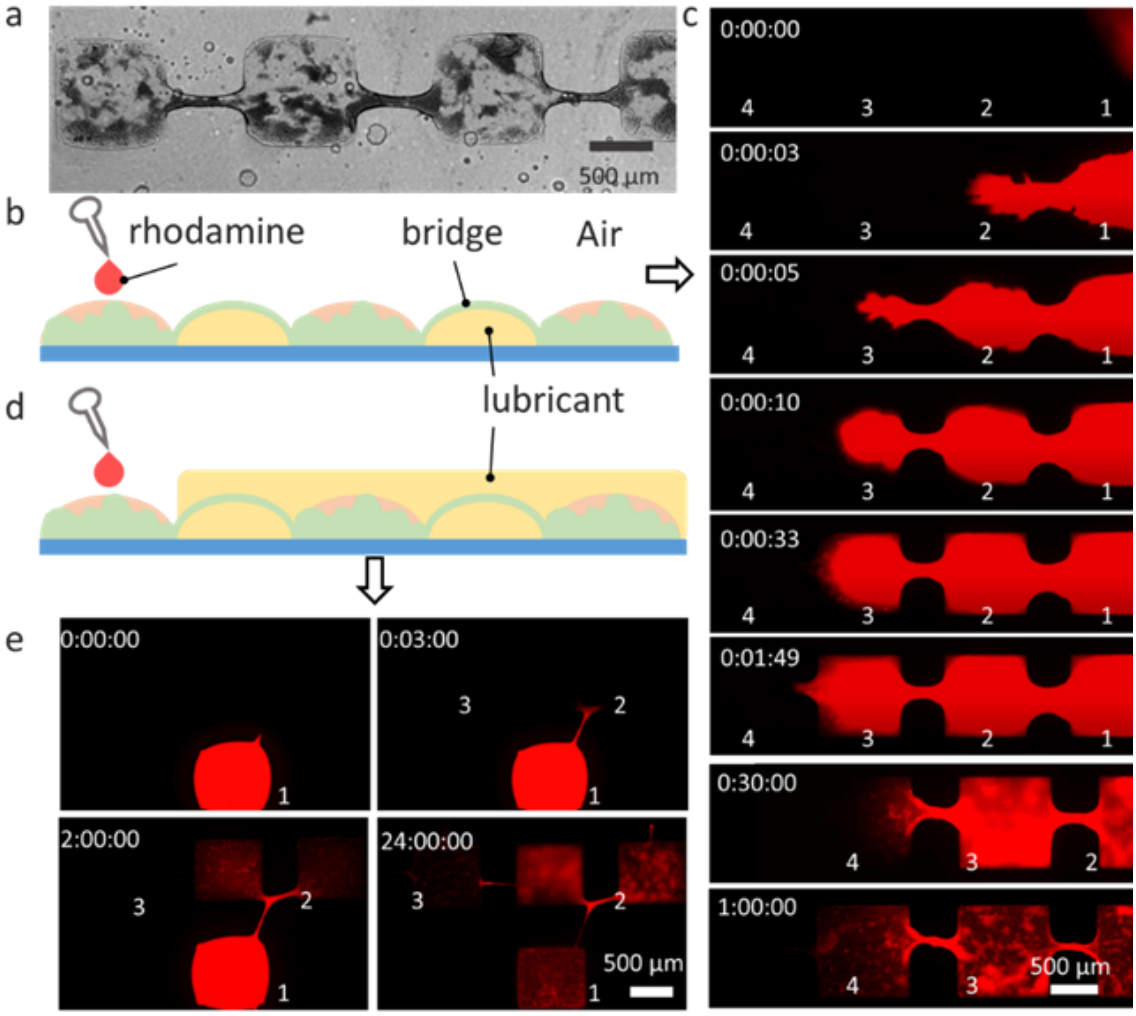

Figure 33. Flow of rhodamine B solution through bridges. (a) Bright field image of *P. aeruginosa* PA49 on hydrophilic spots after the bacteria suspension was removed. (b) Schematic representation of addition of rhodamine B solution on hydrophilic spots. The surface was exposed to air. (c) Snapshot images at different time points showing the transfer of rhodamine B solution (water, 2 mg mL^{-1}) through the bridge of *P. aeruginosa* PA49. (d) Schematic representation of addition of rhodamine B solution on hydrophilic spots. Rhodamine solution was added on one hydrophilic spot with *P. aeruginosa* PA49 which was exposed to the air. The other area around this spot was covered with lubricant. (e)

Diffusion of rhodamine B solution (water, 2 mg mL^{-1}) under lubricant through a biofilm bridge of *P. aeruginosa* PA49. Time format shown in all images (hh:mm:ss).

To further demonstrate the connectivity of bacterial bridges as bio-microfluidics, we used brain heart infusion medium (BHI medium) as nutrient-rich medium and polymyxin B as effective antibiotic to *P. aeruginosa* PA49 and evaluated their influence on bacteria viability after the transfer through bridges as shown in Figure 34a. [170] Water was used as control. Figure 34b shows that the number of living bacteria in spot 3 was influenced by the chemical added in spot 1, which demonstrates that the chemical solution was successfully transferred from spot 1 to spot 3 through bridges. With BHI medium added in spot 1, the number of living bacteria in spot 3 was 11.3×10^7 CFU mL^{-1}, twice as much as the number of living bacteria in spot 3 when water was added in spot 1. No living bacteria were in spot 3 with polymyxin B added in spot 1. However, there was no significant difference of the number of living bacteria in disconnected spot 3', when different chemicals were added in spot 1', suggesting that the solution did not spread to other spots on the surface without bridges. Therefore, the bridges have good connectivity to function as bio-microfluidics. Such bio-microfluidics could be used to study the biofilm formation, heterogeneous structure of biofilms and the spatial variation associated cell behavior. [90, 181, 215] Comparing to the conventional microfluidic system using solid material to fabricate channels, the bio-fluidic channels made of bacterial bridges have the advantage to study bacteria behavior not only on solid-liquid interfaces but also on liquid-liquid interfaces. And it is an open system with no solid boundary. [135, 216] *P. aeruginosa* PA49 used to form bridges is a multidrug-resistant species. [1] Therefore, the bio-fluidic channels can be used to study the drug susceptibility of bacteria/biofilms. In addition, there are biofilm niches in the human body such as biofilm niches in oral cavity and in pulmonary alveoli, which are physically separated, but able to affect each other. [217, 218] With the bridge-formed bio-microfluidic systems, it is possible to study such systems in-vitro, for example, the influence of anti-biofilm compounds on heterogeneous biofilms or the transfer of signals, nutrients between biofilms communities.

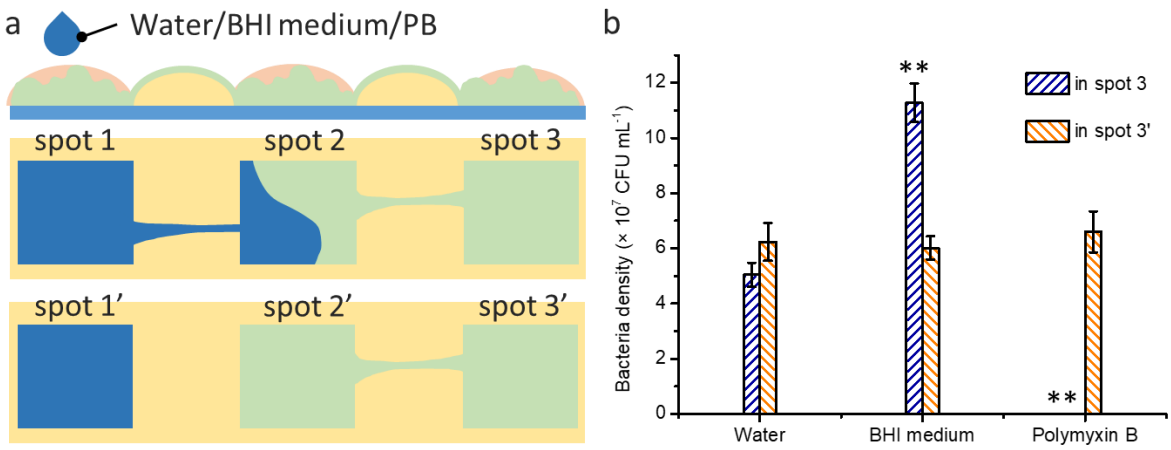

Figure 34. Schematic representation of experiment to study connectivity of the bridges. Side length of hydrophilic spots: 1 mm; lubricant-infused borders: 500 µm wide. Surface was kept under air after the dewetting step of the biofilm bridge formation. 1 µL water, BHI medium or polymyxin B (50 mg mL^{-1}) was added on the hydrophilic spot 1 with *P. aeruginosa* PA49, respectively. (b) The number of bacteria was measured either in the connected spot 3 or disconnected spot 3' 2 h post addition of the solutions to spots 1 or 1′, respectively. Data were presented as mean ± SD of three experiments with three repeats each time.

3.4.3 Summary

Fine control of organization of bacteria or biofilms on surfaces provides great opportunity to study biofilm formation, spreading mechanism or signal exchange between different biofilm colonies. Here we present a strategy to create connective bridge structure between bacterial colonies with defined geometry using patterned lubricant-infused surfaces (pLIS) in a simple dewetting process. We demonstrate that after incubation with bacterial suspensions, bacteria cover the whole surface including lubricant infused borders. During the growth medium removal, discontinuous dewetting leads to the formation of biofilm bridges connecting hydrophilic adhesive hydrophilic spots with irreversibly attached bacterial colonies. The width of lubricant infused borders affects the bridge formation. We demonstrate the possibility to control spatial distribution of bridges by using specific patterns of

hydrophilic spots. Finally, the ability to transfer liquids and dissolved chemicals along the biofilm bridge networks has been demonstrated, which opens a new possibility to investigate the transfer of signals, nutrients, or small molecules through such biofilm structures. Biofilm structures with defined geometry can be used as bio-microfluidic channels to study the fundamental biofilm functionality, the transfer dynamics of pharmaceuticals in medically relevant infectious biofilms or in technical setups where signaling processes impact the stability and function of natural biofilms.

4 Conclusions and Outlook

Within this thesis, droplet-microarray has been applied to solve problems in microbiology, especially in the field of combating multidrug-resistant bacteria. The content of this thesis can be subdivided into two parts:

1) Droplet-microarray was applied as a miniaturized platform of high throughput screening of antimicrobial compounds;

2) Droplet-microarray was used to fabricate patterned liquid infused surfaces to reveal the mechanism of biofilm bridge formation and to spatially control formation of biofilm bridges.

Currently, most conventional platforms of high throughput screening of antimicrobial substances require expensive automation. The high cost of compounds or drug libraries hinders laboratories to investigate new antibacterial agents in a high throughput manner. As a miniaturized high throughput screening platform, droplet-microarray possesses many advantages, including ease of handling, fewer pipetting steps are required, and reduction of reagents. In the first project, an easy and rapid 'droplet sliding' method was used to generate 588 droplets of ~100 nL in seconds containing bacteria, as a benefit of extreme difference of wettability of the patterned hydrophilic-superhydrophobic surface of droplet-microarray. No pipetting was needed in the creation of droplets. Reagents were added into droplets parallelly through a sandwiching approach. No contamination between droplets was observed. The influence of reagents on growth of bacteria can be detected by microscope using a strain producing green fluorescence protein, or applying a staining method. In addition, a visual examination of the turbidity of dried droplets can be used to evaluate the inhibition effects of reagents to bacteria growth. Droplet-microarray was successfully used to screen a small library containing 18 antibiotics to identify the drug resistance of *P. aeruginosa* PA49 isolated from the environment.

In the second project, the working flow of droplet microarray-based high throughput screening was optimized and validated. Multi-resistant *Klebsiella pneumoniae* was used as the target. A non-contact liquid dispenser was used to print compounds onto droplet-microarray first. Then bacteria suspension was printed onto droplet-microarray and incubated with pre-printed compounds. With the help of liquid dispensers, the accuracy of the screening process could be ensured. More importantly, a colorimetric readout method using Cell Counting Kit 8 has been developed. By detecting the color of droplets after staining with Cell Counting Kit 8, compounds presenting positive results, which were colorless, can be easily selected by eyes. Using a cheap paper scanner, the whole droplet-microarray slide can be scanned in six minutes. Scan images enable quantitative evaluation of bacteria growth in droplets by the analysis of color depth of droplets with a MATLAB program. Three candidates of hits have been selected from screened 608 compounds. Further, 3,000 synthesized compounds from the ComPlat library are going to be screened using the droplet microarray-based high throughput system to find hit compounds against *K. pneumoniae*.

Table 1. Direct comparison between droplet-microarray and 384-well plates

	Droplet-microarray	**384-well plate**
Working volume	~ 150 nL per spot	~ 40 µL per well
Amount of reagents (final concentration 10 µM)	1.5 nmol per spot	400 nmol per well
Density of experiment per cm^2	49	4
Time used for the whole assay (152 compounds)	3 days	3 days
Equipment for readout	Paper scanner	Fluorescence microscope/microplate reader
Price of reagents (FDA-approved Drug Library as an example) FDA-approved Drug Library | Targetmol | 96-well	30.00 USD	7180.00 USD

Droplet-microarray was further applied to fabricate patterned liquid infused surfaces. To prepare patterned biofilms with different bacteria, a lubricant containing perfluoropolyether was used to create 'slippery' regions to resist attachment of bacteria by infusing the lubricant into superhydrophobic area of the patterned hydrophilic-superhydrophobic surface of droplet-microarray. Biofilm patterns down to 350 µm were achieved. Between the biofilm patterens, a connection structure, termed 'biofilm bridges' was observed. It was shown that this bridge formation was a ubiquitous structure on patterned liquid infused surfaces for different bacteria including *P. aeruginosa*, *S. maltophilia*, and *S. aureus*. *P. aeruginosa* PA49 presented the highest number of biofilm bridges on surfaces compared with *P. aeruginosa* PA 30 and the other bacteria. By staining with 5-cyano-2,3-ditolyl tetrazolium chloride and 4',6-diamidino-2-phenylindole, it was observed that metabolic active bacteria were surrounded by the biofilm matrix in bridges. With fluorescence in situ hybridization, organisms' distribution in bridges of multi-species biofilms were presented. *S. maltophilia* and *P. aeruginosa* did not mix homogeneously but formed spatial segregation in biofilm bridges.

In the following project, *P. aeruginosa* and *E. coli* were used to reveal the mechanism of bridge formation It was demonstrated that after incubation of patterned liquid infused surfaces with bacterial suspensions, bacteria covered both liquid infused borders and hydrophilic regions. However, on the liquid infused regions, bacteria were not able to attach to the surface. Biofilm bridges were formed during the removal of growth medium from the surface. The distance of liquid infused borders affected the bridge formation. Biofilm bridges were observed with the distance up to 700 µm between 350 µm size patterns. By altering the geometry of patterns and distance between patterns, the number of bridges and distribution of bridges can be changed. Then this strategy was used to control the connective bridge structure on patterned liquid infused surfaces. It is shown that biofilm bridges formed networks along different directions.

Finally, the continuity of biofilm bridges was investigated. Rhodamine solution was added to hydrophilic spots, where biofilm attached. Then the spread of rhodamine through the bridges was observed with the fluorescence microscope. Due to the hydrophilicity of biofilm bridges and the hydrophobicity of the liquid infused regions, aqueous dye solution was restrained in bridges. Rhodamine solution was able to reach neighboring hydrophilic spots in a few minutes. Next, it was shown that Mueller-Hinton medium, which supports growth of bacteria, and polymyxin B solution, which is able to kill *P. aeruginosa*, can be transferred through biofilm bridges respectively and influence the viability of bacteria. The control of distribution of biofilms on surfaces provides great opportunity to study the transfer dynamics of pharmaceuticals in biofilms, biofilm formation and spreading mechanism, and signal exchange between different biofilm colonies, etc.

The present study lays the groundwork for future research into droplet microarray-based high throughput in microbiology. As far as I concerned, that the following points should be explored in future:

1) The target of screening could be altered.
   Up to now, the high throughput screenings with droplet-microarray use planktonic bacteria as targets. The compounds able to inhibit the growth of planktonic bacteria are screened. No anti-biofilm assay was established on droplet-microarray. Anti-biofilm compounds would be clinically relevant since biofilms are a major cause of persistent infections, and they are difficult to eliminate in patients. The study on biofilm bridges is helpful to prepare miniaturized biofilms on droplet-microarray. Corresponding characterization methods of biofilms on DMA should be established, e.g., colorimetric methods, fluorescence staining methods, MALDI-ToF measurements, PCR and sequencing, etc.
2) Detailed and fundamental knowledge of ‘bacteria in droplets’ and ‘biofilms in droplets’ should be studied.

Although it has been demonstrated that droplet-microarray could be used in antibacterial screening, it is still not clear, e.g., the effect of small volume on biofilm formation, the formation of floating biofilms on liquid-air interfaces of droplets, the absorption of substances by the substrate of droplet-microarray, the dissolving process of compounds from surfaces into droplets, etc. That information is significant for future applications of droplet-microarray in antibacterial assays.

3) Droplet-microarray could be used to investigate synergistic effects between drugs against multidrug resistant bacteria, which is a promising direction to find new therapies for infections from existing drugs. Then an efficient and accurate data analysis process should be established for the combinatorial drug screening.

5 Experimental Section

5.1 Materials and Instruments

Patterned superhydrophobic-hydrophilic glass slides (7.5 × 2.5 cm) were obtained from Aquarray GmbH (Eggenstein–Leopoldshafen, Germany). Ethanol, potassium phosphate, $(NH_4)_2SO_4$, $MgSO_4$, $FeSO_4$, NaOH, HCl and glucose were from Merck (Darmstadt, Germany). Müller–Hinton (MH) medium was purchased from Merck (Darmstadt, Germany). Glass slides (Nexterion Glass B) were purchased from Schott (Jena, Germany). (1*H*, 1*H*, 2*H*, 2*H*-perfluorooctyl) silane was purchased from Sigma-Aldrich (Munich, Germany). 5-Cyano-2,3-ditolyl-tetrazolium chloride (CTC) was purchased from Polysciences Europe GmbH (Hirschberg an der Bergstrasse, Germany). Ciprofloxacin was purchased from Fluka (Seelze, Germany). Ceftazidime and tazobactam were purchased from ACROS ORGANICS (Geel, Belgium). Tobramycin, cefotaxime, amoxicillin, ampicillin, polymyxin B, methicillin, colistin sulfate, ceftazidime, erythromycin, kanamycin sulfate, sulfamethoxazole and tetracycline were purchased from Sigma-Aldrich (Munich, Germany). Piperacillin was purchased from Alfa Aesar (Kandel, Germany). Imipenem and meropenem were purchased from Cayman Chemical Company (Michigan, USA). Chloramphenicol was purchased from AppliChem (Darmstadt, Germany). Streptomycin was purchased from Carl Roth (Karlsruhe, Germany). 4′,6-diamidino-2′-phenylindole dihydrochloride (DAPI) was from Sigma-Aldrich (Germany). Brain Heart Infusion (BHI) medium was purchased from Merck (Darmstadt, Germany). DNase was purchased from Peqlab (Erlangen, Germany). For Fluorescent In Situ Hybridization (FISH), we utilized 16S rRNA-targeted oligonucleotide probe Stemal (purchased from Eurofins) for *S. maltophilia*. The probe was labeled with ATTO550 at the sequence (5'-3') of the probe sequence (GTCGTCCAGTATCCACTGC). For *P. aeruginosa*, we utilized 16S rRNA-targeted oligonucleotide probe PseaerB (purchased from Eurofins). The probe was labeled with AT488 at the sequence (5'-3') of the probe sequence (TCTCGGCCTTGAAACCCC). FluoSpheres™

Carboxylate-Modified Microspheres, 1.0 µm, red fluorescent (580/605), 2% solids were purchased from ThermoFisher Scientific (Germany). Krytox GPL 103 (Dupont KrytoxR GPL 103) was purchased from H Costenoble GmbH & Co. KG (Eschborn, Germany). Cell Counting Kit-8 was purchased from MedChemExpress (New Jersey, USA).

The AxioImage M2 system equipped with an Apotome (Carl Zeiss, Oberkochen, Germany) was used for fluorescence microscopy. A DSA 25 contact angle goniometer (Krüss, Hamburg, Germany) was used for water contact angle measurement. The I-DOT non-contact liquid dispenser was purchased from Dispendix (Stuttgart, Germany). LEO 1530 Gemini scanning electron microscope (Zeiss, Jena, Germany) was used to take images of the substrate of patterned LIS. CanoScan 8800F was used to scan DMA slides. Non-contact liquid dispenser SciFlexarrayer S11 (Scienion AG, Germany) and I-DOT (CELLINK, Stuttgart, Germany) were used to print compounds on DMA. Non-contact liquid dispenser I.DOT MINI (CELLINK, Stuttgart, Germany) was used to print bacteria suspension.

5.2 Experimental Procedures to Chapter 3.1

Bacterial strain, medium preparation, and culture conditions

Pseudomonas aeruginosa strain PAO1 was used as a screening target in this study. [200] This strain was tagged by introducing plasmid *pUCP20::GFP* by electroporation, resulting in the production of the green fluorescent protein (GFP) to facilitate monitoring of *P. aeruginosa* PAO1 pUCP20::GFP (designated *P. aeruginosa* PAO1 GFP) by fluorescence microscopy. *P. aeruginosa* PAO1 GFP was routinely grown in Müller–Hinton (MH) broth medium overnight at 37°C. The bacterial suspension was adjusted to OD_{600} = 0.1 with minimal medium Basal Medium 2 (BM2) and then diluted 1:100 with BM2 medium to obtain a bacterial suspension of 10^6 colony forming units CFU mL^{-1}. *Pseudomonas aeruginosa strain* PA49 (designated *P. aeruginosa* PA49) was cultured in BM2 medium overnight at 37°C. The bacterial suspension was adjusted to OD_{600} = 0.1 with BM2 and then diluted 1:100 with BM2 medium to obtain a bacterial suspension of 10^6 CFU mL^{-1}.

Seeding and culture of bacteria on the DMA slide

1.5 mL of solution was added to one of the three compartments of squares on the DMA slide ensuring that all 196 spots were covered. The droplet was left to stand for 30 s to allow the bacteria to settle. The slide was then quickly tilted and the droplets (approximately 90 nL) containing an estimated 90-900 bacteria formed spontaneously as the liquid flowed away.

For incubating bacterial cells, the DMA slide was placed inside a Petri dish within a box with wetted tissues that was closed to prevent evaporation. The box was placed in an incubator at 37°C and the bacteria were cultured for the required period.

To calculate the volume of droplets on the DMA, we first prepared droplets on DMA slides. The height (H), contact angel (θ) and radius (r) of droplets were measured with an DSA 25 contact angle goniometer (Krüss, Hamburg, Germany). Then the volume

of the droplets was then calculated based on the assumption that the droplets formed part of a spherical cap.

To enumerate the bacteria on DMA slides, one of the three compartments in the DMA slide, which contained 196 bacterial droplets on its surface, was immersed into 20 mL BM2 medium and vortexed for 60 s. The suspension was then serially diluted with cell wash buffer and 10 µl of the dilutions were seeded on Luria broth (LB) agar plates. After incubation for 24 h at 37°C, the colony number on LB agar plates was recorded and used to estimate the number of bacteria on the DMA slide. Details of the estimation are shown in the supporting information.

Printing of antibiotics onto fluorinated glass slides

Glass slides were cleaned by immersion in 1 M NaOH solution for 1 h, washed with water for 30 s, and then immersed in 1 M HCl for 30 min. After washing with water for 30 s, the cleaned glass slides were fluorinated by incubation overnight with 30 µL trichloro (1*H*, 1*H*, 2*H*, 2*H*-perfluorooctyl) silane in a pressurized (50 mbar) desiccator. Antibiotics were printed onto the slides using the I-Dot non-contact liquid dispenser. The antibiotics ceftazidime, tobramycin, ampicillin, vancomycin, tetracycline, piperacillin, erythromycin, amoxicillin, and carbenicillin were dissolved in DMSO (2 mg mL^{-1}) whereas ciprofloxacin, polymyxin B, imipenem, and meropenem were dissolved in sterile water (2 mg mL^{-1}). Further dilutions were performed with sterile water to obtain the appropriate amount of antibiotics per square with a printable volume ranging between 5 nL and 100 nL. After printing with antibiotics, the fluorinated glass slides were dried in air to remove traces of DMSO.

Sandwiching DMA with preprinted antibiotics

To expose the bacteria to antibiotics, an antibiotic pre printed slide was sandwiched with the DMA slide using the CellScreenChip (CSC, as described in Figure S1). This novel instrument allows the precise alignment of two glass slides while controlling the distance between them. The DMA slide and the antibiotic printed slide were clamped into the lower and upper frames of the CSC, respectively. The distance

between the two frames was controlled by four micro-screws, fixed at a specific height. This distance was adjusted depending on the height of the droplets, which is influenced by the size of the microarray pattern. The CSC was closed and aligned by four pillars located at the corners of the lower frame that are positioned to align with four reference holes in the upper frame. In this way, the bacteria-containing droplets on the DMA slide were placed in contact with the antibiotic imprinted slide without excess pressure. Since the antibiotics are printed in a specific pattern correlating to the DMA slide, the mirror image of the printed pattern was observed on the DMA slide after sandwiching. Sandwiching was carried immediately after the bacteria were seeded and to prevent evaporation, the sandwiched slides were placed in a humidified chamber during the stamping process. All experiments were conducted at 37°C with a stamping time of 20 min.

Bacteria staining

Using the I-Dot non-contact liquid dispenser, 5-cyano-2,3-ditolyl-tetrazolium chloride (CTC) solution (4 mM freshly prepared in medium) was printed onto a fluorinated glass slide (90 nL per spot). The CTC-stained slides were dried overnight and then exposed to bacteria using the same method used to transfer antibiotics; the stamping time was 10 min. After the addition of CTC, DMA slides loaded with bacteria-containing droplets were incubated for 3 h at 37°C.

Imaging and analyzing growth of bacteria

Before imaging, the DMA slide was dried for 10 min in the dark at room temperature to allow the bacteria to accumulate in a layer on the surface. Images of *P. aeruginosa* PAO1 GFP and CTC-stained *P. aeruginosa* PAO1 GFP were obtained manually with the Zeiss Axio Imager 2 microscope. To compare the fluorescence from bacteria in droplets on DMA slides and in 96-well plates, we transferred the bacteria suspension from the 96-well plate onto DMA slides to form droplets. After drying, squares on DMA slides were imaged.

ImageJ was used for image analysis. The mean fluorescent intensity of hydrophilic squares (1,000 × 1,000 pixels per square) was measured. The mean intensity per pixel of the background was subtracted from this value to calculate the mean intensity produced by the GFP synthesized inside the bacteria. The background was detected on the superhydrophobic border within a square of 100 × 100 pixels.

Time-kill assay of antibiotic on *P. aeruginosa* PAO1 on DMA surface

To investigate the kinetics of antibiotic activity on DMA slides, we incubated suspensions of *P. aeruginosa* PAO1 (initial bacterial density OD_{600} = 1, 10^9 CFU mL^{-1}, BM2 medium) with polymyxin B (40 μg mL^{-1}) for a predetermined time (5, 10, 15, 30, 60, 120, 180, and 240 min) in a 96-well plate (100 mL) and on a DMA slide (90 nL per droplet). To enumerate the bacteria on DMA slides, one of the three compartments in the DMA slide, which contained 196 bacterial droplets on its surface, was immersed into 20 mL BM2 medium and vortexed for 60 s. The suspension was then serially diluted with a cell wash buffer and 10 μL of the dilutions were seeded on Luria–Bertani broth (LB) agar plates. After incubation for 24 h at 37°C, the colony number on LB agar plates was recorded and used to estimate the number of bacteria on the DMA slide. The number of bacteria per well in the 96-well plate was estimated in the same way following a culture of 17.6 μL of bacteria suspension.

Screening of antibiotics on DMA surfaces with multi-drug resistant strain *P. aeruginosa* PA49

Antibiotics (Table S2) were printed onto fluorinated glass slides using the I-Dot. The amount printed was calculated according to the MIC and the droplet volume (90 nL for 1 mm squares). *P. aeruginosa* PA49 suspension (10^6 CFU mL^{-1}) was seeded onto DMA slides, which were then sandwiched with the antibiotic printed glass slides using the CSC instrument. The two surfaces were sandwiched at 37°C for 20 min before the antibiotic printed glass slide was removed and the DMA surface was incubated at 37°C for 24 h. The same screen was performed in a 96-well plate, with

antibiotics added directly into bacterial solution (100 μL) to obtain the same concentration as that of the bacterial droplets on the DMA surface. The solutions were then incubated at 37°C for 24 h. After incubation the DMA surface was dried in air for 10 min.

Statistical analysis

All data were represented as mean ± SD of at least three individual repetitions for each experiment.

5.3 Experimental Procedures to Chapter 3.2

Printing of compounds on DMA slides

All compounds from the ComPlat library were dissolved in DMSO of concentration 10 mM. 1.5 nL compound solution was printed onto individual hydrophilic spots by SciFlexarrayer S11. DMA printed with compounds were placed in a desiccator overnight at room temperature (~ 25 °C). Then the slides were removed from the dessicator for bacteria printing. For experiments with antibiotics, antibiotics (ceftazidime pentahydrate, amoxicillin, and chloramphenicol) were firstly dissolved in DMSO of concentration 1 mg mL^{-1}. Then solutions were diluted to proper concentration with DMSO for further printing. Colistin sulfate was dissolved in water of concentration of 1 mg mL^{-1} and then diluted for further printing. DMA printed with antibiotics were processed in the same way with DMA printed with testing compounds.

Live/dead staining of bacteria

Colonies of *Klebsiella pneumoniae* ATCC BAA-2146 were picked up from LB agar plates and inoculated into MH medium for overnight culture. 150 nL bacteria suspension of the overnight culture was printed on individual hydrophilic spots on DMA slides. Then 10 droplets were collected by pipetting to 0.1 mL MH medium and stained with 0.15 μL SYTO9 and 0.075 PI solution from the LIVE/DEAD™ BacLight™ Bacterial Viability Kit. After 15 min incubation in the dark at room temperature, stained bacteria suspension was removed to microscope slides and observed with epifluorescence microscope. Live/dead staining of initial bacteria suspension was processed in the same way as printed bacteria suspension.

Colony counting tests of bacteria

150 nL of bacteria suspension of determined density was printed on individual spots on DMA. Individual droplets of bacteria suspension on DMA were then removed by pipetting to 1 mL cell wash buffer and diluted to proper bacterial density. Afterwards,

10 µL of prepared suspension was inoculated to MH agar plates and incubated statically at 37 ℃ for 18 h. Colony number of inoculated bacteria was counted, which was used to calculate the bacteria density in droplets.

Printing of bacteria on DMA slides

Colonies of *Klebsiella pneumoniae* were picked up from LB agar plates and inoculated into MH medium for overnight culture. The optical density of cultured bacteria suspension was measured. Bacteria suspension was diluted with MH medium to the calculated OD_{600} value = 0.001, corresponding to 1.2×10^6 CFU mL^{-1}. 150 nL prepared bacteria suspension was printed onto individual spots on DMA using liquid dispenser I.DOT MINI. Then DMA slides with compounds and bacteria were incubated statically at 37 ℃ for 18 h. To prevent evaporation, DMA slides were placed in a sealed box, with a piece of wet tissue inside to create high humidity.

Colorimetric readout method using Kit8

After incubation of DMA slides, 100 nL of Cell Counting Kit-8 solution was printed to individual droplets on DMA slides with I.DOT MINI. Then slides were incubated for another 1 h in the humidity box. Afterwards, DMA slides were placed into a paper scanner to scan the whole slide using the positive-film scan function. High resolution images (6400 dpi) were generated for next data analysis.

Color depth of each droplet was analysed with MATLAB R2020b using a program provided by Prof. Markus Reischl.

Statistical analysis

All data is presented as mean ± SD. Experiments were at least repeated three times individually using $n \geq 3$ repetitions.

5.4 Experimental procedures to Chapter 3.3

Preparation of pLIS

Patterned superhydrophobic-hydrophilic glass slides were dipped into 70% ethanol for 10 min. After drying, the slides were dipped into DI water to form droplets in hydrophilic regions, which were separated by superhydrophobic regions without water. After that, a thin layer of Krytox GPL 103 was spread over the surface to cover the whole slides but only penetrate the hydrophobic regions. The extra Krytox liquid was removed by dipping the slides into water for 20 times and flushing with a stream of water for 30 s.

Biofilm formation on pLIS

Pseudomonas aeruginosa (PA30, PA49) isolated from environmental wastewater, *Stenotrophomonas maltophilia* DSM50170 (*S. maltophilia*) and *Staphylococcus aureus* DSM20231 (*S. aureus*) liquid cultures in Brain Heart Infusion (BHI) medium (1:4 water dilution) with optical density of 600 nm was 0.1 were prepared. To form biofilms, patterned LIS slides were immersed into bacterial suspension and incubated for determined times at 37 °C with 50 rpm shaking for a better nutrient distribution. In parallel biofilms were also cultivated under static conditions without shaking. Biofilm bridging did also occur under these conditions in a comparable way (Supporting Information). The medium was refreshed every 24 h. Slides were washed with buffer (5×10^{-3} M magnesium acetate, 10×10^{-3} M Tris-base, pH = 8) after incubation of defined periods of time. To stain with 5-cyano-2, 3-ditolyl-tetrazolium chloride (CTC) and 4′, 6-diamidino-2′-phenylindole dihydrochloride (DAPI), slides were firstly immersed into a CTC solution (4 mM freshly given to the medium) for 3 h at 37 °C with 50 rpm shaking or without shaking, according to previous incubation condition. After that, the slides were put into DAPI solution (1 μg mL^{-1}, water solution) and incubated for 10 min. Epifluorescence microscopy with AxioImage M2 imaging system was applied to observe and take images of biofilms and bridges. To quantify the biofilm bridges, the number of bridges per area (cm^2), width of bridges

in the middle, and length of bridges in images were counted and measured with ImageJ software. At least 20 images for each sample were taken with the microscope and 5 samples for each bacterial species for statistics.

For bacterial bridges analysis, 1000 folds magnification and Z-stacks were applied to obtain the images of stained biofilm bridges of *P. aeruginosa* PA49.

To stain the biofilm bridges with 1 μm carboxylate-modified microspheres loaded with red dyes, the patterned LIS were incubated in BM2 medium with or without *P. aeruginosa* PA49 (optical density of 600 nm was 0.1) for 24 h at 37 °C. The samples were then stained with DAPI for 10 min as described above. After washing with DI water for three times, 10 mL of the solution of the microbeads (10^5 mL^{-1}, water solution) was added to the sample, followed by 10 min incubation. The samples were taken out of the medium and imaged by epi-fluorescence microscopy.

Formation of biofilm bridges of multiple species bacteria on pLIS and FISH staining

Mixture suspension of *P. aeruginosa* PA49/*S. maltophilia* (DSM50170) (v/v = 1:1) and *P. aeruginosa* PA30/*S. maltophilia* (DSM50170) (v/v = 1:1) were prepared with initial concentration of each species suspension were all the same (OD_{600} = 0.1). LIS samples were incubated in bacteria suspension for 24 h with 50 rpm shaking at 37 ℃. Then samples were removed from the solution, washed, fixed, and treated with FISH hybridization buffer. The samples were fixed with 4% paraformaldehyde solution (in PBS buffer, pH = 7.4) for 1 h at room temperature. Then samples were immersed into lysozyme solution (70,000 U mL^{-1} in Tris-HCL pH = 7.5) for 10 min at 37 ℃. After the fixation and permeabilization, samples were adjusted in hybridization buffer with adequate formamide concentration (0.9 M NaCl, 20 mM Tris-HCL, pH = 7.5, 0.01% SDS, 30% formamide) for 10 min at 46 °C. Samples were immersed in 500 μL of the same solution previously mixed with FISH probes (purchased from Eurofins) for 1.5 - 3 h at 46 °C. The concentration of probes was 6 ng oligonucleotide μL^{-1}. Finally, the samples were immersed in a cell wash buffer for 10 min at 46 °C. After washing with the wash buffer again, the samples were imaged by epi-fluorescence microscopy.

Quantification of biofilm occupation and bridges

DAPI staining presenting DNA (biomass) in biofilm was quantified as biofilm occupation. Binary images were produced using ImageJ software and were inverted to make the biofilms show black or gray color. Then the threshold-adjusting option of ImageJ software was used to choose the biofilm occupation area (DAPI staining). To make sure all DAPI staining areas were chosen for further calculation; we adjusted the threshold to the level, which was able to include all pixels appearing gray or black (not white). Then the biofilm occupation is

$$\boldsymbol{biofilm\ occupation}\ (\%) = \frac{\boldsymbol{area\ of\ DAPI\ staining\ in\ one\ hydrophilic\ square}}{\boldsymbol{total\ area\ of\ one\ hydrophilic\ square}} \times \mathbf{100}\ \%$$

Number of bridges on LIS was visually counted with fluorescence images. Distance between two edges of the middle part of the bridge was calculated as the width of bridges with the distance measuring option of ImageJ software. Distance from one end to another end of bridges in hydrophilic spots was calculated as length of bridges with the distance measuring option of ImageJ software. At least 10 images were analyzed for each sample.

Statistical analysis

All data is presented as mean ± SD. Experiments were at least repeated twice individually using $n \geq 5$ repetitions. All data was analyzed with two-sided Student's t-test using OriginPro (OriginLab Corporation) software. Data with P-values <0.05 were considered statistically significant.

5.5 Experimental procedures for Chapter 3.4

Preparation of pLIS

Patterned LIS was prepared as previously described. [2] Patterned superhydrophobic-hydrophilic glass slides were sterilized by dipping into 70% ethanol for 10 min. After drying in air, the slides were dipped into deionized water to form droplets in hydrophilic regions. A thin layer of Krytox GPL 103 was spread over the slides to cover the droplets of water in hydrophilic regions and infused into the hydrophobic regions. Then the extra Krytox lubricant was immediately removed by dipping the slides into water for 20 times and flushing with a stream of water for 30 s.

Formation of bacterial bridges on pLIS

Pseudomonas aeruginosa strain PA49 (*P. aeruginosa* PA49) isolated from environmental wastewater and *Escherichia coli* DSM 1116 (*E. coli*) were used in this study. [169] *P. aeruginosa* PA49 and *E. coli* were inoculated in Basal Medium 2 (BM2; 62×10^{-3} M potassium phosphate, 7×10^{-3} M $(NH_4)_2SO_4$, 2×10^{-3} M $MgSO_4$, 10×10^{-6} M $FeSO_4$, and 0.4% glucose) separately and incubated at 37 °C with shaking (150 rpm) overnight. The overnight culture suspensions of two bacteria were then adjusted to optical density (OD) of 0.1 ($\approx 1 \times 10^7$ bacteria per mL) with BM2 medium. Patterned LIS slides were immersed into bacterial suspension and incubated at 37 °C with 50 rpm shaking for 3 h. To show the metabolic activity of bacteria, CTC was added into BM2 medium (4×10^{-3} M) from the beginning of the incubation. Slides in the medium were observed with a microscope after incubation. Then the medium was removed with a pump set up (extraction speed: 2 mL min^{-1}) to form bridges. Samples were observed with the microscope. To investigate the influence of glucose, BM2 medium without glucose (62×10^{-3} m potassium phosphate, 7×10^{-3} M $(NH_4)_2SO_4$, 2×10^{-3} M $MgSO_4$, 10×10^{-6} M $FeSO_4$) was used for incubation. To investigate the influence of bacterial density on bridge formation, overnight culture of *P. aeruginosa* PA49 was adjusted to (OD) of 0.01 ($\approx 1 \times 10^6$ bacteria per mL) and used for the following incubation. To investigate the influence of DNase on bridge

formation, DNase (4 U mL^{-1}) was added into the bacteria suspension from the beginning of the incubation. Bacteria suspension was then extracted after 3 h to form bridges.

Rhodamine B, and antibacterial chemicals flowing through bridges

Patterned LIS were incubated with *P. aeruginosa* PA49 suspension ($\approx 1 \times 10^7$ bacteria per mL, BM2 medium) at 37 °C with 50 rpm shaking for 3 h. Then the medium was removed to form bridges. 1 μL Rhodamine B water solution (2 mg mL^{-1}) was placed on the hydrophilic spots with grown biofilm. The flow of rhodamine solution was recorded with the epifluorescence microscope (Axioplane 2, Carl Zeiss, Oberkochen, Germany). To investigate the flow of Rhodamine B under lubricant, the surface including the formed bridges were covered with a layer of Krytox GPL 103 again, with only one hydrophilic spot exposed to air. Then 1 μL rhodamine B water solution was placed on the hydrophilic spot with biofilm again. The flowing of rhodamine B from this hydrophilic spot to the other spots through bridges was recorded with a microscope.

To investigate the transfer of nutrients and antibacterial chemicals through bridges. 1 μL of BHI medium, water and polymyxin B (50 mg mL^{-1}) was added in one spot respectively. The samples were placed in a box with high humidity and incubated for 2 h. The number of living bacteria in the neighboring spots was counted with plate count method, which means 1 μL of bacteria suspension was aspirated from the spot, then the bacterial suspension was diluted to proper density. Diluted bacteria suspension was spread on LB agar plates and incubated overnight. Colony number on agar plates was counted and then the number of living bacteria in the initial spot was calculated.

Statistical Analysis

A two-sided Student's t-test was used for statistical data evaluation. Experiments were at least repeated three times using $n \geq 3$ samples. The statistical significance of

the experimental data was determined with a two-tailed Student t -test (* p -value < 0.05, ** p -value < 0.001).

6 Appendix

6.1 List of Figures

6.2 Supporting Information

6.2.1 Supporting Information of Chapter 3.1

Table S1. Water contact angle of hydrophilic area and superhydrophobic area on DMA slides.

	Advancing water contact angle	Receding water contact angle	CA hysteresis
Hydrophilic area	23.1°± 4.0°	0°	23.1°± 4.0°
Super-hydrophobic area	172.0°± 5.4°	163.3°± 4.2°	8.6°± 5.1°

The water contact angle of DMA surfaces was analyzed with DSA 25 contact angle goniometer (Krüss, Germany) using the sessile drop technique. Advancing contact angles were obtained by measuring the angle while the liquid was slowly added at a rate of 0.1 mL s^{-1} from a ~4 μL droplet to 14 μL in contact with the sample and a micrometer syringe. Receding contact angles were obtained with liquid slowly retracting at a rate of 0.1 mL s^{-1} from a ~14 μL droplet to 4 μL. The data were represented as mean ± SD. For each kind of surface, the dynamic water contact angle was measured with 9 spots from three different slides (three spots from each slide).

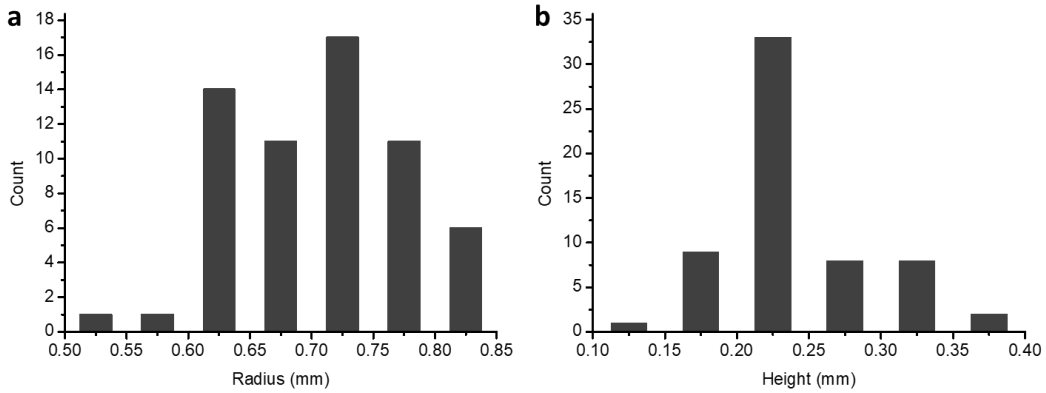

Figure S1. (a) Distribution of the radius of droplets formed on DMA slides. (b) Distribution of the height of droplets formed on DMA slides. 61 droplets of BM2 medium formed on three DMA slides were randomly chosen and images of the droplets were obtained using DSA 25 contact angle goniometer (Krüss, Germany). Radius and height of the droplets were measured using ImageJ.

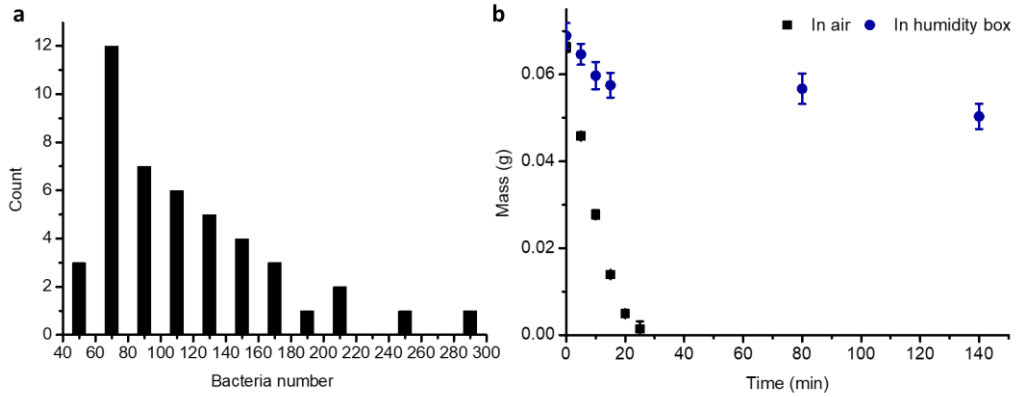

Figure S2. (a) Distribution of bacteria number in individual droplets on DMA slides after the seeding of bacteria using the "standing droplet" method. Droplets of bacteria suspension (*P. aeruginosa* O1 GFP, 10^6 CFU mL^{-1}) formed on DMA slides were collected separately with the pipette. The collected bacteria suspension was diluted with cell wash buffer and then inoculated on LB agar plates. Colony number on agar plates was counted after overnight incubation. Bacteria number in each droplet was calculated according to the colony number. Bacteria number in 45 droplets from 3 different DMA was counted (15 droplets were randomly chosen from each DMA slide). (b) Mass change of droplets on DMA

slides placed in air and in the humidity box. BM2 medium was used to form droplets on DMA. DMA slides were placed in the open air at 24 ℃. The mass change of the total 588 droplets on one DMA slide was measured with a microbalance at predetermined time points. To measure the mass change of droplets on DMA slides placed in humidity box, which was a sealed plastic box with a wet tissue in it at 24 ℃, the DMA slides were taken out from the box and measured the weight at predetermined time points.

$$\text{The mass of 588 droplets} =$$

$$\text{The mass of the DMA slide with 588 droplets} - \text{The mass of the bare DMA slide}$$

The mass change of the droplets placed in humidity box at 37 ℃ over 24 h was measured as well. The total mass of the 588 droplets was decreased from 0.0671 ± 0.0025 g to 0.0519 ± 0.0017 g.

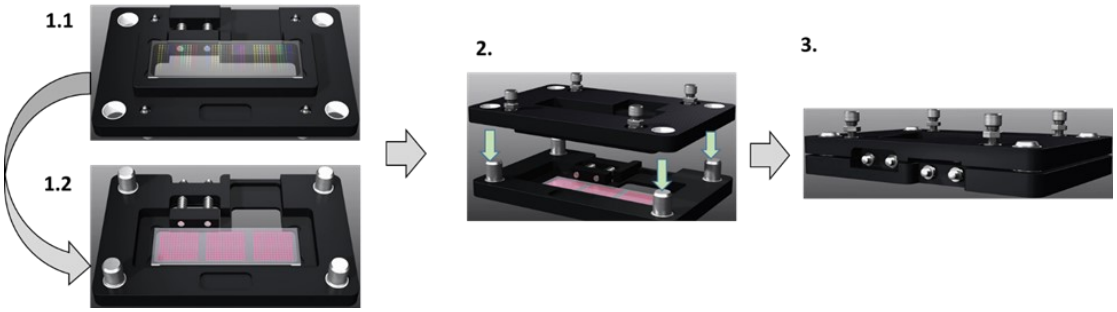

Figure S3. Scheme of workflow of sandwiching a DMA slide and an antibiotic preprinted slide using CellScreenChip (CSC). 1.1. Antibiotic printed slide is fixed in the upper frame of the CSC. 1.2. The DMA slide loaded with bacterial droplets on its surface is fixed in the lower frame of the CSC. 2. The upper frame is inverted and placed onto the lower frame of the CSC. 3. The CSC is closed, with the two frames aligned by four pillars and four micro-screws that define the distance between the DMA slide and antibiotic pre-printed slide.

The CellScreenChip (CSC) is a tool used to align two parallel glass slides. This instrument was designed in our laboratory and manufactured by Maschinenbau Kaltenbach GmbH (Crailsheim, Germany). It comprises two frames (upper and lower) that are manufactured to the same dimensions (127 mm × 85 mm). Four pillars located at the corners of the lower frame are positioned to align with four reference holes in the upper frame in x and y direction. The upper frame contains four micro-screws that define the distance between the parts. A clamp is embedded in each of the two frames, which have a notch that enables live observation of both glass slides while sandwiching using an automated screening microscope. The DMA slide containing the bacteria is fixed into the lower frame of the CSC, while the LMA slide pre-printed with antibiotics is fixed into the upper frame. The CSC is then closed and the micro-screws adjusted to fix the upper frame at a distance that allows contact between the droplets on the DMA slide pre-printed antibiotics on the LMA slide.

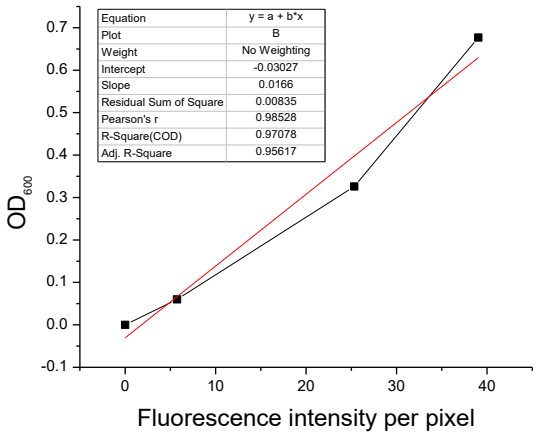

Figure S4. Relationship between OD value of bacteria suspensions and fluorescent intensity of the dried spots on the DMA slide. The OD values of dilutions of *P. aeruginosa* PAO1 bacteria suspension were measured. These dilutions were then used to form droplets of bacteria suspension on the spots on DMA slides. The fluorescence intensity of the dried spots was measured using a fluorescence microscope.

Estimation of bacterial density based on colony number on agar plates

To enumerate the bacteria on DMA slides, one of the three compartments in the DMA slide, which contained 196 bacterial droplets on its surface, was immersed into 20 mL BM2 medium and vortexed for 60 s. The suspension was then diluted with cell wash buffer (1:10^4) and 10 µL of the dilutions were seeded on LB agar plates. After incubation for 24 h at 37°C, the colony number on LB agar plates was recorded used to estimate the number of bacteria on the DMA slide. The bacterial number on the DMA slide was estimated using the following formula:

Bacteria density (CFU mL^{-1}) =

$$Colony\ number\ \times \frac{20\ \text{mL}}{10^{-4}\ \times 10\ \mu\text{L}\ \times 10^{-3}\ \times 90\ \text{nL}\ \times 10^{-6} \times 196}$$

Table S2. Colony number in agar plates. Bacteria were seeded as bacterial suspensions into DMA slides and 96-well plates

	Colony number
DMA slides	1.7 ± 0.5
96-well plates	1.5 ± 0.8

Table S3. Antibiotic concentration printed on glass slides to test resistance of *P. aeruginosa* PA49

Antibiotic	MIC (mg L^{-1})	Reference
piperacillin - tazobactam	4	Eucast2
cefotaxime	10	Eucast2
ceftazidime	2	Eucast2
ciprofloxacin	0.12	Eucast2
methicillin	4	intrinsically resistant [1]
chloramphenicol	4	intrinsically resistant [1]
erythromycin	4	[2]
amoxicillin	64	[3]
carbenicillin	64	[4]
tetracycline	4	intrinsically resistant [1]
ampicillin	64	[3]
kanamycin sulfate	64	Eucast2

streptomycin	5	[5]
polymyxin B	4	[6]
imipenem	1	Eucast2
meropenem	0.5	Eucast2
sulfamethoxazole	4	[7]
tobramycin	1.5	Eucast2

[1] Y. Morita, J. Tomida, Y. Kawamura, *Front. Microbiol.* **2014**, 4, 422.

[2] K. W. Tsang, P. Ng, P. L. Ho, S. Chan, G. Tipoe, R. Leung, J. Sun, J. C. Ho, M. S. Ip, W. K. Lam, *Eur. Respir. J.* **2003**, 21, 401.

[3] H. H. Handsfield, H. Clark, J. F. Wallace, K. K. Holmes, M. Turck, *Antimicrob. Agents Chemother.* **1973**, 3, 262.

[4] D. H. Kwon, C. D. Lu, *Antimicrob. Agents Chemother.* **2006**, 50, 1623.

[5] J. T. Tseng, L. E. Bryan, H. M. Van den Elzen, (1972). *Antimicrob. Agents Chemother.*, **1972**, 2(3), 136-141.

[6] M. Berditsch, T. Jager, N. Strempel, T. Schwartz, J. Overhage, A. S. Ulrich, *Antimicrob. Agents Chemother.* **2015**, 59, 5288.

[7] G. M. Eliopoulos, P. Huovinen, Resistance to trimethoprim-sulfamethoxazole[J]. *Clin. Infect. Dis*., **2001**, 32(11), 1608-1614.

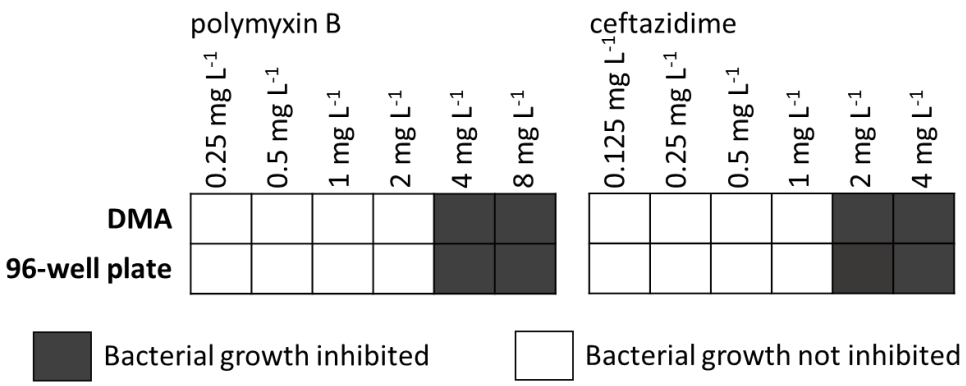

Figure S5. Sensitivity of *P. aeruginosa* PA49 to polymyxin B and ceftazidime tested on DMA slides and in 96-well plates. Different amounts of polymyxin B and ceftazidime were printed on fluorinated glass slides and transferred into droplets of *P. aeruginosa* PA49 suspension (BM2 medium, 10^6 CFU mL^{-1}) using CSC. DMA slides were placed into a humidity box. For 96-well plates, antibiotics were added into wells containing 100 µL bacteria suspension. DMA slides were removed from the humidity box and dried in air after 24 h incubation at 37 ℃. The antibiotic activity was evaluated by visual inspection of the transparency of the wells or droplets (opacity indicates live bacteria). The result was the readout from 10 spots of each concentration on DMA slides and 10 wells of each concentration in 96-well plates. Experiments were repeated twice. The antibiotic was defined as effective when there were ⩾ 8 wells or spots were transparent (without opacity)

6.2.2 Supporting Information of Chapter 3.2

a

X10774	X13110	X13901	X13819	X15558	X12106	X15570	X13853	X15585	X13869	X15513	X12178
	X16136	X13979	X16180	X12355	X16182	X11806	X15817	X12479	X12035	X15878	X15176
X15764	X16176	X15177	X12416	X13217	X13256	X15142	X11113	X11880	X13425	X15160	X15189
	X15100	X11894	X13082	X12358	X13093	X12397	X13098	X12028	X11873	X11860	X12345
X13887	X13839	X15625	X13847	X15104	X12333	X16179	X12395	X16186	X11597	X11366	X10774
X12361	X15571	X13865	X13458	X13815	X13109	X16174	X15158	X16001	X13817	X13851	
X13423	X15496	X13940	X13809	X13478	X15780	X13554	X13840	X12337	X10952	X15686	X15764
X12373	X12329	X13074	X11864	X13230	X11378	X10223	X11891	X10271	X12377	X11884	
X13869	X15513	X15614	X10774	X13110	X15592	X13819	X15558	X13860	X15570	X13853	X15641
X12035	X15878	X16187		X16136	X12317	X16180	X12355	X15872	X11806	X15817	X11871
X13425	X15160	X11375	X15764	X16176	X13225	X12416	X13217	X11634	X15142	X11113	X15605
X11873	X11860	X15595		X15100	X11396	X13082	X12358	X15155	X12397	X13098	X11853
X13847	X13431	X12333	X16179	X16013	X16186	X11597	X16171	X15904	X13887	X15819	X15625
X13458	X12443	X13109	X16174	X13072	X16001	X13817	X13444		X12361	X11858	X13865
X13809	X13557	X15780	X13554	X15103	X12337	X10952	X13943	X15915	X13423	X15612	X13940
X11864	X15650	X11378	X10223	X12385	X10271	X12377	X13055		X12373	X11897	X13074
X13823	X13853	X15641	X12127	X15513	X15614	X15904	X13110	X15592	X13973	X15558	X13860
X12502	X15817	X11871	X16183	X15878	X16187		X16136	X12317	X15796	X12355	X15872
X15121	X11113	X15605	X13495	X15160	X11375	X15915	X16176	X13225	X13479	X13217	X11634
X11895	X13098	X11853	X11376	X11860	X15595		X15100	X11396	X15554	X12358	X15155
X15904	X13887	X15819	X12270	X13847	X13431	X13868	X16179	X16013	X16023	X11597	X16171
	X12361	X11858	X15530	X13458	X12443	X13525	X16174	X13072	X11861	X13817	X13444
X15915	X13423	X15612	X12378	X13809	X13557	X15607	X13554	X15103	X12601	X10952	X13943
	X12373	X11897	X13486	X11864	X15650	X12374	X10223	X12385	X13270	X12377	X13055
X13901	X13860	X13823	X12106	X15641	X12127	X15585	X15614	X12178	X11842	X15592	X13973
X13979	X15872	X12502	X16182	X11871	X16183	X12479	X16187	X15176		X12317	X15796
X15177	X11634	X15121	X13256	X15605	X13495	X11880	X11375	X15189	X15089	X13225	X13479
X11894	X15155	X11895	X13093	X11853	X11376	X12028	X15595	X12345		X11396	X15554
X16171	X11366	X11842	X15819	X12270	X13839	X13431	X13868	X15104	X16013	X16023	X12395
X13444	X13851		X11858	X15530	X15571	X12443	X13525	X13815	X13072	X11861	X15158
X13943	X15686	X15089	X15612	X12378	X15496	X13557	X15607	X13478	X15103	X12601	X13840
X13055	X11884		X11897	X13486	X12329	X15650	X12374	X13230	X12385	X13270	X11891
X13973	X13901	X13819	X13823	X12106	X15570	X12127	X15585	X13869	X12178	X13915	X11842
X15796	X13979	X16180	X12502	X16182	X11806	X16183	X12479	X12035	X15176		
X13479	X15177	X12416	X15121	X13256	X15142	X13495	X11880	X13425	X15189	X15987	X15089
X15554	X11894	X13082	X11895	X13093	X12397	X11376	X12028	X11873	X12345		
X12395	X16186	X11366	X13915	X13915	X12270	X13839	X15625	X13868	X15104	X12333	X16023
X15158	X16001	X13851			X15530	X15571	X13865	X13525	X13815	X13109	X11861
X13840	X12337	X15686	X15987	X15987	X12378	X15496	X13940	X15607	X13478	X15780	X12601
X11891	X10271	X11884			X13486	X12329	X13074	X12374	X13230	X11378	X13270

b

0.51	0.48	0.50	0.55	0.53	0.45	0.43	0.38	0.34	0.28	0.29	0.32
0.03	0.50	0.53	0.47	0.39	0.37	0.39	0.36	0.38	0.44	0.42	0.38
0.54	0.48	0.47	0.44	0.44	0.40	0.33	0.40	0.30	0.33	0.31	0.27
0.55	0.51	0.47	0.47	0.45	0.43	0.41	0.39	0.42	0.33	0.31	0.25
0.56	0.50	0.49	0.48	0.49	0.43	0.32	0.35	0.40	0.36	0.36	0.32
0.60	0.54	0.52	0.50	0.51	0.50	0.56	0.54	0.41	0.41	0.37	0.35
0.57	0.54	0.53	0.50	0.47	0.50	0.42	0.44	0.39	0.34	0.18	0.27
0.62	0.61	0.63	0.53	0.63	0.50	0.47	0.40	0.39	0.51	0.36	0.36
0.58	0.61	0.53	0.62	0.42	0.48	0.47	0.36	0.49	0.41	0.38	0.34
0.59	0.56	0.53	0.03	0.50	0.48	0.48	0.44	0.46	0.39	0.38	0.36
0.60	0.55	0.52	0.53	0.52	0.46	0.46	0.42	0.44	0.41	0.40	0.36
0.59	0.54	0.52	0.58	0.48	0.48	0.50	0.46	0.46	0.43	0.40	0.36
0.61	0.54	0.57	0.61	0.52	0.53	0.50	0.51	0.48	0.41	0.38	0.34
0.60	0.56	0.55	0.56	0.48	0.47	0.49	0.51	0.44	0.41	0.37	0.37
0.59	0.57	0.62	0.53	0.53	0.47	0.46	0.46	0.41	0.40	0.43	0.39
0.62	0.61	0.54	0.62	0.53	0.46	0.45	0.45	0.42	0.41	0.40	0.39
0.63	0.60	0.58	0.58	0.59	0.48	0.47	0.50	0.43	0.44	0.43	0.38
0.62	0.61	0.63	0.52	0.58	0.48	0.03	0.45	0.39	0.41	0.45	0.39
0.62	0.60	0.55	0.51	0.55	0.48	0.52	0.44	0.47	0.50	0.42	0.40
0.62	0.60	0.54	0.57	0.47	0.48	0.48	0.46	0.44	0.42	0.41	0.40
0.63	0.56	0.55	0.53	0.51	0.47	0.49	0.45	0.45	0.53	0.44	0.42
0.62	0.56	0.54	0.54	0.51	0.50	0.47	0.49	0.45	0.43	0.43	0.41
0.61	0.57	0.59	0.57	0.58	0.47	0.48	0.46	0.46	0.44	0.44	0.41
0.62	0.56	0.55	0.59	0.53	0.51	0.49	0.46	0.44	0.53	0.44	0.40
0.63	0.56	0.54	0.51	0.50	0.46	0.49	0.45	0.40	0.45	0.41	0.41
0.60	0.59	0.55	0.53	0.52	0.46	0.51	0.47	0.51	0.03	0.48	0.47
0.62	0.58	0.51	0.52	0.50	0.46	0.45	0.46	0.56	0.49	0.47	0.54
0.59	0.61	0.54	0.51	0.50	0.43	0.48	0.48	0.55	0.50	0.47	0.47
0.63	0.59	0.57	0.51	0.50	0.48	0.56	0.51	0.53	0.51	0.59	0.45
0.63	0.59	0.56	0.51	0.52	0.47	0.53	0.50	0.54	0.48	0.49	0.46
0.63	0.59	0.58	0.56	0.51	0.49	0.52	0.52	0.57	0.48	0.45	0.46
0.63	0.58	0.57	0.54	0.53	0.50	0.56	0.51	0.63	0.45	0.53	0.41
0.63	0.63	0.60	0.56	0.53	0.51	0.51	0.46	0.44	0.44	0.43	0.43
0.63	0.63	0.63	0.58	0.49	0.51	0.47	0.47	0.46	0.46	0.45	0.03
0.63	0.63	0.62	0.56	0.55	0.53	0.50	0.48	0.49	0.46	0.45	0.46
0.63	0.63	0.63	0.57	0.58	0.56	0.47	0.49	0.47	0.48	0.49	0.47
0.63	0.63	0.63	0.63	0.63	0.59	0.53	0.52	0.55	0.47	0.51	0.57
0.63	0.63	0.63	0.63	0.63	0.62	0.57	0.54	0.34	0.53	0.55	0.53
0.63	0.63	0.63	0.63	0.63	0.62	0.61	0.63	0.56	0.57	0.56	0.52
0.63	0.63	0.63	0.63	0.63	0.63	0.63	0.63	0.62	0.63	0.58	0.59

Figure S1. (a) Layout of compounds on one DMA slide. (b) Value of color depth of stained droplets incubated overnight on DMA printed with compounds from ComPlat as shown in (a).

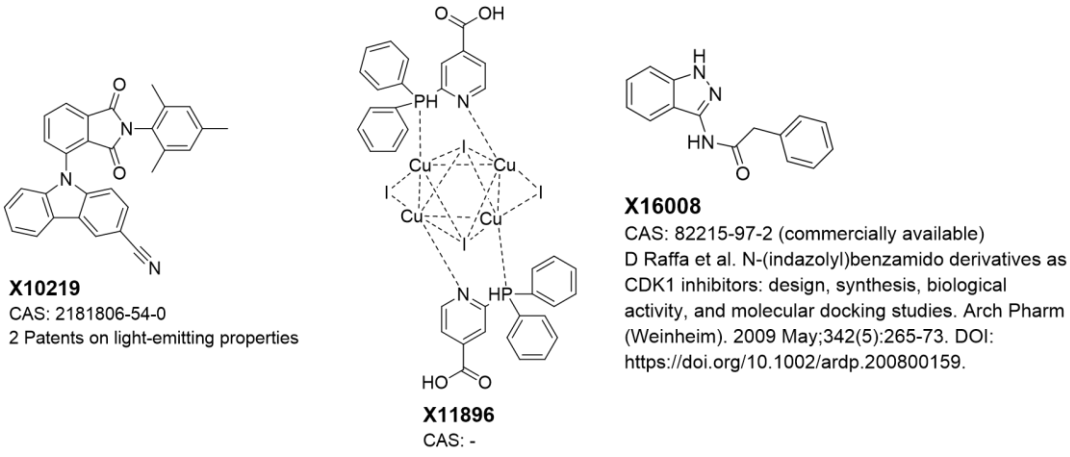

Figure S2. Structures of three compounds presenting positive results in the screening.

6.2.3 Supporting information of Chapter 3.3

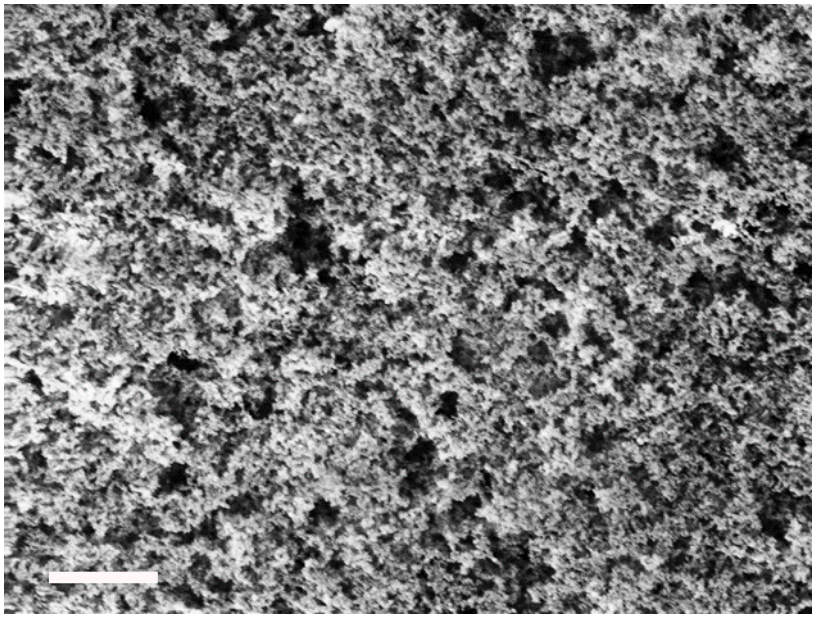

Figure S1. SEM image of the substrate of patterned LIS without lubricant. The scale bar: 1 μm.

Surfaces without lubricant were prepared. Prior to SEM measurements, samples were sputtered with a 10 nm gold layer using a Cressington 108 auto sputter coater. LEO 1530 Gemini scanning electron microscope (Zeiss, Germany) was used to take images of the substrate of patterned LIS. The SEM image shows the porous structure of the surface, which is required to lock the lubricant for LIS preparation.

Table S1 Water contact angle and sliding angle of different area on patterned LIS.

	Static water contact angle	Advancing water contact angle	Receding water contact angle	Sliding angle for water
Hydrophilic area	0 °	-	-	-
Hydrophobic area	156.5°± 3°	162.6°± 4°	152.5°± 4°	1.9°± 0.4°
LIS area	100.3°± 1°	100.4°± 5°	95.5°± 2°	1.6°± 0.2°

We measured the water contact angle and sliding angle with DSA 25 contact angle goniometer (Krüss, Germany) using the sessile drop technique. Advancing contact angles were obtained by measuring the angle while the liquid was slowly added at a rate of 0.1 mL s^{-1} from a ~4 μL droplet to 14 μL in contact with the sample and a micrometer syringe. Receding contact angles were obtained with liquid slowly retracting at a rate of 0.1 mL s^{-1} from a ~14 μL droplet to 4 μL. Sliding angles were measured by using the tilting option with the rate of 60° min^{-1}. The table shows small sliding angles of the lubricant infused surfaces, while the advancing water contact angles and receding water contact angles of the surface were smaller than those of the hydrophobic area, indicating the hydrophobic surfaces turned into slippery surfaces after the spread of lubricant.

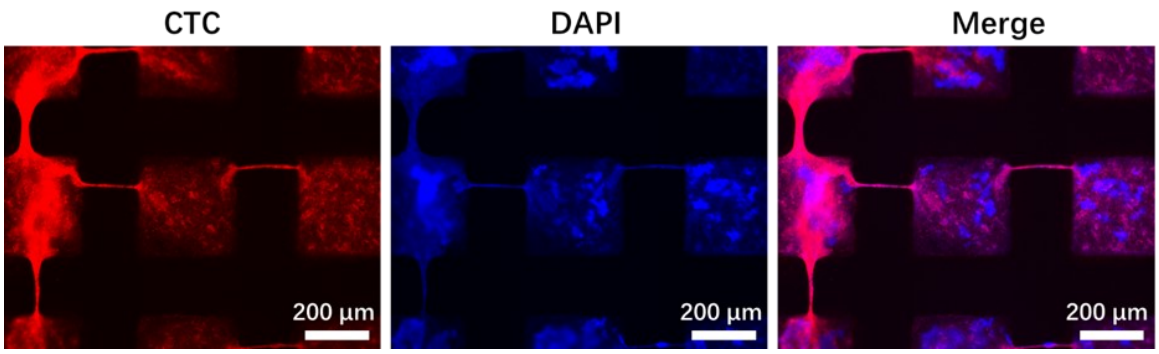

Figure S2. Fluorescence microscope images of biofilms of *P. aeruginosa* PA49 on patterned LIS after 1 day incubation in BM2 medium under static condition (without shaking). Biofilms were stained with CTC for 3 h then with DAPI for 10 min before images were produced. Red color represents active bacteria from CTC staining and blue color represents DNA (external+inside of bacteria). The microscope observations were completed by ImageJ software.

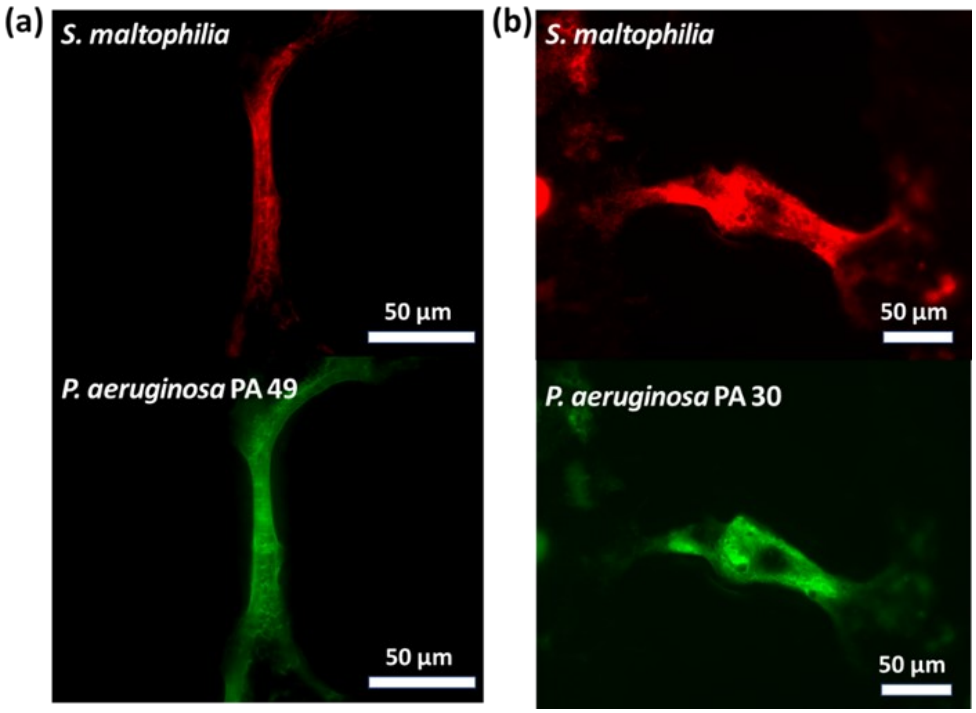

Figure S3. Images of mixed species biofilm bridges after FISH staining (individual fluorescence channel). (a) A single biofilm bridge where red fluorescence is from *S. maltophilia* (top) and green fluorescence comes from *P. aeruginosa* PA49 (bottom). (b) Biofilm bridges of a mixed population of PA 30 (green fluorescence, bottom) and

S.maltopohilia (red fluorescence, top). Patterned LIS slides were incubated with the bacteria mixture solution for 24 h, followed by FISH staining.

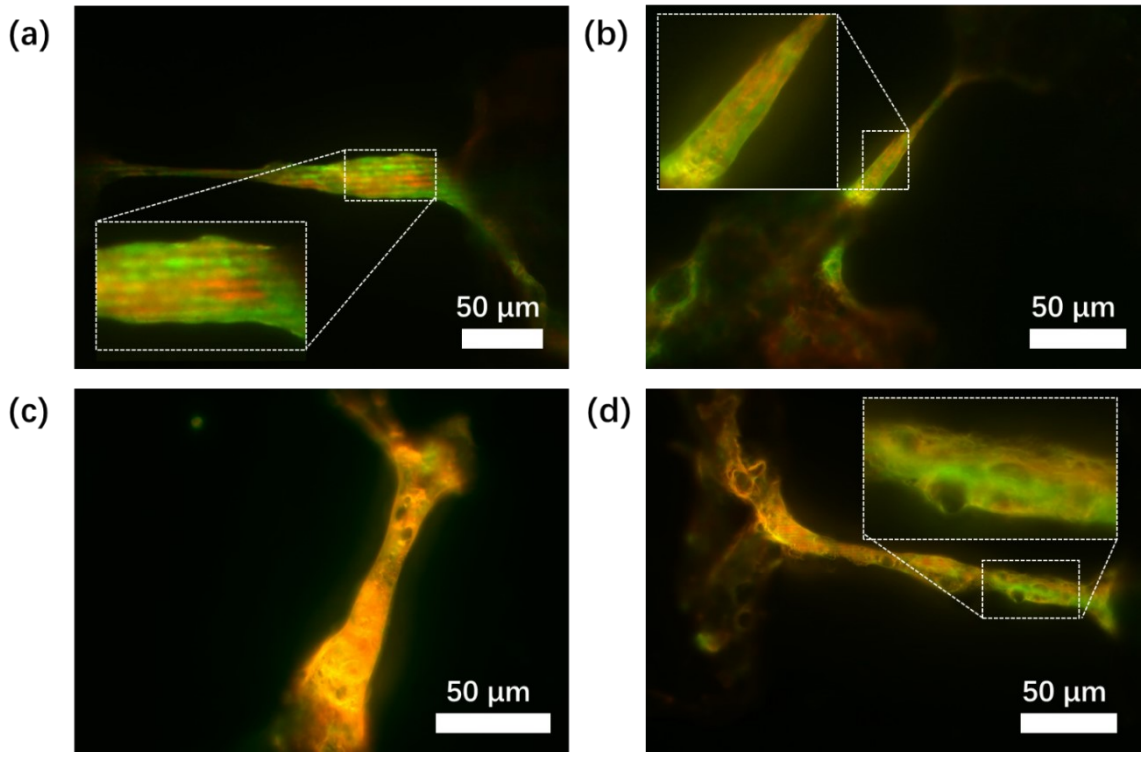

Figure S4. Images of mixed species biofilm bridges after FISH staining. (a) A single biofilm bridge where red fluorescence is from *S. maltophilia* and green fluorescence comes from *P. aeruginosa* PA 30. (b)(c)(d) Biofilm bridges of a mixed population of *P. aeruginosa* PA49 (green fluorescence) and *S. maltophilia* (red fluorescence). Patterned LIS slides were incubated with the bacteria mixture solution for 24 h, followed by FISH staining.

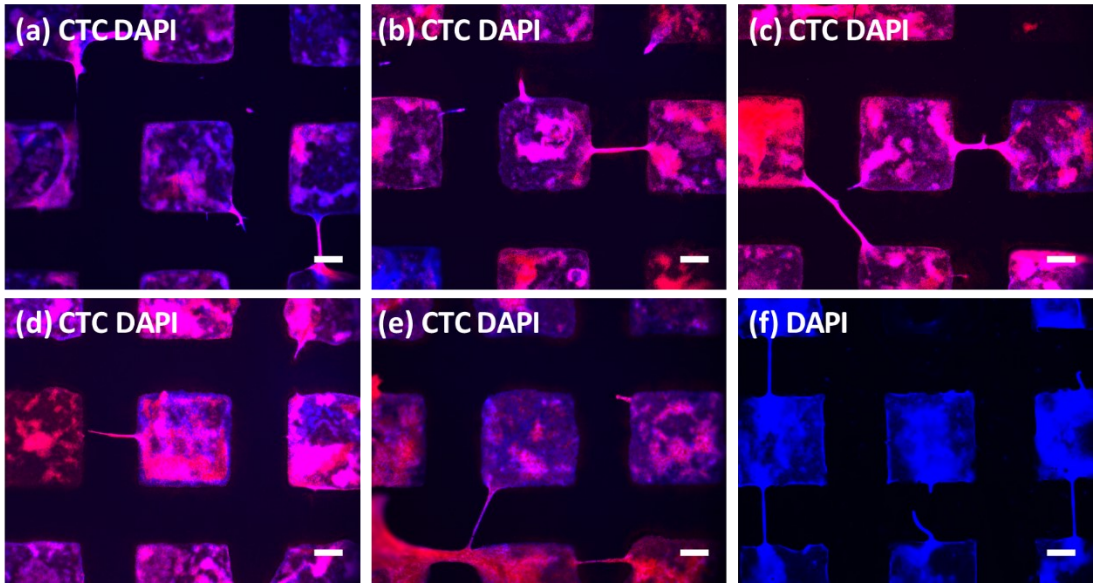

Figure S5. Fluorescence microscope images of biofilm bridges of *P. aeruginosa* PA49 of different length on patterned LIS after 1 day incubation in BM2 medium. Biofilms were stained with CTC for 3 h then with DAPI for 10 min before images were produced. Red color represents active bacteria from CTC staining and blue color represents DNA (external + inside of bacteria). The microscope observations were completed by ImageJ software. The scale bar is 100 µm.

6.2.4 Supporting Information of Chapter 3.4

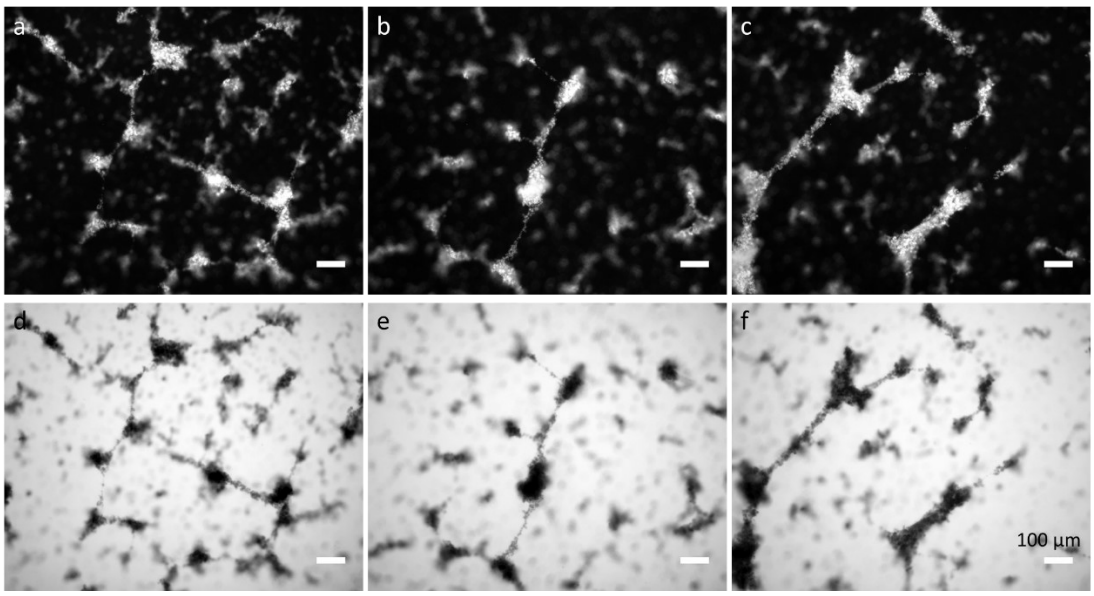

Figure S1. (a)(b)(c) Fluorescence images of *P. aeruginosa* PA49 incubated with pLIS after 3 h. Images were taken before the medium was removed. (d)(e)(f) Bright field images of *P. aeruginosa* PA49 incubated with patterned lubricant infused surfaces after 3 h. Images were taken before the medium was removed.

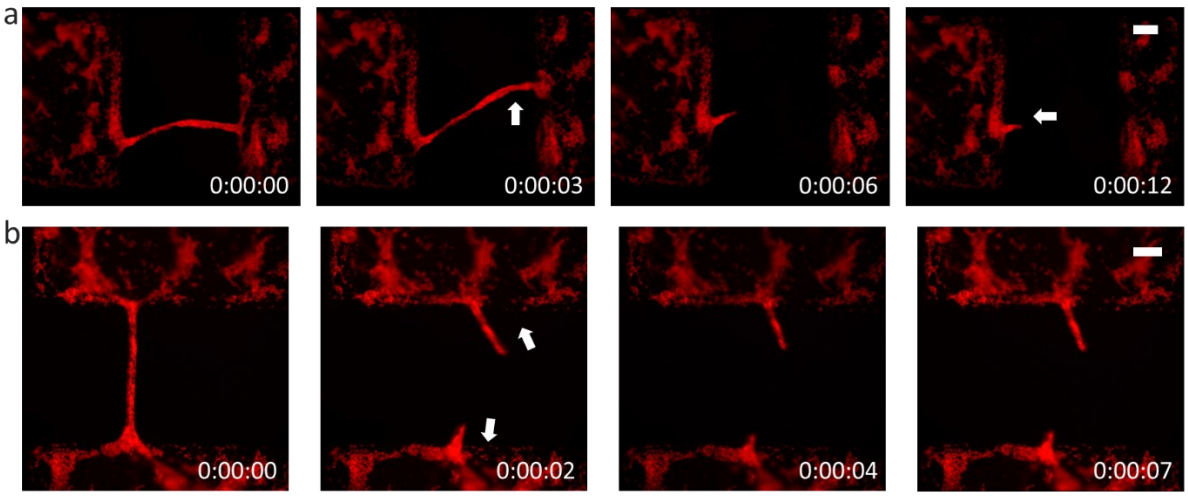

Figure S2. (a) Fluorescence images showing breaking of a bacterial bridge of *P. aeruginosa* PA49 using a needle after the bacterial suspension was aspirated. A needle touched the bridge before the third second, then due to the touch of the needle, the bridge moved in the direction showing with the white arrow. Then the bridge was cut off by the needle. Part of the bridge was removed with the needle, while the remaining part shrank towards the

hydrophilic bacteria attached area. The video shows that the ends of the bridge were attached to the hydrophilic area, while the bridge was not attached to the lubricant infused area. The video S2 is available as supporting information. (b) Fluorescence images showing breaking of a bridge of *P. aeruginosa* PA49. The pLIS slide was incubated in *P. aeruginosa* PA49 suspension for 3 h. Then the bacterial bridge was formed by aspirating the liquid. After the incubation of the bridge in air for 24 h, it was broken by a needle. The video S3 is available as supporting information. Time format shown in all images (hh:mm:ss). Scale bars: 100 μm.

LIS borders	1	2	3	4	5	6	7	8	9	10
Height (μm)	10.4	12.7	6.8	7.6	11.5	9.7	9.0	11.4	12.0	9.3

Table S1. Height of the LIS borders. The pLIS (side length of hydrophilic square: 1 mm. Width of lubricant infused borders: 500 μm) slide was incubated with *P. aeruginosa* PA49 in BM2 medium for 3 h. Then the slide was observed using bright field view of a microscope. Since the focusing plane of bacteria precipitated on the LIS borders and the bacteria attached to the hydrophilic area is different, we could use the difference of the focusing plane to measure the height of the LIS borders. 10 LIS borders on one slide were randomly measured.

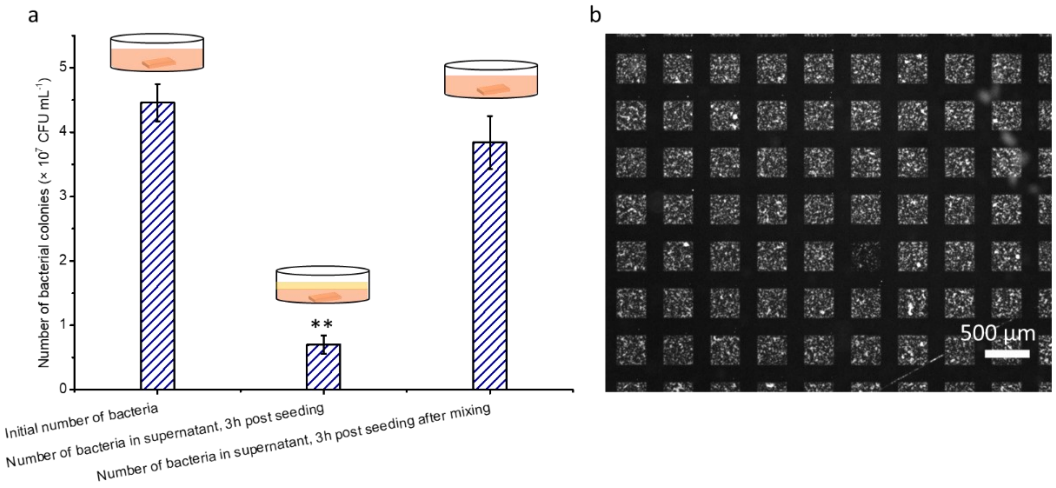

Figure S3. (a) Bacteria number of the bacteria suspension before 3 h incubation, the supernatant of bacterial suspension after 3 h incubation and fully mixed bacterial suspension after 3 h incubation. Data were presented as mean ± SD of three experiments with three repeats each time. (b) Fluorescence image of patterned lubricant infused surface incubated vertically in bacterial suspension of *P. aeruginosa* PA49. CTC was added into bacterial suspension from the beginning of the incubation.

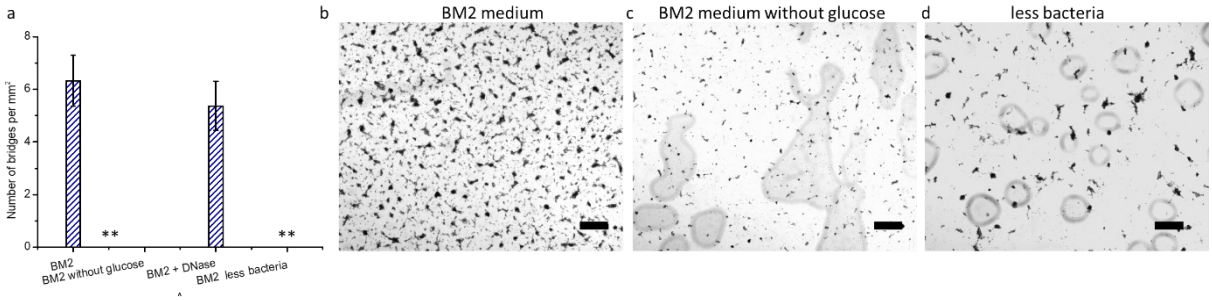

Figure S4. (a) Number of bridges of *P. aeruginosa* PA49 on surfaces under different incubation conditions. PLIS (side length of hydrophilic square: 350 µm. Width of lubricant infused borders: 200 µm) were incubated with *P. aeruginosa* PA49 in BM2 medium, BM2 medium without glucose, BM2 medium with DNase and BM2 medium with lower density of bacteria (low density 10^6 bacteria per mL vs. normal density of bacteria 10^7 bacteria per mL during the seeding step) for 3 h. The number of bridges was counted visually after the liquid was removed. Data were presented as mean ± SD of three experiments with three

repeats each time. (b) Bright field image of *P. aeruginosa* PA49 on pLIS after 3 h incubation in BM2 medium. (c) Bright field image of *P. aeruginosa* PA49 on pLIS after 3 h incubation in BM2 medium without glucose. (d) Bright field image of *P. aeruginosa* PA49 of low density (10^6 bacteria per mL) on pLIS after 3 h incubation in BM2 medium. Scale bars: 500 μm.

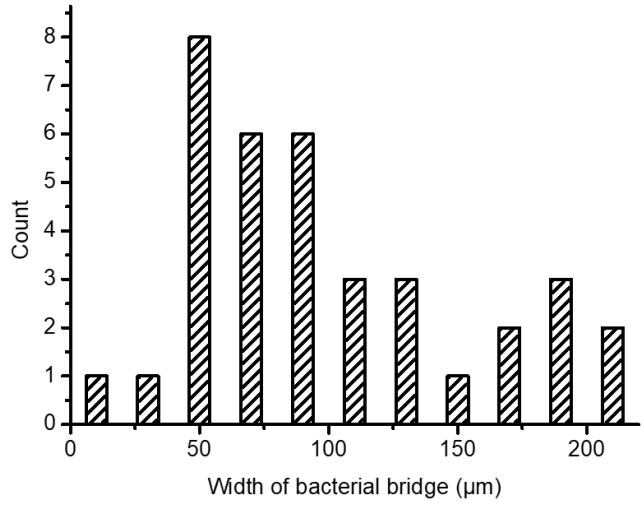

Figure S5. Distribution of width of bacterial bridges. PLIS (side length of hydrophilic square:1 mm. Distance of lubricant infused borders: 500 μm) were incubated with *P. aeruginosa* PA49 in BM2 medium for 3 h. The width of bacterial bridges was measured using ImageJ with images of the bridges after the liquid was removed from the surfaces. 12 bridges were randomly selected from three surfaces to measure the width, and the experiment was repeated three times.

6.3 List of Abbreviations

MIC	Minimum inhibitory concentration
ATP	Adenosine triphosphate
FDA	U.S. Food and Drug Administration
P. aeruginosa	*Pseudomonas aeruginosa*
S. aureus	*Staphylococcus aureus*
E. coli	*Escherichia coli*
M. tuberculosis	*Mycobacterium tuberculosis*
PDMS	Polydimethylsiloxane
RNA	Ribonucleic ccid
MRSA	Methicillin-resistant *Staphylococcus aureus*
PEG	Polyethylene glycol
PCR	Polymerase chain reaction
MALDI-ToF	Matrix-assisted laser desorption/ionization time-of-flight mass spectrometer
OD	Optical density
RAFT	Reversible addition−fragmentation chain-transfer

6.4 Curriculum Vitae

Personal Data

Name	Wenxi Lei
Date of Birth	1993.11.25
Email	wenxi.lei@kit.edu
Address	Pirmasenser str. 8 Karlsruhe

Education

09.2017-present	PhD studies Karlsruhe Institute of Technology (KIT), Germany Institute of Biological and Chemical Systems – Functional Molecular Systems (IBCS-FMS) Supervisor: Prof. Dr. Pavel A. Levkin Research Topic: Applications of Droplet Microarray in Microbiology: from High Throughput Screening Platform to Biofilm Control
09.2014-06.2017	Master studies Zhejiang University, China Department of Polymer Science and Engineering Supervisor: Prof. Kefeng Ren Research Topic: Bioinspired Antibacterial Coatings

09.2010-06.2014	Bachelor studies Tianjin University, China Department of Material Science and Engineering
09.2007-06.2010	Secondary school Hongqi Zhongxue, China

6.5 Publications and Conference Contributions

1) **Lei, W.**, Bruchmann, J., Rüping, J. L., Levkin, P. A., & Schwartz, T. (**2019**). Biofilm Bridges Forming Structural Networks on Patterned Lubricant - Infused Surfaces. *Advanced Science*, 6(13), 1900519.
2) **Lei, W.**, Demir, K., Overhage, J., Grunze, M., Schwartz, T., & Levkin, P. A. (**2020**). Droplet - Microarray: Miniaturized Platform for High - Throughput Screening of Antimicrobial Compounds. *Advanced Biosystems*, 4(10), 2000073.
3) **Lei, W.**, Krolla, P., Schwartz, T., & Levkin, P. A. (**2020**). Controlling Geometry and Flow Through Bacterial Bridges on Patterned Lubricant - Infused Surfaces (pLIS). *Small*, 16(52), 2004575.
4) **Lei, W.**, Deckers, A., Popova, A., Reischl, M., Jung, N., Bräse, S., Schwartz, T., & Levkin, P. A. (**2020**). DMA-based ultra HTS of a Library of 608 Compounds with Carbapenem-resistant *Klebsiella pneumoniae*. Manuscript in preparation.
5) Behboodi-Sadabad, F., Li, S., **Lei, W.**, Liu, Y., Sommer, T., Friederich, P., Sobek, C., Messersmith, P. B. & Levkin, P. A. (**2021**). High-throughput screening of multifunctional nanocoatings based on combinations of polyphenols and catecholamines. *Materials Today Bio*, 10, 100108.

06.2018	Participants
BioInterfaces International Graduate School RETREAT	
06.2019	Poster presentation
BioInterfaces International Graduate School RETREAT	
06.2021	Oral presentation
BioInterfaces International Graduate School RETREAT	

7 Literature

[1] W.X. Lei, K. Demir, J. Overhage, M. Grunze, T. Schwartz, P.A. Levkin, *Adv. Biosyst.* 4 (10) (**2020**) 2000073.

[2] W.X. Lei, J. Bruchmann, J.L. Ruping, P.A. Levkin, T. Schwartz, *Adv. Sci.* 6 (13) (**2019**) 1900519.

[3] W.X. Lei, P. Krolla, T. Schwartz, P.A. Levkin, *Small* 16 (52) (**2020**) 2004575.

[4] P.W. Smith, K. Watkins, A. Hewlett, *Am. J. Infect. Control* 40 (1) (**2012**) 35-42.

[5] B.R. da Cunha, L.P. Fonseca, C.R.C. Calado, *Antibiotics-Basel* 8 (2) (**2019**) 45.

[6] R. Norrby, M Powell, B. Aronsson, D.L. Monnet, I. Lutsar, I.S. Bocsan, O. Cars, H. Giamarellou, I.C Gyssens, *Eur. J. Clin. Pharm.* 15 (5) (**2009**) 15.

[7] E. Martens, A.L. Demain, *J. Antibiot.* 70 (5) (**2017**) 520-526.

[8] J.M.A. Blair, M.A. Webber, A.J. Baylay, D.O. Ogbolu, L.J.V. Piddock, *Nat. Rev. Microbiol.* 13 (1) (**2015**) 42-51.

[9] F.C. Tenover, *Am. J. Infect. Control* 34 (5) (**2006**) S3-S10.

[10] S.N. Khan, A.U. Khan, *Front. Microbiol.* 7 (**2016**) 174.

[11] M. Frieri, K. Kumar, A. Boutin, *J. Infect. Public Health* 10 (4) (**2017**) 369-378.

[12] J.H. Song, P.R. Hsueh, D.R. Chung, K.S. Ko, C.I. Kang, K.R. Peck, J.S. Yeom, S.W. Kim, H.H. Chang, Y.S. Kim, S.I. Jung, J.S. Son, T.M.K. So, M.K. Lalitha, Y.H. Yang, S.G. Huang, H. Wang, Q.A. Lu, C.C. Carlos, J.A. Perera, C.H. Chiu, J.W. Liu, A. Chongthaleong, V. Thamlikitkul, P.H. Van, A.S. Grp, *J. Antimicrob. Chemother.* 66 (5) (**2011**) 1061-1069.

[13] P. Nordmann, T. Naas, L. Poirel, *Emerg. Infect. Dis.* 17 (10) (**2011**) 1791-1798.

[14] R. Laxminarayan, P. Matsoso, S. Pant, C. Brower, J.A. Rottingen, K. Klugman, S. Davies, *Lancet* 387 (10014) (**2016**) 168-175.

[15] G.A. Durand, D. Raoult, G. Dubourg, *Int. J. Antimicrob. Agents* 53 (4) **(2019**) 371-382.

[16] L.L. Silver, *Clin. Microbiol. Rev.* 24 (1) (**2011**) 71-109.

[17] J.A. DiMasi, H.G. Grabowski, R.W. Hansen, *J. Health Econ.* 47 (**2016**) 20-33.

[18] C. Merlin, *Front. Microbiol.* 11 (**2020**) 33.

[19] K. E. Zulauf, J. E. Kirby, *Proc. Natl. Acad. Sci. U. S. A.* 117 (47) (**2020**) 29839-29850.

[20] W. Phuklia, P. Panyanivong, D. Sengdetka, P. Sonthayanon, P.N. Newton, D.H. Paris, N.P.J. Day, S. Dittrich, *J. Antimicrob. Chemother* 74 (1) (**2019**) 74-81.

[21] F. Stocker, M.M. Obermeier, K. Resch, G. Berg, C.A. Muller Bogota, *Antibiotics* (Basel) 9 (11) (**2020**) 726.

[22] S. Wen, D.M. Yao, X.Y. Liu, F.H. Wang, *J. Agric. Food Chem.* 67 (45) (**2019**) 12584-12589.

[23] M. Balouiri, M. Sadiki, S.K. Ibnsouda, *J. Pharm. Anal.* 6 (2) (**2016**) 71-79.

[24] B. Cauwelier, B. Gordts, P. Descheemaecker, H. Van Landuyt, *Eur. J. Clin. Microbiol. Infect. Dis.* 23 (5) (**2004**) 389-392.

[25] G. Kampf, C. Lecke, A.K. Cimbal, K. Weist, H. Ruden, *J. Clin. Microbiol.* 36 (8) (**1998**) 2254-2257.

[26] O. Rangasamy, G. Raoelison, F.E. Rakotoniriana, K. Cheuk, S. Urverg-Ratsimamanga, J. Quetin-Leclercq, A. Gurib-Fakim, A.H. Subratty, *J. Ethnopharmacol.* 109 (2) (**2007**) 331-337.

[27] S.R. Fitzpatrick, M. Garvey, K. Jordan, J. Flynn, B. O'Brien, D. Gleeson, *Vet. World* 12 (5) (**2019**) 629-637.

[28] Y. Imai, K.J. Meyer, A. Iinishi, Q. Favre-Godal, R. Green, S. Manuse, M. Caboni, M. Mori, S. Niles, M. Ghiglieri, C. Honrao, X.Y. Ma, J.J. Guo, A. Makriyannis, L. Linares-Otoya, N. Boehringer, Z.G. Wuisan, H. Kaur, R. Wu, A. Mateus, A. Typas, M.M. Savitski, J.L. Espinoza, A. O'Rourke, K.E. Nelson, S. Hiller, N. Noinaj, T.F. Schaberle, A. D'Onofrio, K. Lewis, *Nature* 576 (7787) (**2019**) 459-464.

[29] E.A. Idelevich, K. Becker, J. Schmitz, D. Knaack, G. Peters, R. Kock, *PloS one* 11 (7) (**2016**) e0159183.

[30] K.R. Fiebelkorn, S.A. Crawford, M.L. McElmeel, J.H. Jorgensen, *J. Clin. Microbiol.* 41 (10) (**2003**) 4740-4744.

[31] R.R. Hansen, A.C. Timm, C.M. Timm, A.N. Bible, J.L. Morrell-Falvey, D.A. Pelletier, M.L. Simpson, M.J. Doktycz, S.T. Retterer, *PloS one* 11 (7) (**2016**) e0155080.

[32] C.J. Ingham, A. Sprenkels, J. Bomer, D. Molenaar, A. van den Berg, J.E.T.V. Vlieg, W.M. de Vos, *Proc. Natl. Acad. Sci. U. S. A.* 104 (46) (**2007**) 18217-18222.

[33] D.S.P.D. Auld, P.B.S. Coassin, N.P.P.D. Coussens, P. Hensley, C. Klumpp-Thomas, S. Michael, G.S.P.D. Sittampalam, O.B.S. Trask, B.K.P.D. Wagner, J.R.P.D. Weidner, M.J.P.D. Wildey, J.L.P.D. Dahlin M.D, *Assay Guidance Manual, Bethesda (MD)* **2004**.

[34] S. Gilbert-Girard, K. Savijoki, J. Yli-Kauhaluoma, A. Fallarero, *Microorganisms* 8 (11) (**2020**) 1834.

[35] S. Gilbert-Girard, K. Savijoki, J. Yli-Kauhaluoma, A. Fallarero, *J. Clin. Microbiol.* 21 (9) (**2020**) 3034.

[36] S.A. Siles, A. Srinivasan, C.G. Pierce, J.L. Lopez-Ribot, A.K. Ramasubramanian, *Antimicrob. Agents Chemother.* 57 (8) (**2013**) 3681-3687.

[37] J.J. Harrison, C.A. Stremick, R.J. Turner, N.D. Allan, M.E. Olson, H. Ceri, *Nat. Protoc.* 5 (7) (**2010**) 1236-1254.

[38] S. Kitamura, A. Owensby, D. Wall, D.W. Wolan, *Cell Chem. Biol.* 25 (3) (**2018**) 301-308.

[39] A.R. Brochado, A. Telzerow, J. Bobonis, M. Banzhaf, A. Mateus, J. Selkrig, E. Huth, S. Bassler, J.Z. Beas, M. Zietek, N. Ng, S. Foerster, B. Ezraty, B. Py, F. Barras, M.M. Savitski, P. Bork, S. Gottig, A. Typas, *Nature* 559 (7713) (**2018**) 259-263.

[40] S.J. Li, P.F. She, L.Y. Zhou, X.H. Zeng, L.L. Xu, Y.Q. Liu, L.H. Chen, Y. Wu, *Front. Microbiol.* 11 (**2020**) 3109.

[41] Y.Q. Zheng, Y. Luo, K. Feng, W.D. Zhang, G.J. Chen, *ACS Macro Lett.* 8 (3) (**2019**) 326-330.

[42] J.L. Garcia-Cordero, Z.H. Fan, *Lab Chip* 17 (13) (**2017**) 2150-2166.

[43] F. Wu, B.G. van Schie, J.E. Keymer, C. Dekker, *Nat. Nanotechnol.* 10 (8) (**2015**) 719-26.

[44] B. Berdy, A.L. Spoering, L.L. Ling, S.S. Epstein, *Nat. Protoc.* 12 (10) (**2017**) 2232-2242.

[45] X. Liu, R.E. Painter, K. Enesa, D. Holmes, G. Whyte, C.G. Garlisi, F.J. Monsma, M. Rehak, F.F. Craig, C.A. Smith, *Lab Chip* 16 (9) (**2016**) 1636-1643.

[46] K. Churski, T.S. Kaminski, S. Jakiela, W. Kamysz, W. Baranska-Rybak, D.B. Weibel, P. Garstecki, *Lab Chip* 12 (9) (**2012**) 1629-1637.

[47] J.P. Yang, Z.G. Chen, P.Y. Ching, Q.J. Shi, X.C. Li, *Lab Chip* 13 (17) (**2013**) 3373-3382.

[48] J.P. Yang, M.Q. Zheng, F. Yang, X.L. Zhang, W. Yin, X.J. Liu, G.J. Zhang, Z.G. Chen, *Sens. Actuators B Chem.* 275 (**2018**) 373-381.

[49] L.L. Ling, T. Schneider, A.J. Peoples, A.L. Spoering, I. Engels, B.P. Conlon, A. Mueller, T.F. Schaberle, D.E. Hughes, S. Epstein, M. Jones, L. Lazarides, V.A. Steadman, D.R. Cohen, C.R. Felix, K.A. Fetterman, W.P. Millett, A.G. Nitti, A.M. Zullo, C. Chen, K. Lewis, *Nature* 517 (7535) (**2015**) 455-459.

[50] N. Qin, P. Zhao, E.A. Ho, G.M. Xin, C.L. Ren, *ACS Sens.* 6 (1) (**2021**) 3-21.

[51] R. Seemann, M. Brinkmann, T. Pfohl, S. Herminghaus, *Rep. Prog. Phys.* 75 (1) (**2012**) 016601.

[52] P. Zhu, L. Wang, *Lab Chip* 17 (1) (**2016**) 34-75.

[53] M. Sesen, T. Alan, A. Neild, *Lab Chip* 17 (14) (**2017**) 2372-2394.

[54] C.M. Betanzos, M.J. Gonzalez-Moa, K.W. Boltz, B.D.V. Werf, S.A. Johnston, S.A. Svarovsky, *ChemBioChem* 10 (5) (**2009**) 877-888.

[55] M. Kazemzadeh-Narbat, H. Cheng, R. Chabok, M.M. Alvarez, C. De La Fuente-Nunez, K.S. Phillips, A. Khademhosseini, *Crit. Rev. Biotechnol.* 41 (1) (**2021**) 94-120.

[56] S.A. Svarovsky, M.J. Gonzalez-Moa, *ACS Comb. Sci.* 13 (6) (**2011**) 634-638.

[57] G.B. Qi, Y.J. Gao, L. Wang, H. Wang, *Adv. Mater.* 30 (22) (**2018**) 1703444.

[58] K. Hilpert, D.F.H. Winkler, R.E.W. Hancock, *Nat. Protoc.* 2 (6) (**2007**) 1333-1349.

[59] R. Frank, *J. Immunol. Methods* 267 (1) (**2002**) 13-26.

[60] C. Schirwitz, F.F. Loeffler, T. Felgenhauer, V. Stadler, F. Breitling, F.R. Bischoff, *Biointerphases* 7 (1) (**2012**) 47.

[61] J.B. Legutki, Z.G. Zhao, M. Greving, N. Woodbury, S.A. Johnston, P. Stafford, Scalable high-density peptide arrays for comprehensive health monitoring, *Nat. Commun.* 5 (**2014**) 1-7.

[62] R. Popov, G.K. Shankara, C. von Bojnicic-Kninski, P. Barua, D. Mattes, F. Breitling, A. Nesterov-Mueller, *Sci. Rep.* 9 (**2019**) 1-10.

[63] F.F. Loeffler, T.C. Foertsch, R. Popov, D.S. Mattes, M. Schlageter, M. Sedlmayr, B. Ridder, F.X. Dang, C. von Bojnicic-Kninski, L.K. Weber, A. Fischer, J. Greifenstein, V. Bykovskaya, I. Buliev, F.R. Bischoff, L. Hahn, M.A.R. Meier, S. Brase, A.K. Powell, T.S. Balaban, F. Breitling, A. Nesterov-Mueller, *Nat. Commun.*7 (1) (**2016**) 1-9.

[64] L.W. Jiang, D. Watkins, Y. Jin, C. Gong, A. King, A.Z. Washington, K.D. Green, S. Garneau-Tsodikova, A.K. Oyelere, D.P. Arya, *ACS Chem. Biol.* 10 (5) (**2015**) 1278-1289.

[65] E.F. Haney, S.C. Mansour, A.L. Hilchie, C. de la Fuente-Nunez, R.E.W. Hancock, *Peptides* 71 (**2015**) 276-285.

[66] M. Benz, A. Asperger, M. Hamester, A. Welle, S. Heissler, P.A. Levkin, *Nat. Commun.*11 (1) (**2020**) 1-10.

[67] C.T. Kuo, J.Y. Wang, A.M. Wo, B.P.C. Chen, H. Lee, *Adv. Biosyst.* 1 (5) (**2017**) 1700048.

[68] M. Kim, J. Noh, *MICROMACHINES-BASEL* 9 (5) (**2018**) 208.

[69] D.G. Anderson, S. Levenberg, R. Langer, *Nat. Biotechnol.* 22 (7) (**2004**) 863-866.

[70] H.Z. Li, Q. Yang, G.N. Li, M.Z. Li, S.T. Wang, Y.L. Song, *ACS Appl. Mater. Interfaces* 7 (17) (**2015**) 9060-9065.

[71] Y. Zhu, Y.X. Zhang, W.W. Liu, Y. Ma, Q. Fang, B. Yao, *Sci. Rep.* 5 (**2015**) 1-7.

[72] A.I. Neto, C.R. Correia, C.A. Custodio, J.F. Mano, *Adv. Funct. Mater.* 24 (32) (**2014**) 5096-5103.

[73] H.J. Cui, X.X. Wang, J. Wesslowski, T. Tronser, J. Rosenbauer, A. Schug, G. Davidson, A.A. Popova, P.A. Levkin, *Adv. Mater.* 33 (4) (**2021**) 2006434.

[74] A.I. Neto, P.A. Levkin, J.F. Mano, *Mater. Horiz.* 5 (3) (**2018**) 379-393.

[75] A.A. Popova, K. Demir, T.G. Hartanto, E. Schmitt, P.A. Levkin, *RSC Adv.* 6 (44) (**2016**) 38263-38276.

[76] B. Chang, Q. Zhou, R.H.A. Ras, A. Shah, Z.G. Wu, K. Hjort, *Appl. Phys. Lett.* 108 (15) (**2016**) 154102.

[77] A.A. Popova, S.M. Schillo, K. Demir, E. Ueda, A. Nesterov-Mueller, P.A. Levkin, *Adv. Mater.* 27 (35) (**2015**) 5217-5222.

[78] W.Q. Feng, E. Ueda, P.A. Levkin, *Adv. Mater.* 30 (20) (**2018**) 1706111.

[79] M. Brehm, S. Heissler, S. Afonin, P.A. Levkin, *Small* 16 (10) (**2020**) 1905971.

[80] D. Qin, Y.N. Xia, G.M. Whitesides, *Nat. Protoc.* 5 (3) (**2010**) 491-502.

[81] Y. Li, P. Chen, Y. Wang, S. Yan, X. Feng, W. Du, S.A. Koehler, U. Demirci, B.F. Liu, *Adv. Mater.* 28 (18) (**2016**) 3543-8.

[82] H. Wu, L. Wu, X.H. Zhou, B.S. Liu, B. Zheng, *Small* 14 (38) (**2018**) 1802128.

[83] S.K. Kuster, M. Pabst, R. Zenobi, P.S. Dittrich, *Angew. Chem. Int. Ed.* 54 (5) (**2015**) 1671-1675.

[84] X. Liu, Z. Lei, D.J. Liu, Z.X. Wang, *Anal. Chim. Acta* 917 (**2016**) 93-100.

[85] Y.J. Ren, C. Wang, Z. Chen, E. Allan, H.C. van der Mei, H.J. Busscher, *FEMS Microbiol. Rev.* 42 (3) (**2018**) 259-272.

[86] D. Sharma, L. Misba, A.U. Khan, *Antimicrob. Resist. Infect. Control* 8 (**2019**) 1-10.

[87] W. Yin, Y.T. Wang, L. Liu, J. He, *Int. J. Mol. Sci.* 20 (14) (**2019**) 3423.

[88] R.M. Donlan, *Emerg. Infect. Dis.* 7 (2) (**2001**) 277-281.

[89] M. Burmolle, T.R. Thomsen, M. Fazli, I. Dige, L. Christensen, P. Homoe, M. Tvede, B. Nyvad, T. Tolker-Nielsen, M. Givskov, C. Moser, K. Kirketerp-Moller, H.K. Johansen, N. Hoiby, P.O. Jensen, S.J. Sorensen, T. Bjarnsholt, *FEMS Microbiol. Immunol.* 59 (3) (**2010**) 324-336.

[90] P.S. Stewart, M.J. Franklin, *Nat. Rev. Microbiol.* 6 (3) (**2008**) 199-210.

[91] L.R. Damgaard, L.P. Nielsen, N.P. Revsbech, *Water Res.* 35 (6) (**2001**) 1379-1386.

[92] S.K. Hansen, J.A.J. Haagensen, M. Gjermansen, T.M. Jorgensen, T. Tolker-Nielsen, S. Molin, *J. Bacteriol. Res.* 189 (13) (**2007**) 4932-4943.

[93] A.M. Baty, C.C. Eastburn, Z. Diwu, S. Techkarnjanaruk, A.E. Goodman, G.G. Geesey, *Appl. Environ. Microbiol.* 66 (8) (**2000**) 3566-3573.

[94] H. Gu, D.C. Ren, *FRONT CHEM SCI ENG* 8 (1) (**2014**) 20-33.

[95] C.R. Arciola, D. Campoccia, L. Montanaro, Implant infections: adhesion, biofilm formation and immune evasion, *Nat. Rev. Microbiol.* 16 (7) (**2018**) 397-409.

[96] H. Gu, S.W. Lee, J. Carnicelli, T. Zhang, D.C. Ren, *Nat. Commun.* 11 (1) (**2020**) 1-11.

[97] I. De-la-Pinta, M. Cobos, J. Ibarretxe, E. Montoya, E. Eraso, T. Guraya, G. Quindos, *J. Mater. Sci.: Mater. Med.* 30 (7) (**2019**) 1-11.

[98] E.K. Riga, M. Vohringer, V.T. Widyaya, K. Lienkamp, *Macromol. Rapid Commun.* 38 (20) (**2017**) 1700216.

[99] H.M. Pouran, S.A. Banwart, M. Romero-Gonzalez, *Environ. Sci.: Process. Impacts* 19 (4) (**2017**) 622-634.

[100] J.X. Meng, P.C. Zhang, S.T. Wang, *Chem. Asian J.* 9 (8) (**2014**) 2004-2016.

[101] F. Chen, J. Ricken, D.D. Xu, S.V. Wegner, *Adv. Biosyst.* 3 (3) (**2019**) 1800269.

[102] F. Chen, S.V. Wegner, *ACS Synth. Biol.* 6 (12) (**2017**) 2170-2174.

[103] N.B. Arnfinnsdottir, V. Ottesen, R. Lale, M. Sletmoen, *PloS One* 10 (6) (**2015**) e0128162.

[104] S. Rozhok, Z.F. Fan, D. Nyamjav, C. Liu, C.A. Mirkin, R.C. Holz, *Langmuir* 22 (26) (**2006**) 11251-11254.

[105] S. Rozhok, C.K.F. Shen, P.L.H. Littler, Z.F. Fan, C. Liu, C.A. Mirkin, R.C. Holz, *Small* 1 (4) (**2005**) 445-451.

[106] Z.Y. Suo, R. Avci, X.H. Yang, D.W. Pascual, *Langmuir* 24 (8) (**2008**) 4161-4167.

[107] W.A. Velema, J.P. van der Berg, W. Szymanski, A.J.M. Driessen, B.L. Feringa, *Org. Biomol. Chem.* 13 (6) (**2015**) 1639-1642.

[108] M. Palacios-Cuesta, A.L. Cortajarena, O. Garcia, J. Rodriguez-Hernandez, *Polym. Chem.* 6 (14) (**2015**) 2677-2684.

[109] A.K. Epstein, A.I. Hochbaum, P. Kim, J. Aizenberg, *Nanotechnology* 22 (49) (**2011**) 494007.

[110] A.I. Hochbaum, J. Aizenberg, *Nano Lett.* 10 (9) (**2010**) 3717-3721.

[111] M. Yang, Y.H. Ding, X. Ge, Y. Leng, *Colloids Surf. B* 135 (**2015**) 549-555.

[112] J. Kim, Y.H. Shin, S.H. Yun, D.S. Choi, J.H. Nam, S.R. Kim, S.K. Moon, B.H. Chung, J.H. Lee, J.H. Kim, K.Y. Kim, K.M. Kim, J.H. Lim, *J. Am. Chem. Soc.* 134 (40) (**2012**) 16500-16503.

[113] J. Merrin, S. Leibler, J.S. Chuang, *PloS One* 2 (7) (**2007**) e663.

[114] A. Majerle, D.T. Schmieden, R. Jerala, A.S. Meyer, *Biochemistry* 58 (16) (**2019**) 2095-2104.

[115] V.S. Cheptsov, E.S. Churbanova, V.I. Yusupov, M.V. Gorlenko, L.V. Lysak, N.V. Minaev, V.N. Bagratashvili, B.N. Chichkov, *Lett. Appl. Microbiol.* 67 (6) (**2018**) 544-549.

[116] L.P. Xu, L. Robert, O.Y. Qi, F. Taddei, Y. Chen, A.B. Lindner, D. Baigl, *Nano Lett.* 7 (7) (**2007**) 2068-2072.

[117] D.B. Weibel, A. Lee, M. Mayer, S.F. Brady, D. Bruzewicz, J. Yang, W.R. DiLuzio, J. Clardy, G.M. Whitesides, *Langmuir* 21 (14) (**2005**) 6436-6442.

[118] T. Xu, S. Petridou, E.H. Lee, E.A. Roth, N.R. Vyavahare, J.J. Hickman, T. Boland, *Biotechnol. Bioeng.* 85 (1) (**2004**) 29-33.

[119] J.L. Connell, E.T. Ritschdorff, M. Whiteley, J.B. Shear, *Proc. Natl. Acad. Sci. U.S.A.* 110 (46) (**2013**) 18380-18385.

[120] K. Dubbin, Z.Y. Dong, D.M. Park, J. Alvarado, J. Su, E. Wasson, C. Robertson, J. Jackson, A. Bose, M.L. Moya, Y.Q. Jiao, W.F. Hynes, *Nano Lett.* 21 (3) (**2021**) 1352-1359.

[121] J.F. Huang, S.Y. Liu, C. Zhang, X.Y. Wang, J.H. Pu, F. Ba, S. Xue, H.F. Ye, T.X. Zhao, K. Li, Y.Y. Wang, J.C. Zhang, L.H. Wang, C.H. Fan, T.K. Lu, C. Zhong, *Nat. Chem. Biol.* 15 (1) (**2019**) 34-41.

[122] M. Schaffner, P.A. Ruhs, F. Coulter, S. Kilcher, A.R. Studart, *Sci. Adv.* 3 (12) (**2017**) eaao6804.

[123] R.S. Gona, A.S. Meyer, *MRS Bull.* 45 (12) (**2020**) 1034-1038.

[124] L.M. Gonzalez, N. Mukhitov, C.A. Voigt, *Nat. Chem. Biol.* 16 (2) (**2020**) 126-133.

[125] X.Y. Liu, H. Yuk, S.T. Lin, G.A. Parada, T.C. Tang, E. Tham, C. de la Fuente-Nunez, T.K. Lu, X.H. Zhao, *Adv. Mater.* 30 (4) (**2018**) 1704821.

[126] S. Joshi, E. Cook, M.S. Mannoor, *Nano Lett.* 18 (12) (**2018**) 7448-7456.

[127] B.A.E. Lehner, D.T. Schmieden, A.S. Meyer, *ACS Synth. Biol.* 6 (7) (**2017**) 1124-1130.

[128] D.T. Schmieden, S.J. Basalo Vazquez, H. Sanguesa, M. van der Does, T. Idema, A.S. Meyer, *ACS Synth. Biol.* 7 (5) (**2018**) 1328-1337.

[129] X.F. Jin, I.H. Riedel-Kruse, *Proc. Natl. Acad. Sci. U.S.A.* 115 (14) (**2018**) 3698-3703.

[130] Y.Y. Wang, B.L. An, B. Xue, J.H. Pu, X.L. Zhang, Y.Y. Huang, Y. Yu, Y. Cao, C. Zhong, *Nat. Chem. Biol.* 17 (3) (**2021**) 351-359.

[131] Y.J. Huang, A.G. Xia, G. Yang, F. Jin, *ACS Synth. Biol.* 7 (5) (**2018**) 1195-1200.

[132] E.T. Felix Moser, Lina M. González, Timothy K. Lu, Christopher A. Voigt, *Adv. Funct. Mater.* 29 (30) (**2019**) 1901788.

[133] S.H. Hong, J.B. Gorce, H. Punzmann, N. Francois, M. Shats, H. Xia, *Sci. Adv.* 6 (22) (**2020**) eaaz9386.

[134] Z. Jahed, H. Shahsavan, M.S. Verma, J.L. Rogowski, B.B. Seo, B.X. Zhao, T.Y. Tsui, F.X. Gu, M.R.K. Mofrad, *Acs Nano* 11 (1) (**2017**) 675-683.

[135] V. Kantsler, E. Ontanon-McDonald, C. Kuey, M.J. Ghanshyam, M.C. Roffin, M. Asally, *ACS Synth. Biol.* 9 (6) (**2020**) 1277-1283.

[136] A. Susarrey-Arce, A. Marin, A. Massey, A. Oknianska, Y. Diaz-Fernandez, J.F. Hernandez-Sanchez, E. Griffiths, J.G.E. Gardeniers, J.H. Snoeijer, D. Lohse, R. Rayal, *Langmuir* 32 (28) (**2016**) 7159-7169.

[137] S. Peppou-Chapman, J.K. Hong, A. Waterhouse, C. Neto, *Chem. Soc. Rev.* 49 (11) (**2020**) 3688-3715.

[138] J. Bruchmann, I. Pini, T.S. Gill, T. Schwartz, P.A. Levkin, *Adv. Healthc. Mater.* 6 (1) (**2017**) 1601082.

[139] T.S. Wong, S.H. Kang, S.K.Y. Tang, E.J. Smythe, B.D. Hatton, A. Grinthal, J. Aizenberg, *Nature* 477 (7365) (**2011**) 443-447.

[140] J.S. Li, E. Ueda, D. Paulssen, P.A. Levkin, *Adv. Funct. Mater.* 29 (4) (**2019**) 1802317.

[141] M. Villegas, Y.X. Zhang, N. Abu Jarad, L. Soleymani, T.F. Didar, *Acs Nano* 13 (8) (**2019**) 8517-8536.

[142] N. Vogel, R.A. Belisle, B. Hatton, T.S. Wong, J. Aizenberg, *Nat. Commun.* 4 (**2013**) 1-10.

[143] D. Paulssen, W.Q. Feng, I. Pini, P.A. Levkin, *Adv. Mater. Interfaces* 5 (18) (**2018**) 1800852.

[144] L.Y. Fang, J.H. Zhang, Y.C. Chen, S.L. Liu, Q.Y. Chen, A. Ke, L.T. Duan, S.L. Huang, X.L. Tian, Z. Xie, *Adv. Funct. Mater.* (**2021**) 2100447.

[145] T.C. Scanlon, S.M. Dostal, K.E. Griswold, *Biotechnol. Bioeng.* 111 (2) (**2014**) 232-243.

[146] N.C. Parsley, A.L. Smythers, L.M. Hicks, *FRONT CELL INFECT MI* 10 (**2020**) 547177.

[147] K. Lewis, *Nat. Rev. Drug Discov.* 12 (5) (**2013**) 371-387.

[148] R. Tommasi, D.G. Brown, G.K. Walkup, J.I. Manchester, A.A. Miller, *Nat. Rev. Drug Discov.* 14 (9) (**2015**) 662-662.

[149] J.M. Blair, M.A. Webber, A.J. Baylay, D.O. Ogbolu, L.J. Piddock, *Nat. Rev. Microbiol.* 13 (1) (**2015**) 42-51.

[150] F. Antonanzas, H. Goossens, *Eur. J. Health Econ.* 20 (4) (**2019**) 483-485.

[151] A. Luther, M. Urfer, M. Zahn, M. Mueller, S.Y. Wang, M. Mondal, A. Vitale, J.B. Hartmann, T. Sharpe, F. Lo Monte, H. Kocherla, E. Cline, G. Pessi, P. Rath, S.M. Modaresi, P. Chiquet, S. Stiegeler, C. Verbree, T. Remus, M. Schmitt, C. Kolopp, M.A. Westwood, N. Desjonqueres, E. Brabet, S. Hell, K. LePoupon, A. Vermeulen, R. Jaisson, V. Rithie, G. Upert, A. Lederer, P. Zbinden, A. Wach, K. Moehle, K. Zerbe, H.H. Locher, F. Bernardini, G.E. Dale, L. Eberl, B. Wollscheid, S. Hiller, J.A. Robinson, D. Obrecht, *Nature* 576 (7787) (**2019**) 452-458.

[152] E.M. Hart, A.M. Mitchell, A. Konovalova, M. Grabowicz, J. Sheng, X.Q. Han, F.P. Rodriguez-Rivera, A.G. Schwaid, J.C. Malinverni, C.J. Balibar, S. Bodea, Q. Si, H. Wang, M.F. Homsher, R.E. Painter, A.K. Ogawa, H. Sutterlin, T. Roemer, T.A. Black, D.M. Rothman, S.S. Walker, T.J. Silhavy, *Proc. Natl. Acad. Sci. U.S.A.* 116 (43) (**2019**) 21748-21757.

[153] B. Ruhmann, J. Schmid, V. Sieber, *Front. Microbiol.* 6 (**2015**) 565.

[154] C. Rani, R. Mehra, R. Sharma, R. Chib, P. Wazir, A. Nargotra, I.A. Khan, *Tuberculosis* 95 (6) (**2015**) 664-77.

[155] E.K. Sully, N. Malachowa, B.O. Elmore, S.M. Alexander, J.K. Femling, B.M. Gray, F.R. DeLeo, M. Otto, A.L. Cheung, B.S. Edwards, L.A. Sklar, A.R. Horswill, P.R. Hall, H.D. Gresham, *PLoS Pathog.* 10 (6) (**2014**) e1004174.

[156] S.A. Stanley, S.S. Grant, T. Kawate, N. Iwase, M. Shimizu, C. Wivagg, M. Silvis, E. Kazyanskaya, J. Aquadro, A. Golas, M. Fitzgerald, H. Dai, L. Zhang, D.T. Hung, *ACS Chem. Biol.* 7 (8) (**2012**) 1377-1384.

[157] X. Jin, M. H. Li, J. W. Wang, C. Marambio-Jones, F. B. Peng, X. F. Huang, R. Damoiseaux, E. M. V. Hoek, *Environ. Sci. Technol*. (**2010)** 7321-7328.

[158] X.M. Kang, F.F. Wang, H. Zhang, Q. Zhang, W. Qiana, *Appl. Environ. Microbiol.* 81 (4) (**2015**) 1200-1209.

[159] G. Choi, D.J. Hassett, S. Choi, *Analyst.* 140 (12) (**2015**) 4277-83.

[160] C.J. Ingham, A. Sprenkels, J. Bomer, D. Molenaar, A. van den Berg, J.E. van Hylckama Vlieg, W.M. de Vos, *Proc. Natl. Acad. Sci. U.S.A.* 104 (46) (**2007**) 18217-18222.

[161] W.Q. Feng, L.X. Li, E. Ueda, J.S. Li, S. Heissler, A. Welle, O. Trapp, P.A. Levkin, *Adv. Mater. Interfaces* 1 (7) (**2014**) 1400269.

[162] A.A. Popova, T. Tronser, K. Demir, P. Haitz, K. Kuodyte, V. Starkuviene, P. Wajda, P.A. Levkin, *Small* 15 (25) (**2019**) 1901299.

[163] Y. Morita, J. Tomida, Y. Kawamura, *Front. Microbiol.* 4 (**2014**) 422.

[164] Y. Ren, G. Ma, L. Peng, Y. Ren, F. Zhang, *Cell Biochem. Biophys.* 71 (2) (**2015**) 1235-1238.

[165] S.T. Micek, R.G. Wunderink, M.H. Kollef, C. Chen, J. Rello, J. Chastre, M. Antonelli, T. Welte, B. Clair, H. Ostermann, E. Calbo, A. Torres, F. Menichetti, G.E. Schramm, V. Menon, *Crit. Care* 19 (**2015**) 219.

[166] G.D. Wright, *Nat. Rev. Microbiol.* 5 (3) (**2007**) 175-86.

[167] T. Rasamiravaka, M. El Jaziri, *Curr. Microbiol.* 73 (5) (**2016**) 747-753.

[168] Z.M. Djordjevic, M.M. Folic, S.M. Jankovic, *J. Glob. Antimicrob.* 13 (**2018**) 60-64.

[169] T. Schwartz, H. Volkmann, S. Kirchen, W. Kohnen, K. Schon-Holz, B. Jansen, U. Obst, *FEMS Microbiol. Ecol.* 57 (1) (**2006**) 158-167.

[170] M. Berditsch, T. Jager, N. Strempel, T. Schwartz, J. Overhage, A.S. Ulrich, *Antimicrob. Agents Chemother.* 59 (9) (**2015**) 5288-5296.

[171] A.P. Magiorakos, A. Srinivasan, R.B. Carey, Y. Carmeli, M.E. Falagas, C.G. Giske, S. Harbarth, J.F. Hindler, G. Kahlmeter, B. Olsson-Liljequist, D.L. Paterson, L.B. Rice, J. Stelling, M.J. Struelens, A. Vatopoulos, J.T. Weber, D.L. Monnet, *Clin. Microbiol. Infect.* 18 (3) (**2012**) 268-281.

[172] S. Petersen-Morfin, P. Bocanegra-Ibarias, R. Morfin-Otero, E. Garza-Gonzalez, H.R. Perez-Gomez, E. Gonzalez-Diaz, S. Esparza-Ahumada, G. Leon-Garnica, G. Amezcua-Salazar, E. Rodriguez-Noriega, *Am. J. Med. Case Rep.* 18 (**2017**) 805-809.

[173] K. Chamchoy, D. Pakotiprapha, P. Pumirat, U. Leartsakulpanich, U. Boonyuen, *BMC Biochem.* 20 (**2019**) 1-14.

[174] I.M. Bezerra, O. Chiavone, S. Mattedi, *Braz. J. Chem. Eng.* 30 (1) (**2013**) 45-54.

[175] C. de la Fuente-Nunez, F. Reffuveille, L. Fernandez, R.E.W. Hancock, *Curr. Opin. Microbiol.* 16 (5) (**2013**) 580-589.

[176] D. Davies, *Nat. Rev. Drug Discov.* 2 (2) (**2003**) 114-122.

[177] E.P. Greenberg, *Nature* 424 (6945) (**2003**) 134.

[178] E.S. Gloag, L. Turnbull, A. Huang, P. Vallotton, H. Wang, L.M. Nolan, L. Mililli, C. Hunt, J. Lu, S.R. Osvath, L.G. Monahan, R. Cavaliere, I.G. Charles, M.P. Wand, M.L. Gee, R. Prabhakar, C.B. Whitchurch, *Proc. Natl. Acad. Sci. U.S.A.* 110 (28) (**2013**) 11541-11546.

[179] D.T. Hughes, V. Sperandio, *Nat. Rev. Microbiol.* 6 (2) (**2008**) 111-120.

[180] L.R. Hoffman, D.A. D'Argenio, M.J. MacCoss, Z.Y. Zhang, R.A. Jones, S.I. Miller, *Nature* 436 (7054) (**2005**) 1171-1175.

[181] H.C. Flemming, J. Wingender, *Nat. Rev. Microbiol.* 8 (9) (**2010**) 623-633.

[182] E. Karatan, P. Watnick, Signals, *Microbiol. Mol. Biol. Rev.* 73 (2) (**2009**) 310.

[183] P. Stoodley, R. Cargo, C.J. Rupp, S. Wilson, I. Klapper, *J. Ind. Microbiol. Biotechnol.* 29 (6) (**2002**) 361-367.

[184] R. Rusconi, S. Lecuyer, L. Guglielmini, H.A. Stone, *J. R. Soc. Interface* 7 (50) (**2010**) 1293-1299.

[185] K. Drescher, Y. Shen, B.L. Bassler, H.A. Stone, *Proc. Natl. Acad. Sci. U.S.A.* 110 (11) (**2013**) 4345-4350.

[186] M. Badv, S.M. Imani, J.I. Weitz, T.F. Didar, *Acs Nano* 12 (11) (**2018**) 10890-10902.

[187] M. Badv, I.H. Jaffer, J.I. Weitz, T.F. Didar, *Sci. Rep.*7 (**2017**) 1-10.

[188] J.S. Li, T. Kleintschek, A. Rieder, Y. Cheng, T. Baumbach, U. Obst, T. Schwartz, P.A. Levkin, *ACS Appl. Mater. Interfaces* 5 (14) (**2013**) 6704-6711.

[189] C. Howell, T.L. Vu, J.J. Lin, S. Kolle, N. Juthani, E. Watson, J.C. Weaver, J. Alvarenga, J. Aizenberg, *ACS Appl. Mater. Interfaces* 6 (15) (**2014**) 13299-13307.

[190] A.K. Epstein, T.S. Wong, R.A. Belisle, E.M. Boggs, J. Aizenberg, *Proc. Natl. Acad. Sci. U.S.A.* 109 (33) (**2012**) 13182-13187.

[191] A. Oliver, R. Canton, P. Campo, F. Baquero, J. Blazquez, *Science* 288 (5469) (**2000**) 1251-1253.

[192] S.E. Vartivarian, K.A. Papadakis, E.J. Anaissie, *Arch. Intern. Med.* 156 (4) (**1996**) 433-435.

[193] S.Y.C. Tong, J.S. Davis, E. Eichenberger, T.L. Holland, V.G. Fowler, *Clin. Microbiol. Rev.* 28 (3) (**2015**) 603-661.

[194] P.S. Stewart, J.W. Costerton, *Lancet* 358 (9276) (**2001**) 135-138.

[195] A. Potron, L. Poirel, P. Nordmann, *Int. J. Antimicrob. Agents* 45 (6) (**2015**) 568-585.

[196] J. Bruchmann, K. Sachsenheimer, B.E. Rapp, T. Schwartz, *PloS One* 10 (2) (**2015**) e0117300.

[197] I. Olsen, *Eur. J. Clin. Microbiol. Infect. Dis.* 34 (5) (**2015**) 877-886.

[198] S.I. Khan, G. Blumrosen, D. Vecchio, A. Golberg, M.C. McCormack, M.L. Yarmush, M.R. Hamblin, W.G. Austen, *Biotechnol. Bioeng.* 113 (3) (**2016**) 643-650.

[199] L.A. Yang, Y. Liu, H. Wu, N. Hoiby, S. Molin, Z.J. Song, *Int. J. Oral Sci.* 3 (2) (**2011**) 74-81.

[200] C.K. Stover, X.Q. Pham, A.L. Erwin, S.D. Mizoguchi, P. Warrener, M.J. Hickey, F.S.L. Brinkman, W.O. Hufnagle, D.J. Kowalik, M. Lagrou, R.L. Garber, L. Goltry, E. Tolentino, S. Westbrock-Wadman, Y. Yuan, L.L. Brody, S.N. Coulter, K.R. Folger, A. Kas, K. Larbig, R. Lim, K. Smith, D. Spencer, G.K.S. Wong, Z. Wu, I.T. Paulsen, J. Reizer, M.H. Saier, R.E.W. Hancock, S. Lory, M.V. Olson, *Nature* 406 (6799) (**2000**) 959-964.

[201] O. Ciofu, T. Tolker-Nielsen, P.O. Jensen, H.Z. Wang, N. Hoiby, *Adv. Drug Deliv. Rev.* 85 (**2015**) 7-23.

[202] E.R. Rojas, G. Billings, P.D. Odermatt, G.K. Auer, L. Zhu, A. Miguel, F. Chang, D.B. Weibel, J.A. Theriot, K.C. Huang, *Nature* 559 (7715) (**2018**) 617-621.

[203] X.Z. Li, P. Plesiat, H. Nikaido, *Clin. Microbiol. Rev.* 28 (2) (**2015**) 337-418.

[204] Z. Pang, R. Raudonis, B.R. Glick, T.J. Lin, Z.Y. Cheng, *Biotechnol. Adv.* 37 (1) (**2019**) 177-192.

[205] S. Amini, S. Kolle, L. Petrone, O. Ahanotu, S. Sunny, C.N. Sutanto, S. Hoon, L. Cohen, J.C. Weaver, J. Aizenberg, N. Vogel, A. Miserez, *Science* 357 (6352) (**2017**) 668-673.

[206] S. Peppou-Chapman, J.K. Hong, A. Waterhouse, C. Neto, *Chem. Soc. Rev.* (**2020**) 3688-3715.

[207] C.S. Ware, T. Smith-Palmer, S. Peppou-Chapman, L.R.J. Scarratt, E.M. Humphries, D. Balzer, C. Neto, *ACS Appl. Mater. Interfaces* 10 (4) (**2018**) 4173-4182.

[208] H.X. Zhao, Q.Q. Sun, X. Deng, J.X. Cui, *Adv. Mater.* 30 (29) (**2018**) 1802141.

[209] H.Y. Geng, S.K. Cho, *Lab Chip* 19 (13) (**2019**) 2275-2283.

[210] C. Howell, A. Grinthal, S. Sunny, M. Aizenberg, J. Aizenberg, *Adv. Mater.* 30 (50) (**2018**) 1802724.

[211] N. Keller, J. Bruchmann, T. Sollich, C. Richter, R. Thelen, F. Kotz, T. Schwartz, D. Helmer, B.E. Rapp, *ACS Appl. Mater. Interfaces* 11 (4) (**2019**) 4480-4487.

[212] P.F. She, Y.L. Wang, Y.Q. Liu, F. Tan, L.H. Chen, Z. Luo, Y. Wu, *Microbiologyopen* 8 (12) (**2019**) e933.

[213] G.Y. Celik, B. Aslim, Y. Beyatli, *Carbohydr. Polym*. 73 (1) (**2008**) 178-182.

[214] J. Wimpenny, W. Manz, U. Szewzyk, *FEMS Microbiol. Rev.* 24 (5) (**2000**) 661-671.

[215] C. Li, Z. Hite, J.W. Warrick, J.Y. Li, S.H. Geller, V.G. Trantow, M.N. McClean, D.J. Beebe, *Sci. Adv.* 6 (16) (**2020**) eaay9919.

[216] E.A. Naumova, L. Weber, V. Pankratz, V. Czenskowski, W.H. Arnold, *Arch. Oral Biol.* 97 (**2019**) 91-96.

[217] A.J. Adami, J.L. Cervantes, *Tuberculosis* 95 (6) (**2015**) 651-658.